*Available online at* www.joac.info

ISSN: 2278-1862

Journal of Applicable Chemistry

2024, 13 (4): 594-652

(International Peer Reviewed Journal)

New Chemistry News

$^{-}N=C=N^{-}$

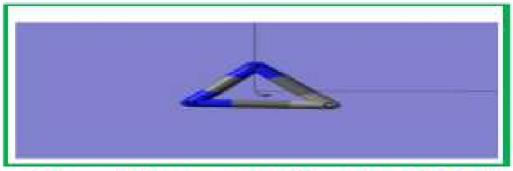

New News of Chem (NNC)

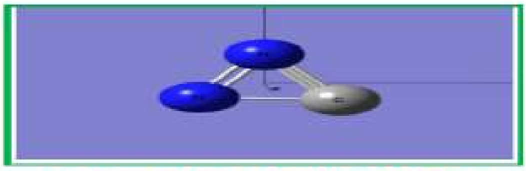

ChemNewsNew (CNN)

## CNN – 64b... *I am ...*

# ...*Intelligence Augmented Medical...* *Urology/Nephrology*

| | Information Source | sciencedirect.com; |
|---|---|---|
| **S. Narasinga Rao M D**<br>**Associate Professor,**<br>**Emergency Medicine dept.,**<br>**Andhra Medical College,**<br>**King George Hospital**<br>**Visakhapatnam, A.P., India** | **K. SomasekharaRao, Ph D**<br>**Dept. of Chemistry,**<br>**Acharya Nagarjuna Univ.,**<br>**Dr. M.R.Appa Rao Campus,**<br>**Nuzvid-521 201, India** | **R. Sambasiva Rao, Ph D**<br>**Dept. of Chemistry,**<br>**Andhra University,**<br>**Visakhapatnam 530 003,**<br>**India** |
| snrnaveen007@gmail.com<br>(+91 9848136704) | sr_kaza1947@yahoo.com<br>(+91 98 48 94 26 18) | rsr.chem@gmail.com<br>(+91 99 85 86 01 82) |

***Keywords*:**Artificial intelligence (AI); Medical diagnosis, Surgery; Urologist/Nephrologist

CNN : [C [Computations; Computer; Chemistry, Cell, Celestial,Cerebrum] NN [New News; News New; Neural Nets; Nature News; News of Nature;] ]

Fits : [Figure Image Table Script;]

K(nowledge)Lab

rsr.chem1979

08

**Overall Experimental Procedure of the Study**

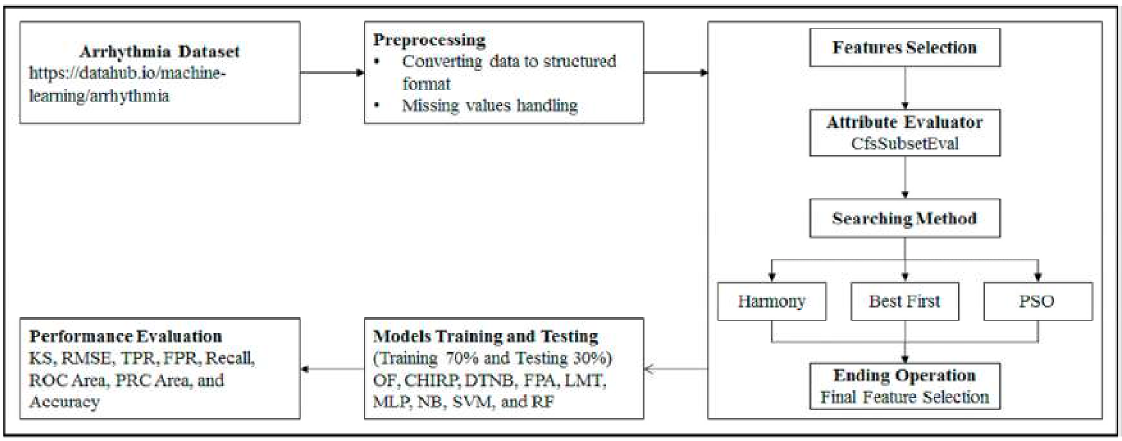
Arrhythmia Dataset
https://datahub.io/machine-learning/arrhythmia
Preprocessing
Converting data to structured format
Missing values handling
Features Selection
Attribute Evaluator
CfsSubsetEval
Searching Method
Harmony
Best First
PSO
Ending Operation
Final Feature Selection
Models Training and Testing
(Training 70% and Testing 30%)
OF, CHIRP, DTNB, FPA, LMT, MLP, NB, SVM, and RF
Performance Evaluation
KS, RMSE, TPR, FPR, Recall, ROC Area, PRC Area, and Accuracy

Chronic Kidney Disease (CKD)

## virtual reality
## Augmented reality
## Real reality

09

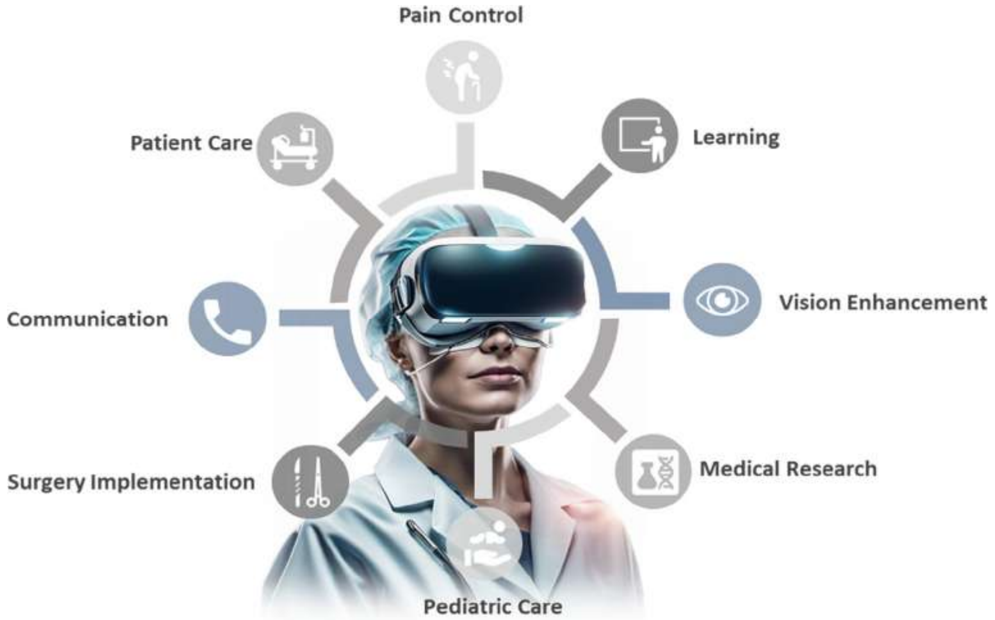
Pain Control
Patient Care
Learning
Communication
Vision Enhancement
Surgery Implementation
Medical Research
Pediatric Care

**Possible application of new headsets for medical enhanced virtual reality/augmented reality**

10

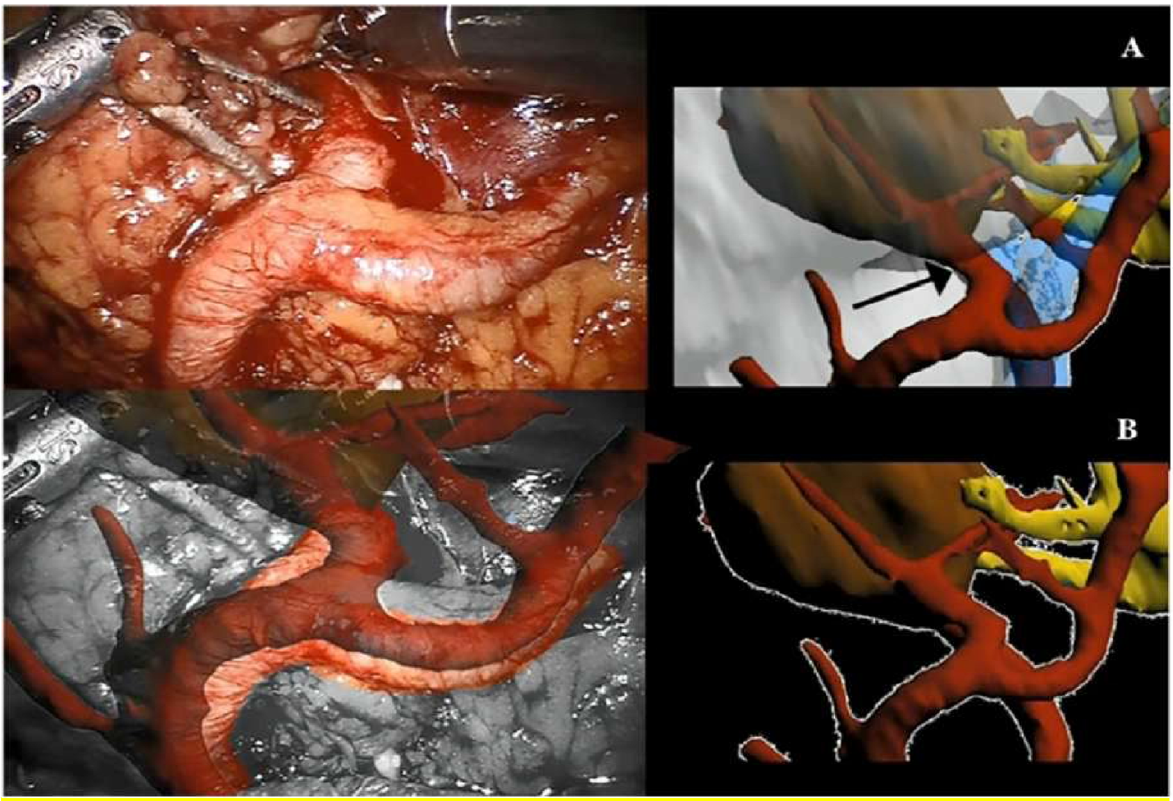

Dissection of the renal pedicle guided by an augmented reality three-dimensional reconstruction

# Segmentation

10

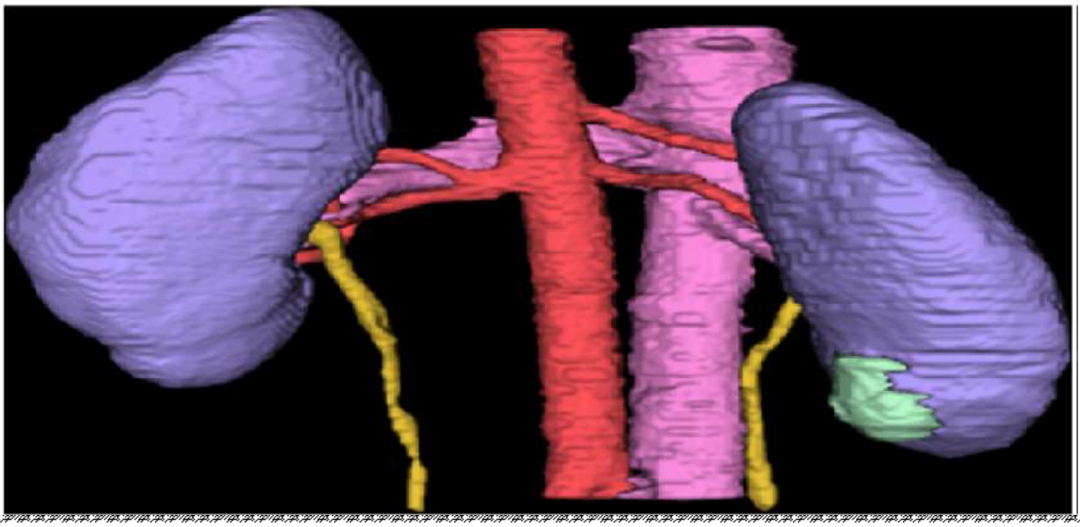

Segmentation of
kidneys, ureters, renal vessels, and a tumor
(https://kits21.kits-challenge.org).

# Cancer

11

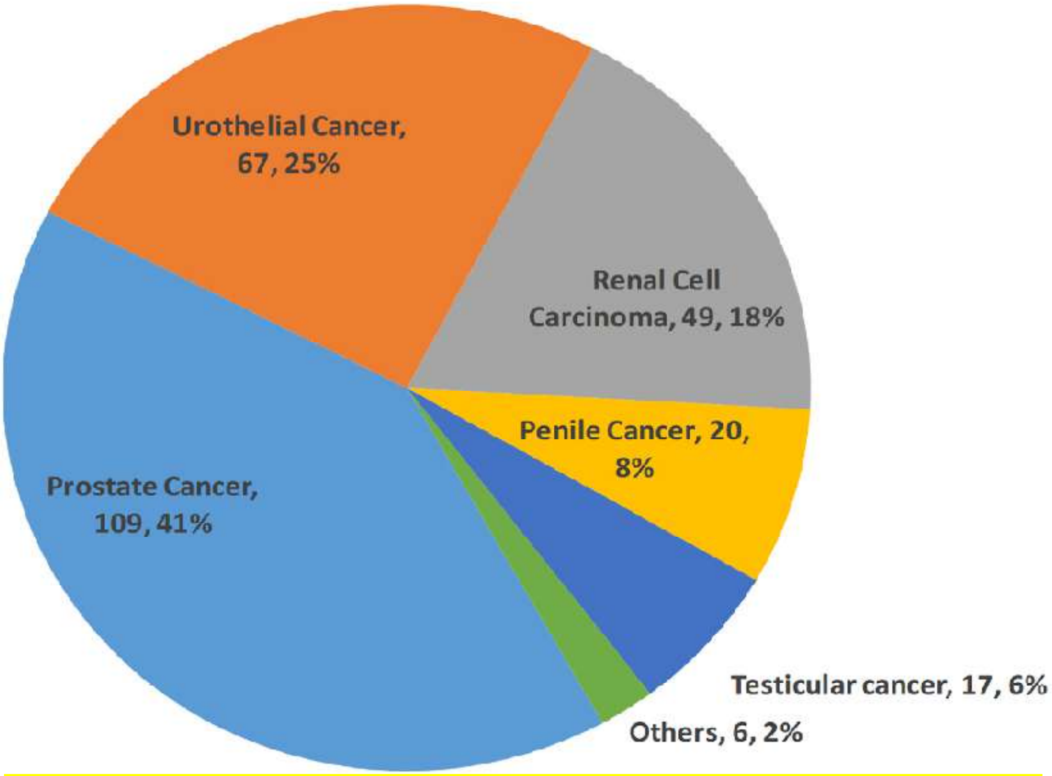

Breakdown of the number of histology reports by cancer types (2008–2018) (n = 268).

11

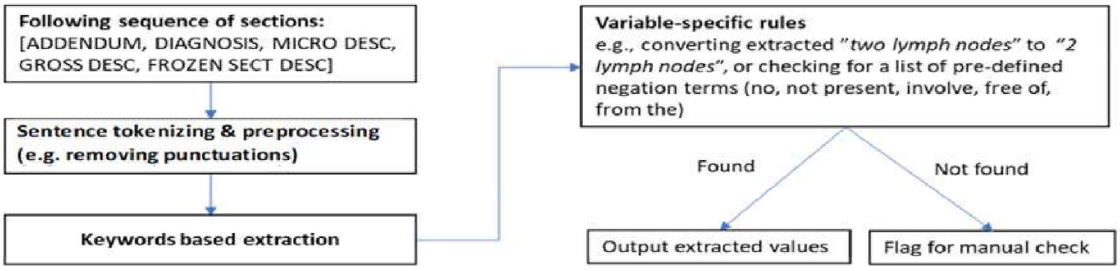
Following sequence of sections: [ADDENDUM, DIAGNOSIS, MICRO DESC, GROSS DESC, FROZEN SECT DESC]
Sentence tokenizing & preprocessing (e.g. removing punctuations)
Keywords based extraction
Variable-specific rules e.g., converting extracted "two lymph nodes" to "2 lymph nodes", or checking for a list of pre-defined negation terms (no, not present, involve, free of, from the)
Found
Not found
Output extracted values
Flag for manual check

Method-flow for General rule-based extraction

# Math. Models

11

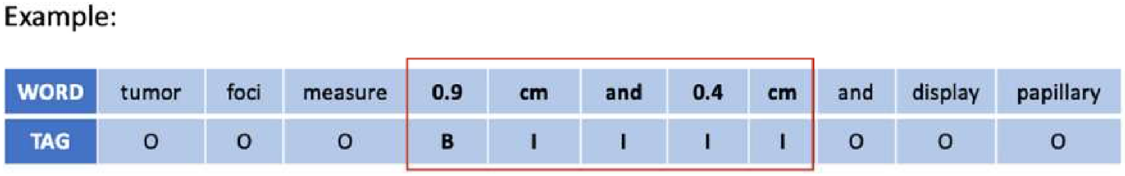

Example:

| WORD | tumor | foci | measure | 0.9 | cm | and | 0.4 | cm | and | display | papillary |
|---|---|---|---|---|---|---|---|---|---|---|---|
| TAG | O | O | O | B | I | I | I | I | O | O | O |

Sample of a BIO tagged sentence1

# LLMs
# Bert Model

11

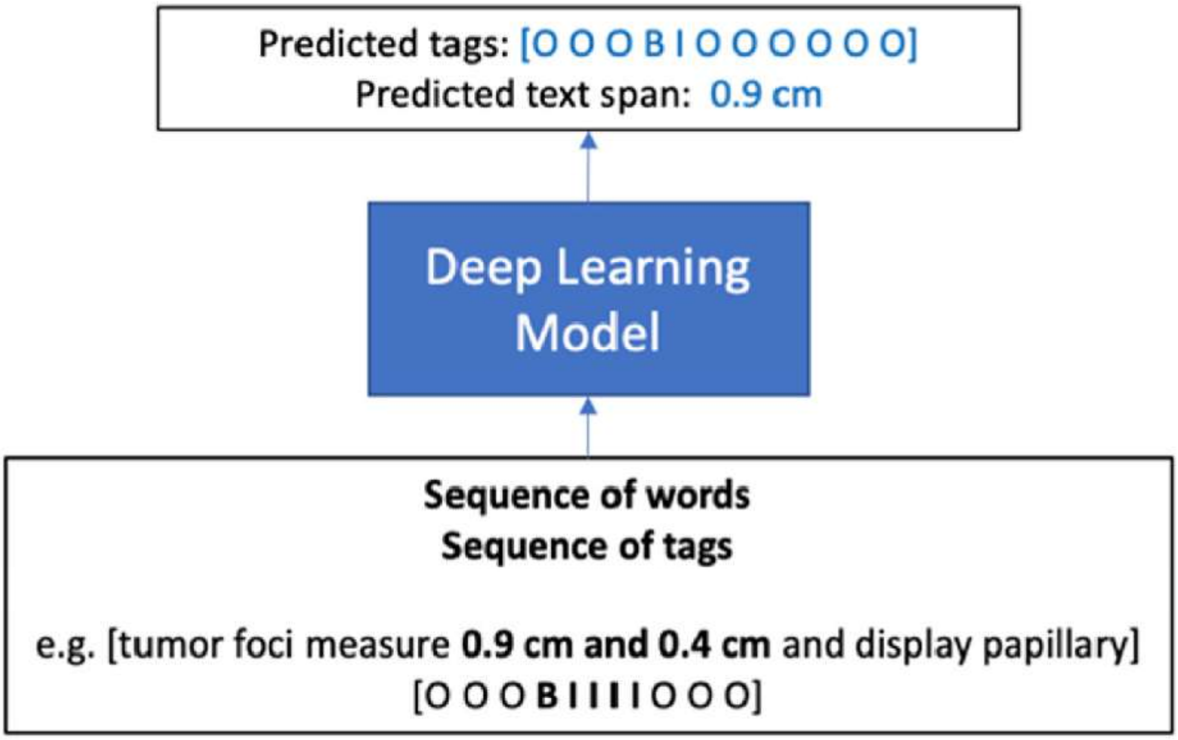

Predicted tags: [O O O B I O O O O O O]
Predicted text span: 0.9 cm

Deep Learning Model

**Sequence of words**
**Sequence of tags**

e.g. [tumor foci measure **0.9 cm and 0.4 cm** and display papillary]
[O O O **B I I I I** O O O]

**Sample of predicted labels for an input sentence**

11

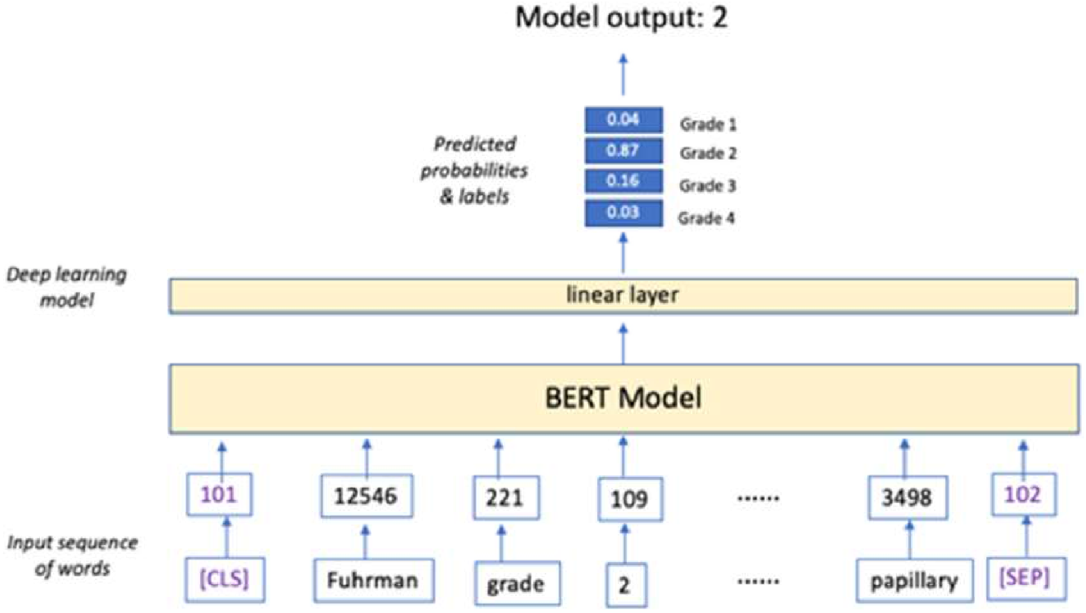
Model output: 2
Predicted probabilities & labels
0.04 Grade 1
0.87 Grade 2
0.16 Grade 3
0.03 Grade 4
Deep learning model
linear layer
BERT Model
101
12546
221
109
......
3498
102
Input sequence of words
[CLS]
Fuhrman
grade
2
......
papillary
[SEP]

**Language model framework**

12

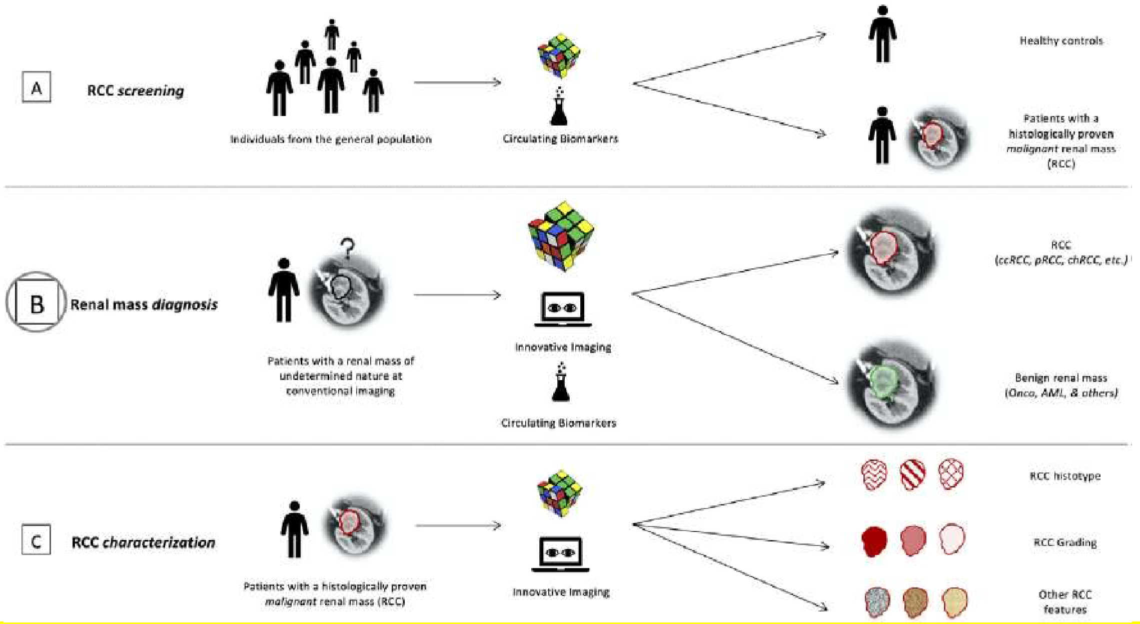
A
RCC screening
Individuals from the general population
Circulating Biomarkers
Healthy controls
Patients with a histologically proven malignant renal mass (RCC)
B
Renal mass diagnosis
?
Patients with a renal mass of undetermined nature at conventional imaging
Innovative Imaging
Circulating Biomarkers
RCC (ccRCC, pRCC, chRCC, etc.)
Benign renal mass (Onco, AML, & others)
C
RCC characterization
Patients with a histologically proven malignant renal mass (RCC)
Innovative Imaging
RCC histotype
RCC Grading
Other RCC features

**Pictorial overview of the potential impact of novel liquid biomarkers and/or innovative imaging modalities on kidney cancer screening diagnosis, and characterisation**

Only the studies focused on kidney cancer diagnosis and fulfilling all other prespecified PICOS criteria were finallyincluded in the qualitative analysis of this review.

- ✓ (A ) Liquid biomarkers may allow discrimination between healthy individuals (without any renal mass) and patients with (histologically confirmed) renal cell carcinoma (RCC). Such biomarkers could potentially be integrated into RCC screening programs. All studies evaluating this kind of biomarkers were excluded from the review but were the subject of supplementary qualitative analysis.
- ✓ (B ) In patients presenting with a renal mass of undetermined nature (discovered at onventional cross-sectional imaging), liquid biomarkers and/or innovative imaging modalities may allow discrimination between malignant RCC and benign masses (oncocytomas, fat-poor ngiomyolipomas, adenomas). Such biomarkers could be integrated into the current diagnostic algorithms for patients with renal masses of undetermined nature, and then implemented in kidney cancer diagnosis and potentially clinical practice (decision-making regarding a management strategy of active surveillance, ablative therapy, or surgery).
- ✓ (C ) For patients with (histologically confirmed) RCC, innovative imaging modalities, with or without the use of deep learning or machine learning algorithms, may aid in characterisingtumour grade or histotype, as well as other specific features (eg, presence of necrosis). All studies evaluating this kind of imaging technique were excluded from the review but were the subject of supplementary qualitative analysis.
- ✓

RCC = renal cell carcinoma; ccRCC = clear-cell RCC; pRCC = papillary RCC; chRCC = chromophobe RCC; Onco = oncocytoma; AML = angiomyolipoma

# Med. Literature survey

12

**Systematic Reviews and Meta-analyses (PRISMA) statement recommendations**

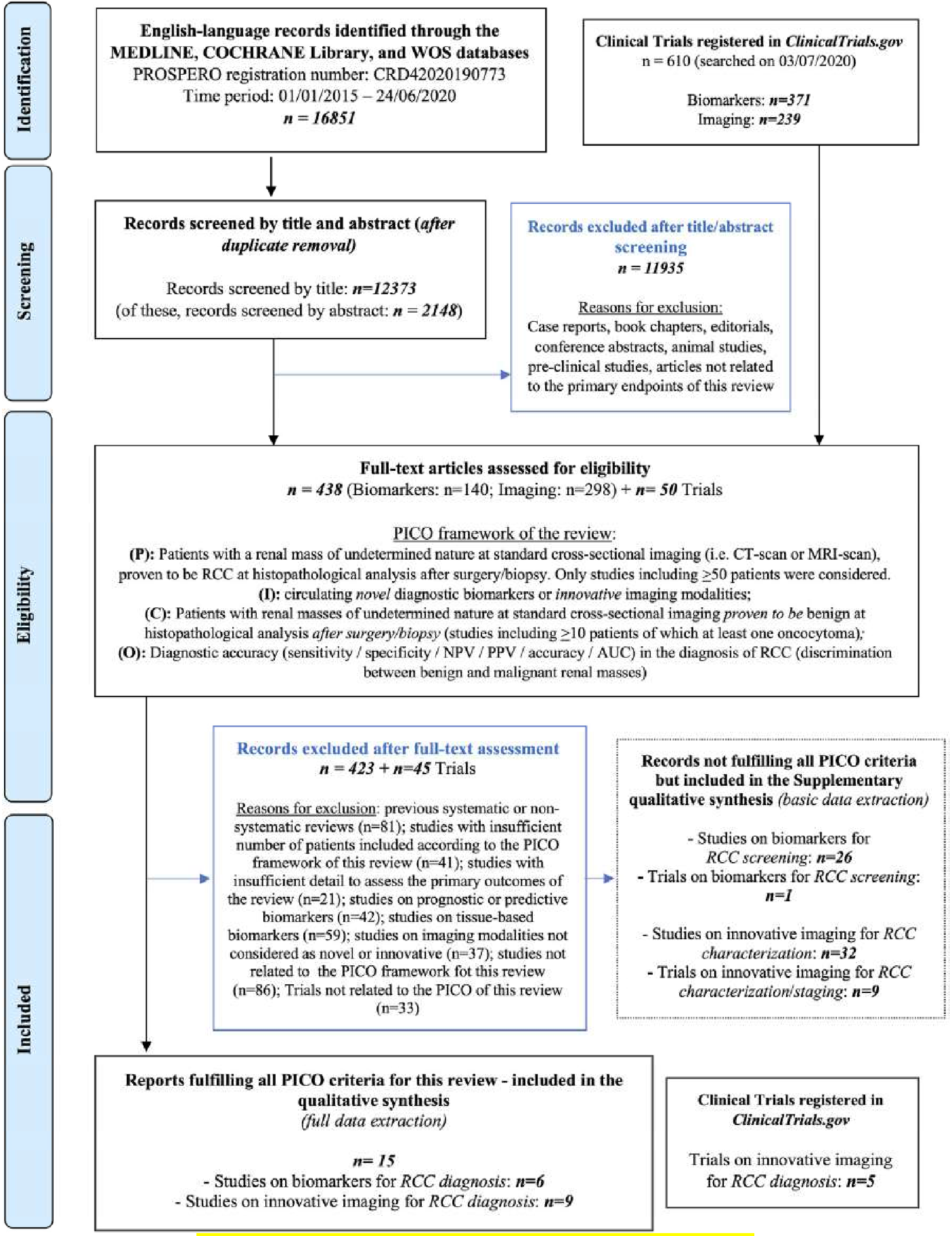

**English-language records identified through the MEDLINE, COCHRANE Library, and WOS databases**
PROSPERO registration number: CRD42020190773
Time period: 01/01/2015 – 24/06/2020
***n = 16851***

**Clinical Trials registered in *ClinicalTrials.gov***
n = 610 (searched on 03/07/2020)

Biomarkers: ***n=371***
Imaging: ***n=239***

**Records screened by title and abstract (*after duplicate removal*)**

Records screened by title: ***n=12373***
(of these, records screened by abstract: ***n = 2148***)

**Records excluded after title/abstract screening**
***n = 11935***

Reasons for exclusion:
Case reports, book chapters, editorials, conference abstracts, animal studies, pre-clinical studies, articles not related to the primary endpoints of this review

**Full-text articles assessed for eligibility**
***n = 438*** (Biomarkers: n=140; Imaging: n=298) + ***n= 50*** Trials

PICO framework of the review:
**(P):** Patients with a renal mass of undetermined nature at standard cross-sectional imaging (i.e. CT-scan or MRI-scan), proven to be RCC at histopathological analysis after surgery/biopsy. Only studies including ≥50 patients were considered.
**(I):** circulating *novel* diagnostic biomarkers or *innovative* imaging modalities;
**(C):** Patients with renal masses of undetermined nature at standard cross-sectional imaging *proven to be* benign at histopathological analysis *after surgery/biopsy* (studies including ≥10 patients of which at least one oncocytoma);
**(O):** Diagnostic accuracy (sensitivity / specificity / NPV / PPV / accuracy / AUC) in the diagnosis of RCC (discrimination between benign and malignant renal masses)

**Records excluded after full-text assessment**
***n = 423 + n=45*** Trials

Reasons for exclusion: previous systematic or non-systematic reviews (n=81); studies with insufficient number of patients included according to the PICO framework of this review (n=41); studies with insufficient detail to assess the primary outcomes of the review (n=21); studies on prognostic or predictive biomarkers (n=42); studies on tissue-based biomarkers (n=59); studies on imaging modalities not considered as novel or innovative (n=37); studies not related to the PICO framework fot this review (n=86); Trials not related to the PICO of this review (n=33)

**Records not fulfilling all PICO criteria but included in the Supplementary qualitative synthesis** *(basic data extraction)*

- Studies on biomarkers for *RCC screening*: ***n=26***
- Trials on biomarkers for *RCC screening*: ***n=1***

- Studies on innovative imaging for *RCC characterization*: ***n=32***
- Trials on innovative imaging for *RCC characterization/staging*: ***n=9***

**Reports fulfilling all PICO criteria for this review - included in the qualitative synthesis**
*(full data extraction)*

***n= 15***
- Studies on biomarkers for *RCC diagnosis*: ***n=6***
- Studies on innovative imaging for *RCC diagnosis*: ***n=9***

**Clinical Trials registered in *ClinicalTrials.gov***

Trials on innovative imaging for *RCC diagnosis*: ***n=5***

Flowchart showing the main steps of the review process

**WOS = World of Science;**
**RCC = renal cell carcinoma; CT = computed tomography; MRI = magnetic resonance imaging; NPV = negative predictive value;PPV = positive predictive value; AUC = area under the receiver operating characteristic curve**

12

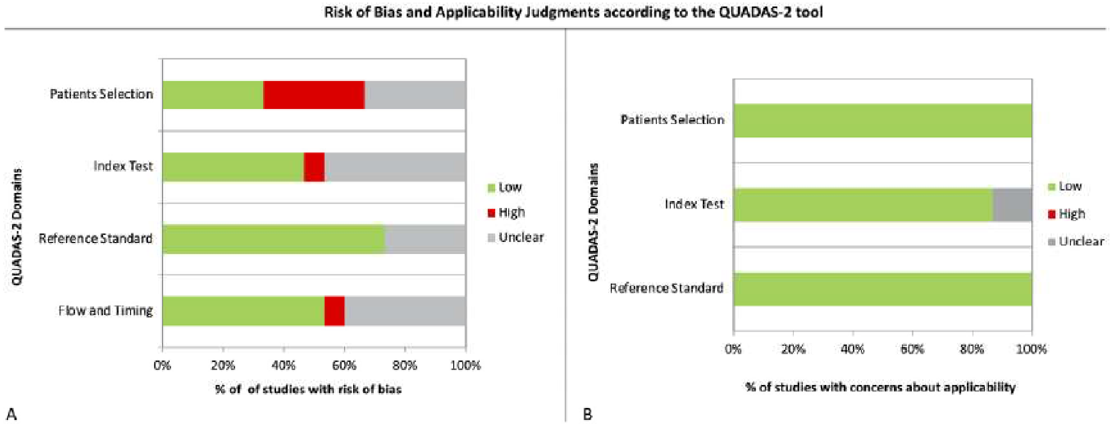

**Graphical overview of the overall risk of bias and applicability judgements for the 15 studies included in the review**

QualityAssessment of Diagnostic Accuracy Studies (QUADAS) 2 tool

16

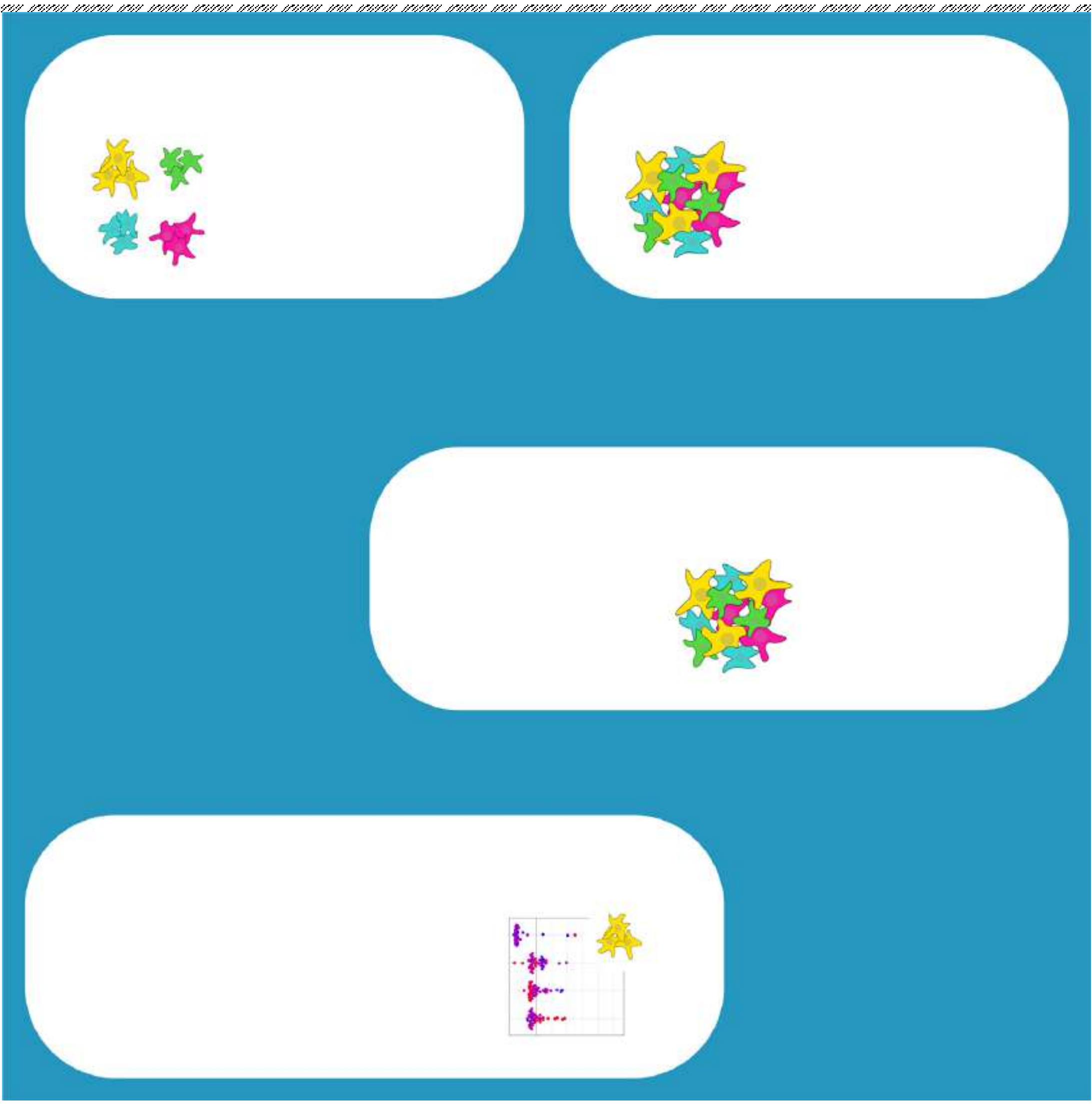

x

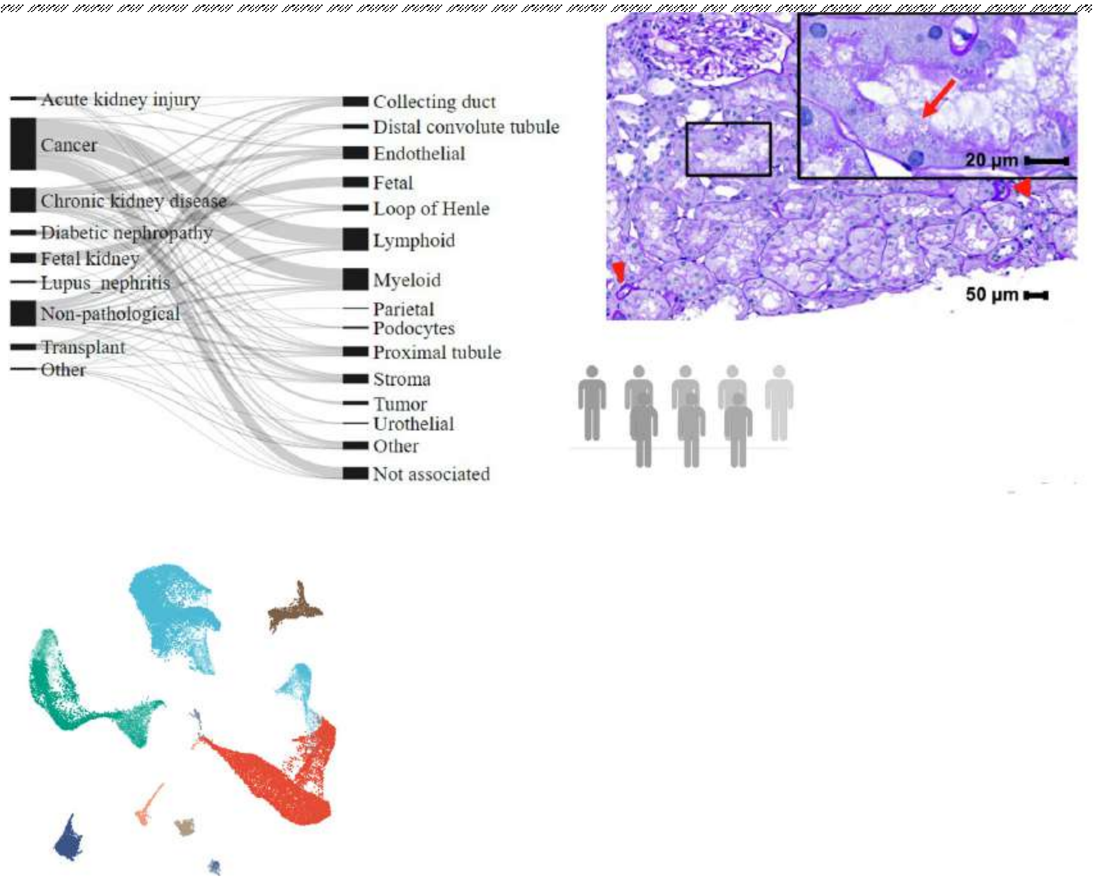
Acute kidney injury
Cancer
Chronic kidney disease
Diabetic nephropathy
Fetal kidney
Lupus_nephritis
Non-pathological
Transplant
Other
Collecting duct
Distal convolute tubule
Endothelial
Fetal
Loop of Henle
Lymphoid
Myeloid
Parietal
Podocytes
Proximal tubule
Stroma
Tumor
Urothelial
Other
Not associated
20 µm
50 µm

**Atlas of human transcriptional profiles of kidney cells**

- ✓ (A ) Overview of the atlas composition.
- ✓ (B ) Histopathology of a representative renal cortical area showing diffuse acute tubular lesions characterized by nonisometric sloughing of tubular epithelial cells
- ✓ and brush border loss (boxed area). Sparse foci of atrophic tubules are noted (red arrows heads). Red arrow indicates complete loss of the brush border. Periodic
- ✓ Acid-Schiff stain.
- ✓ (C ) Schematic of the data integration strategy.
- ✓ (D ) Uniform manifold approximation and projection (UMAP) representation of the 13 cell types identified by unsupervised clustering of the whole dataset.
- ✓ (E )Dotplot of cell cluster marker genes identified in AKI and control samples (dot size indicates the percentage of positive cells and color indicated relative
- ✓ expression).
- ✓ (F ) Relative abundance of major cell types in each sample.
- ✓ (G ) Relative abundance of major cell types in individuals with AKI and controls (mean with bootstraped confidence interval).
- ✓ (H ) Absolute and relative numbers of differentially expressed genes upregulated and downregulated in AKI versus controls within major kidney cell types.
- ✓ (I ) Principal component analysis of all study individuals using pseudobulk data per individual from all proximal tubule (PT) cells

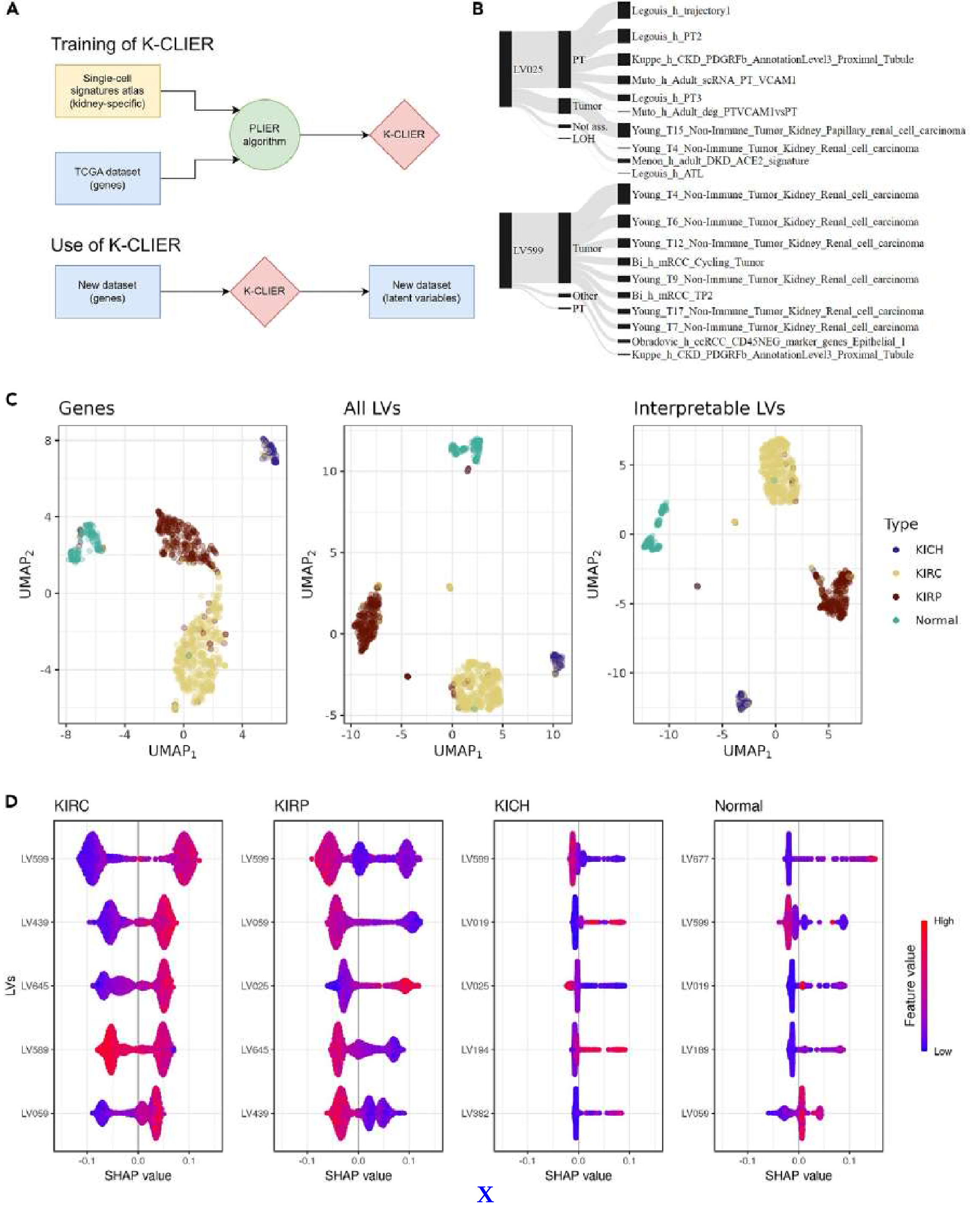

X

- A ) Schematic representation of K-CLIER framework.
- (B ) Association between latent variable (LV), cell type and single-cell signature for two relevant LVs.
- (C ) Graphical two-dimensional representation of the original KIPAN gene expression dataset (31k genes), the dataset obtained by applying K-CLIER to it (700 LVs), and a subset of this latter containing interpretable LVs (96). UMAP was applied to all datasets.
- Samples are colored according to their histological type.

- (D ) Most characterizing LVs for the different histological types in KIPAN dataset. Characterization is provided by training a model for prediction of the histological type and extracting Shapley values (the five most relevant LVs are shown).
- For each histological type, LVs with a positive impact on the target show positive Shapley values for higher-value of the LV (in red), e.g., LV599 for KIRC, whereas LVs with a negative impact show positive Shapley values for lower-value of the LV (in blue), e.g., LV599 for KIRP.

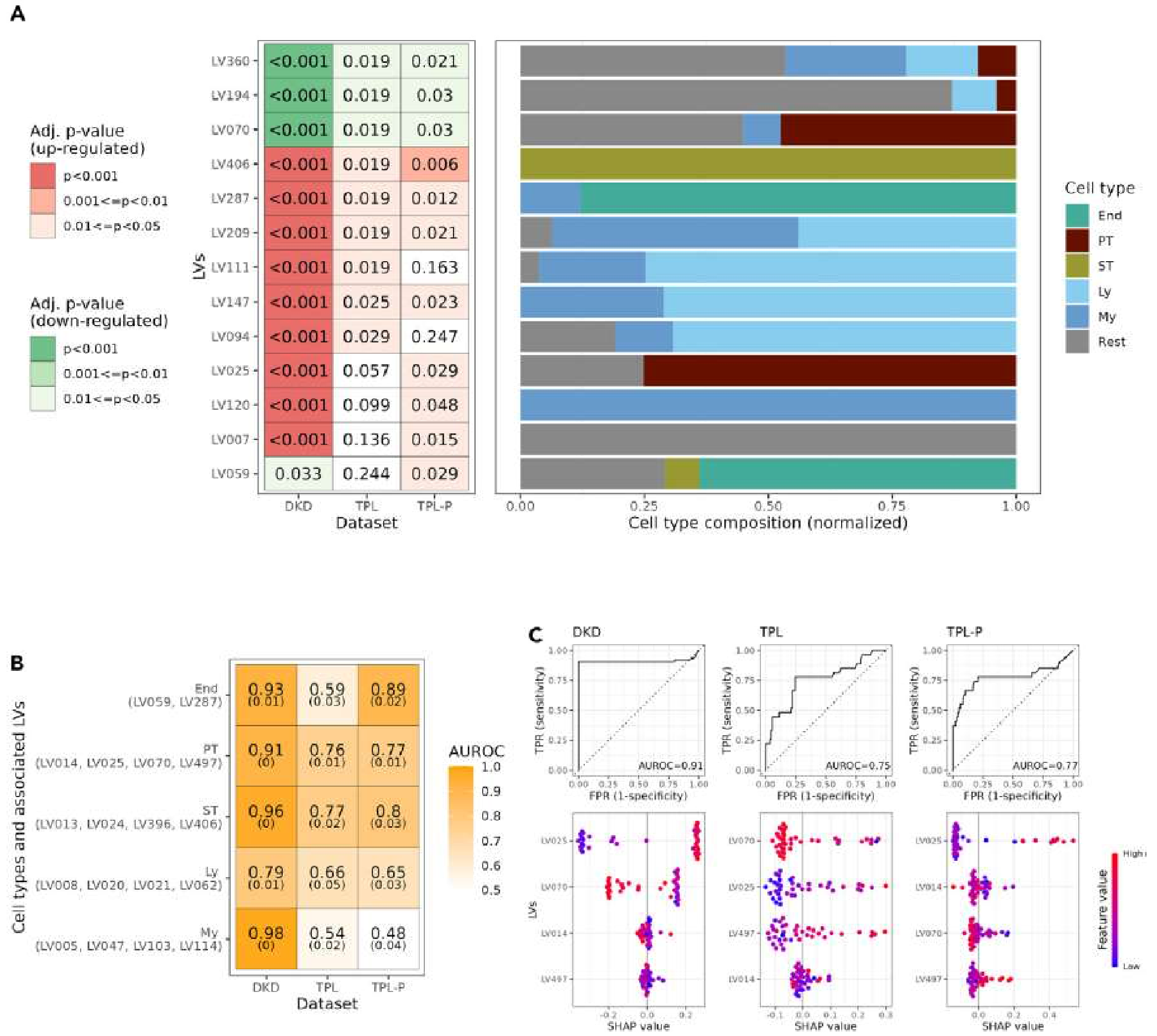

## K-CLIER for studying CKD

- (A ) Most significant interpretable LVs for distinguishing patients with and without CKD in DKD, TPL and TPL-P cohorts. The set of LVs with adjusted p value <0.05 both in the DKD and in at least one of the TPL cohorts is shown. Hypothesis tests were limited to interpretable LVs.
- End, endothelial; PT, proximal tubule; ST, stroma; Ly, lymphoid; My, Myeloid; Rest includes all other cell types (tumor, loop of Henle, distal convolute tubule collecting duct, podocytes, urothelial, fetal, parietal, not associated, other).
- (B ) CKD predictive power of cell-type-specific sets of LVs. For each cell type, its 4 (if present) most associated LVs are extracted. These are used to train models for prediction of

CKD in the DKD, TPL and TPL-P case (in 10-fold 10-repetition cross-validation). AUROCs of such models and their standard deviations are shown.

✓ (C ) Focus on the models to predict CKD in DKD, TPL, and TPL-P cohorts using PT LVs. In the upper panel, ROC curves from models trained in cross validation; inthe lower panel, Shapley values from models trained on the entire datasets

17

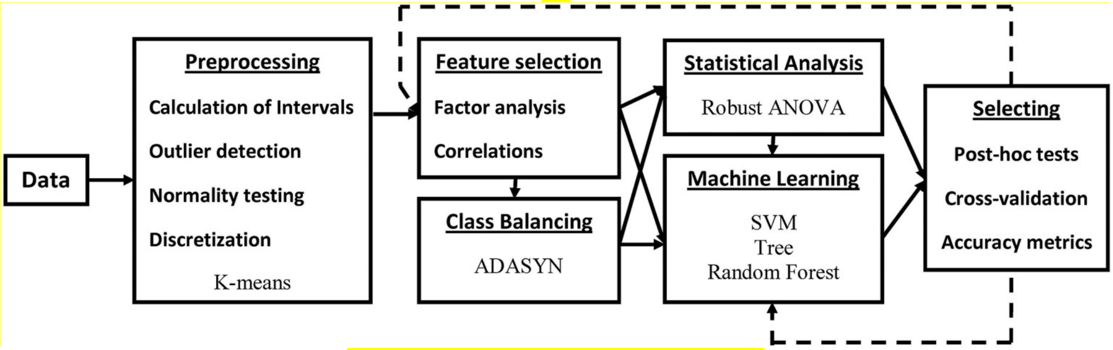
Data
Preprocessing
Calculation of Intervals
Outlier detection
Normality testing
Discretization
K-means
Feature selection
Factor analysis
Correlations
Class Balancing
ADASYN
Statistical Analysis
Robust ANOVA
Machine Learning
SVM
Tree
Random Forest
Selecting
Post-hoc tests
Cross-validation
Accuracy metrics

**Overview of the analytics protocol**

17

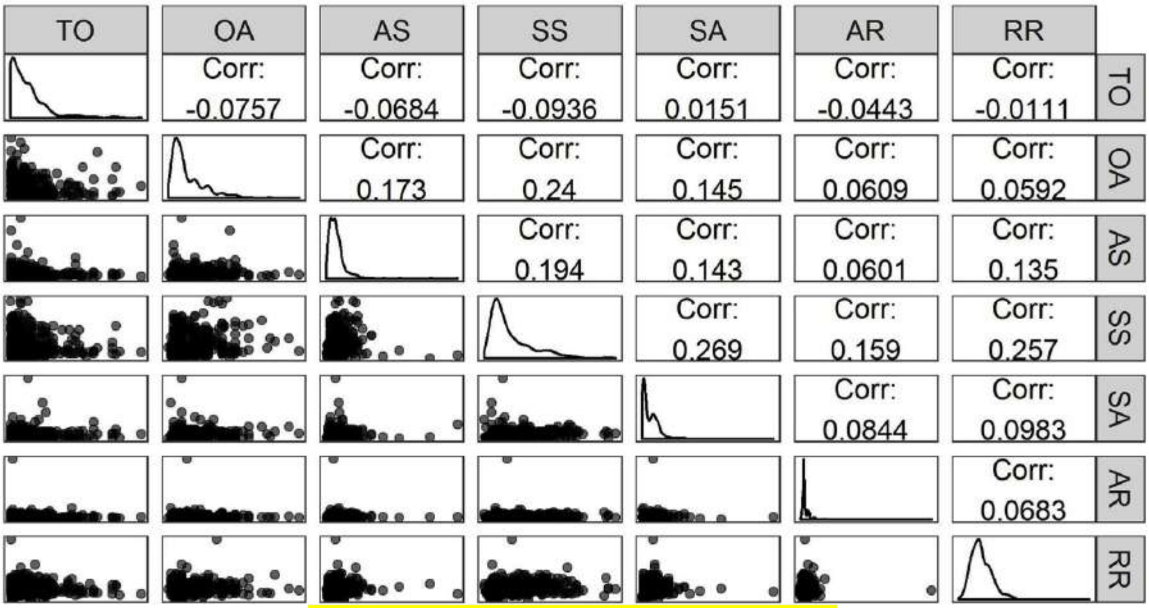

**Scatter plot matrix of duration components**

TO: arrival at the theater to entering to theoperating room,
OA: entering to the operatingroom to the start of anesthesia,
AS: start of anesthesia induction to the start ofsurgical incision,
SS: the beginning to theend of surgery,
SA: end of surgery to the end of anesthesia,
AR: end of anesthesiato entering to the recovery room,
RR: beginning to the end of recovery.

17

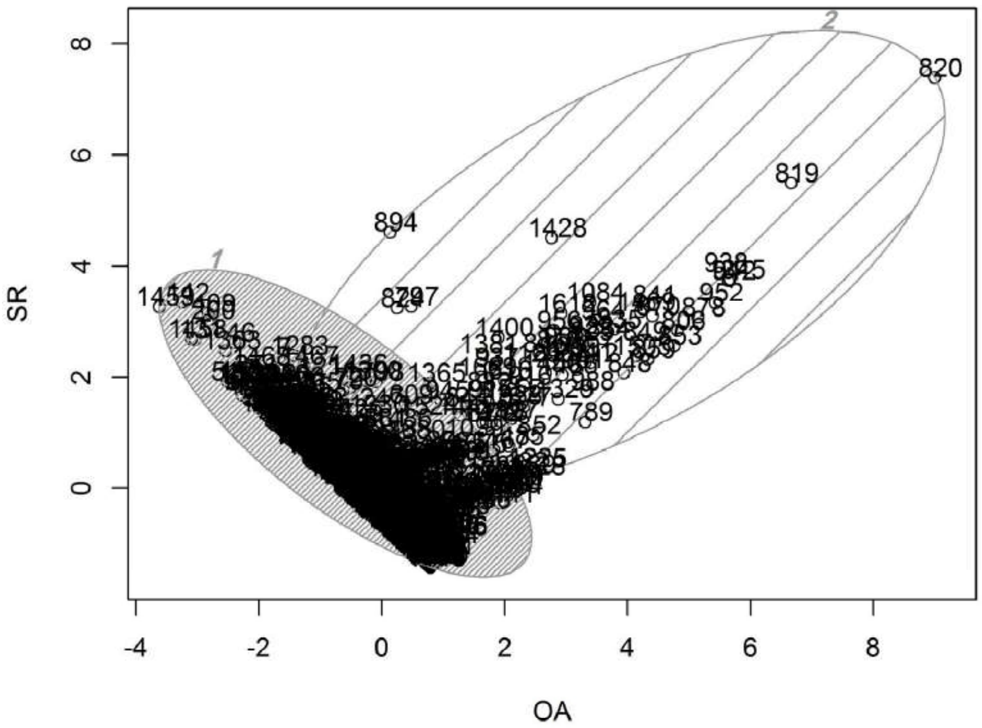

**K-Means Clusters of OA and SR**
**OA: entering the operating room to the start of anesthesia,**
**SR: time from the beginning of surgery to the end of the recovery**

17

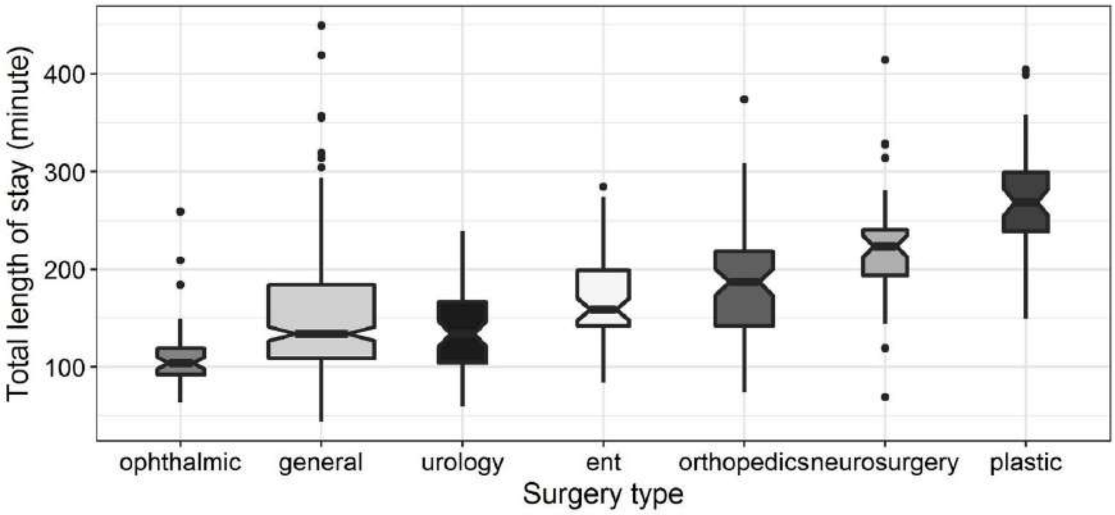

**Total length of stay based on surgical categories (box widths are proportional to the sample sizes**

17

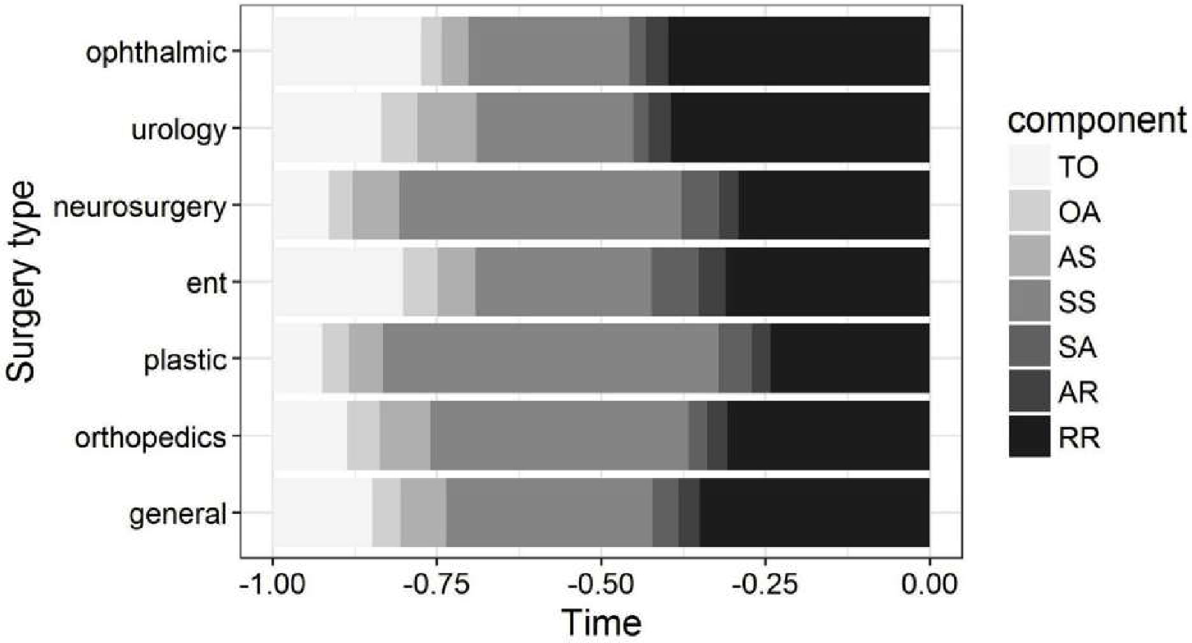

**Percent stack bars for the components of time interval spent in different surgery types**

TO: arrival at the theater to entering to the operatingroom,
OA: entering to the operating room tothe start of anesthesia,
AS: start of anesthesiainduction to the start of surgical incision,
SS: beginning to the end of surgery,
SA: end ofsurgery to the end of anesthesia,
AR: end ofanesthesia to entering to the recovery room,
RR: beginning to the end of recovery

## *Robotic console*

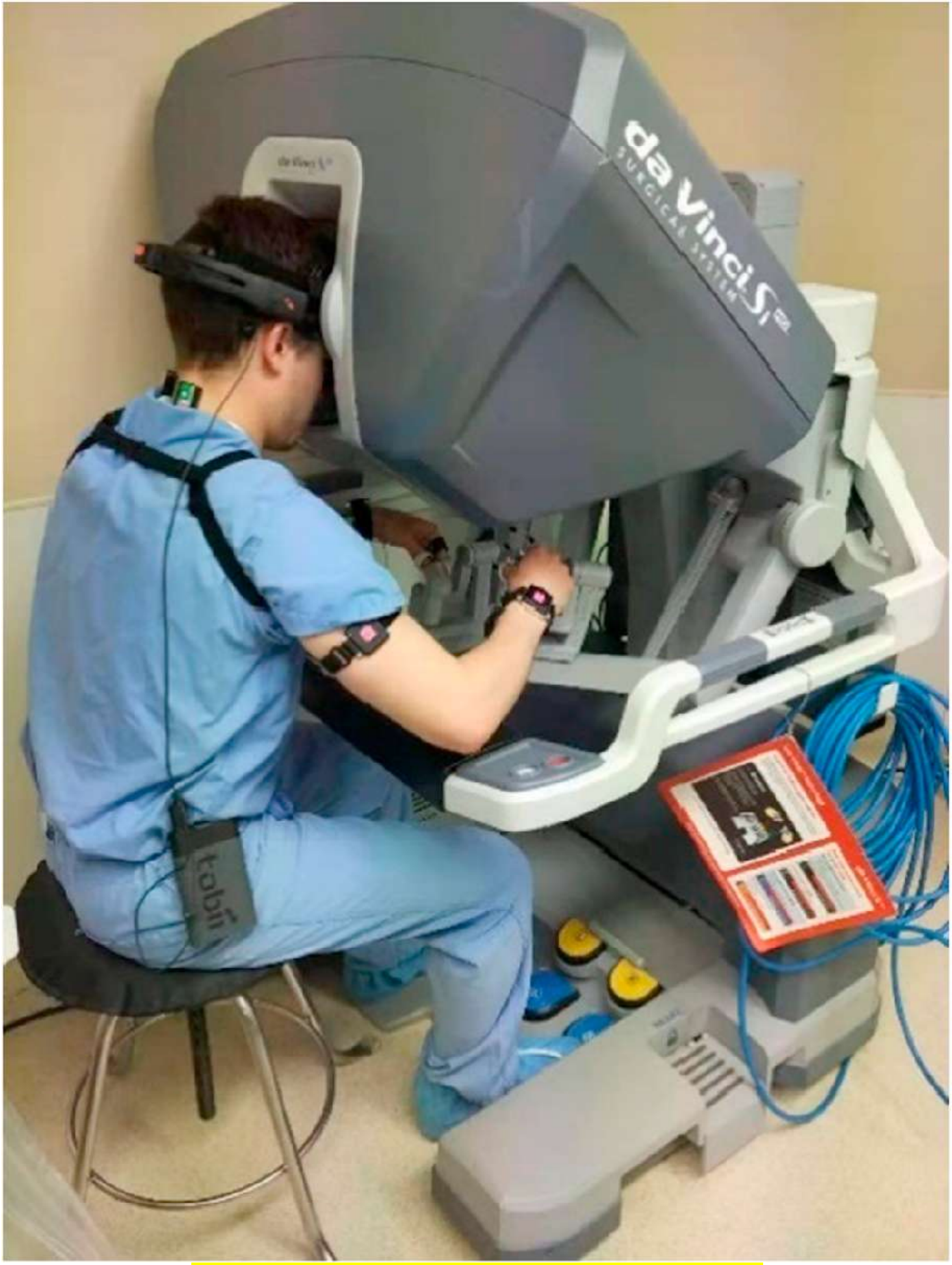
da Vinci Si
SURGICAL SYSTEM
tobii

**Participant performing tasks through the robotic console.**

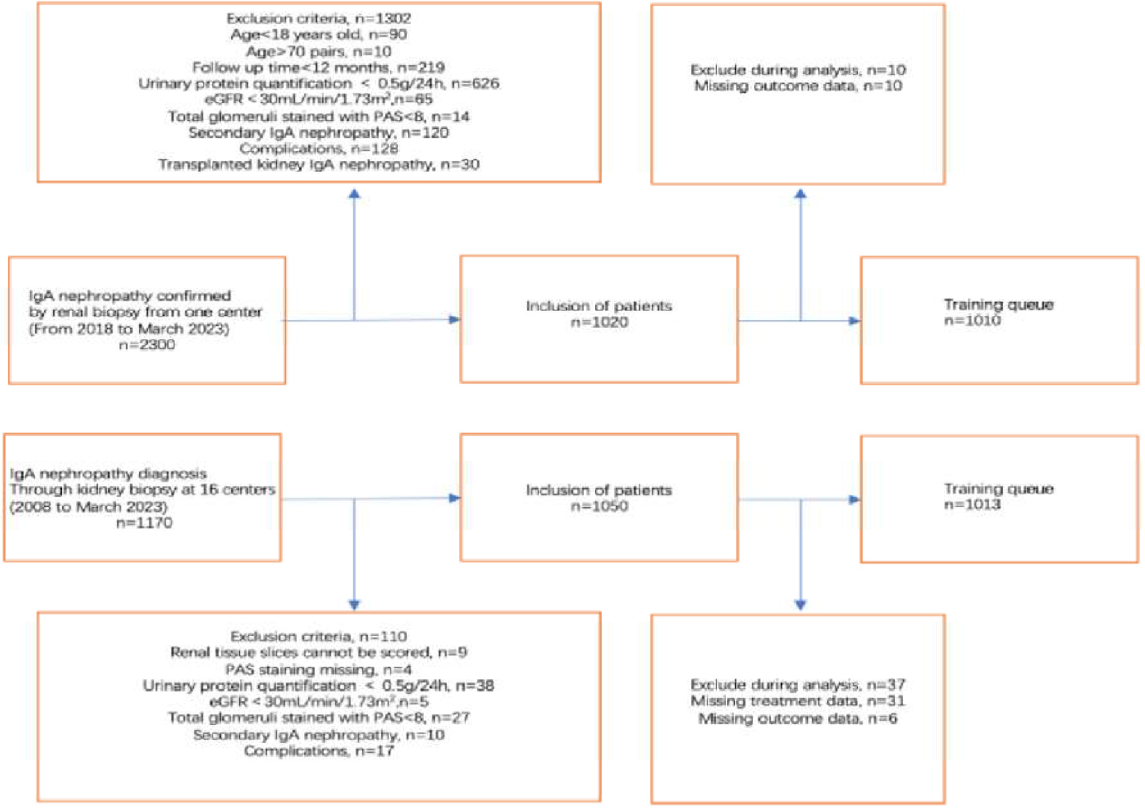
Exclusion criteria, n=1302
Age<18 years old, n=90
Age>70 pairs, n=10
Follow up time<12 months, n=219
Urinary protein quantification < 0.5g/24h, n=626
eGFR < 30mL/min/1.73m², n=65
Total glomeruli stained with PAS<8, n=14
Secondary IgA nephropathy, n=120
Complications, n=128
Transplanted kidney IgA nephropathy, n=30
Exclude during analysis, n=10
Missing outcome data, n=10
IgA nephropathy confirmed by renal biopsy from one center (From 2018 to March 2023) n=2300
Inclusion of patients n=1020
Training queue n=1010
IgA nephropathy diagnosis Through kidney biopsy at 16 centers (2008 to March 2023) n=1170
Inclusion of patients n=1050
Training queue n=1013
Exclusion criteria, n=110
Renal tissue slices cannot be scored, n=9
PAS staining missing, n=4
Urinary protein quantification < 0.5g/24h, n=38
eGFR < 30mL/min/1.73m², n=5
Total glomeruli stained with PAS<8, n=27
Secondary IgA nephropathy, n=10
Complications, n=17
Exclude during analysis, n=37
Missing treatment data, n=31
Missing outcome data, n=6

**Patient enrollment in training and validation queues**

# CNNs
# VGG16

22

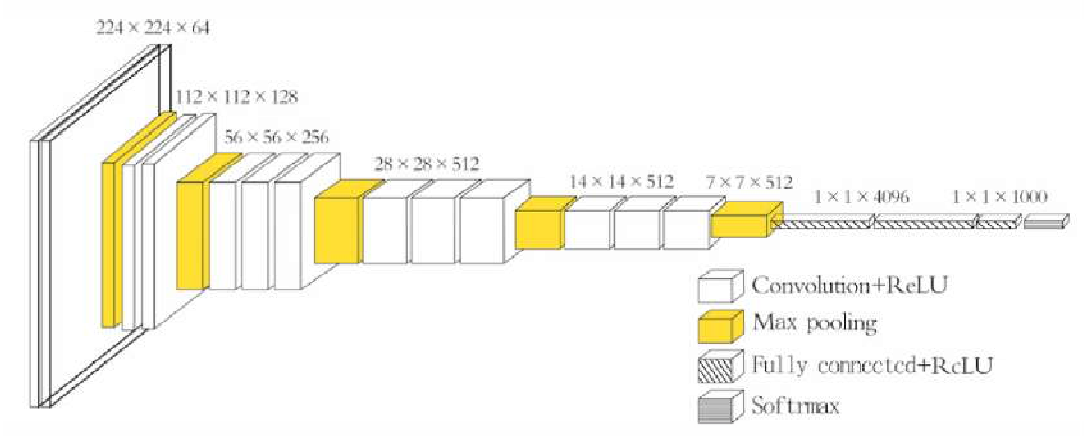
224 × 224 × 64
112 × 112 × 128
56 × 56 × 256
28 × 28 × 512
14 × 14 × 512
7 × 7 × 512
1 × 1 × 4096
1 × 1 × 1000
Convolution+ReLU
Max pooling
Fully connected+ReLU
Softmax

**VGG16 network structure**

22

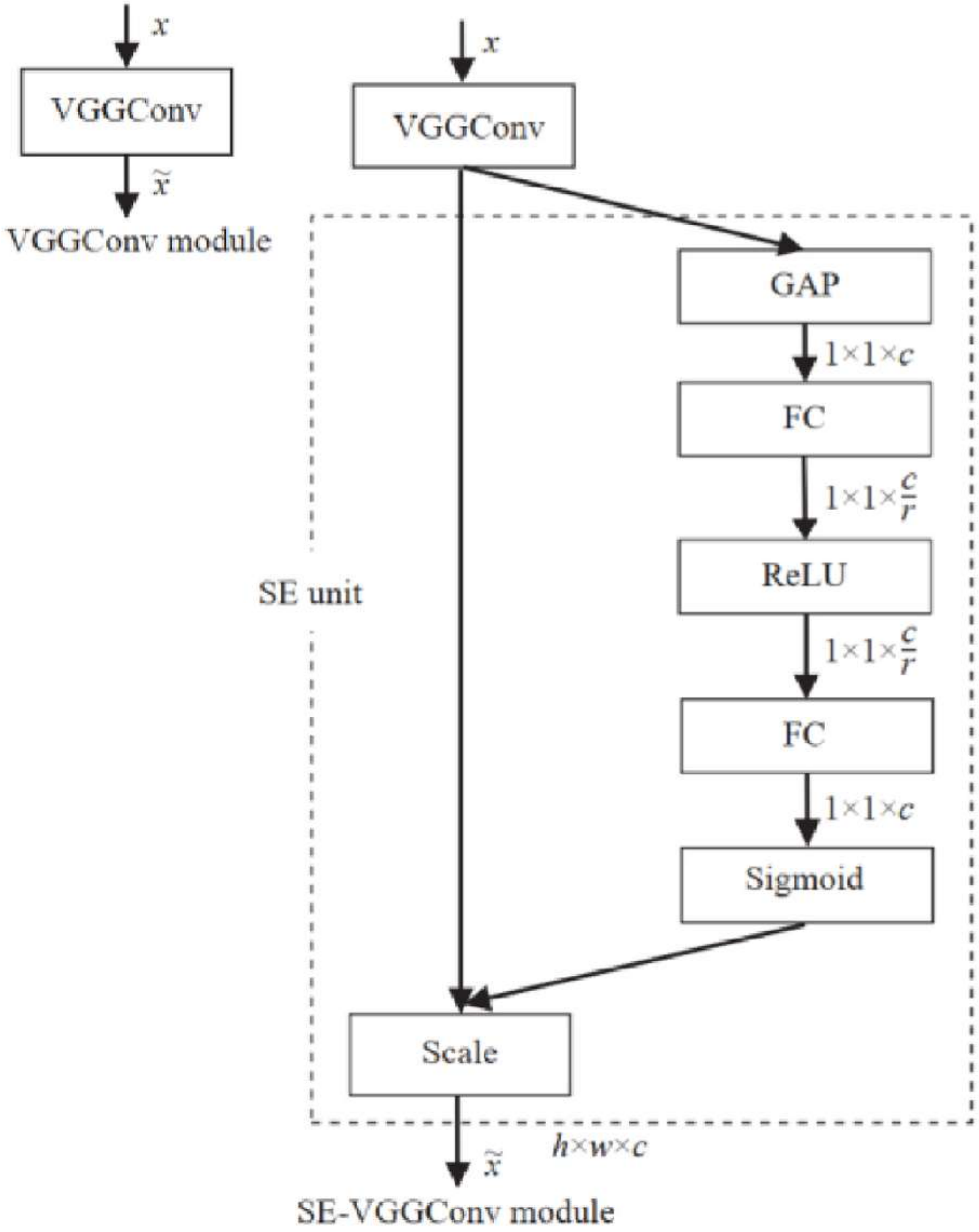
x
VGGConv
$\tilde{x}$
VGGConv module
x
VGGConv
GAP
1×1×c
FC
$1\times1\times\frac{c}{r}$
ReLU
$1\times1\times\frac{c}{r}$
FC
1×1×c
Sigmoid
SE unit
Scale
h×w×c
$\tilde{x}$
SE-VGGConv module

X

# Nephropathy

22

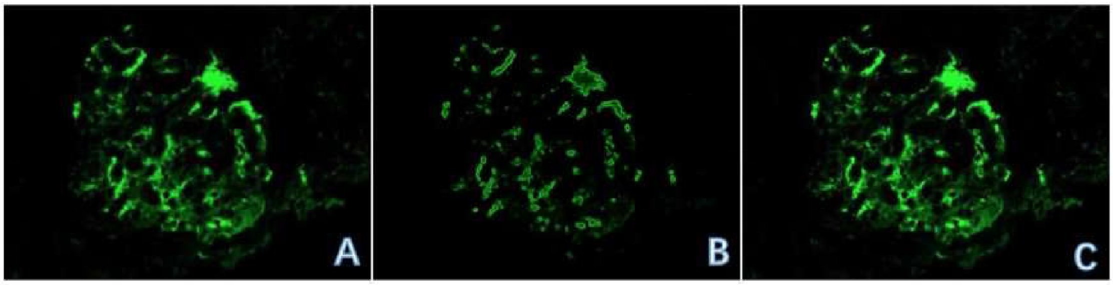

- ✓ (A ) shows the image of a medical cell sample of IgA nephropathy disease observed under a microscope (X200);
- ✓ (B ) is the result (x200) of the sample image segmentation of the fluorescence deposition area using computer Python data analysis and machine learning software;
- ✓ (C ) represents the shape extraction results of fluorescence deposition areas using computer Python data analysis and machine learning software (X200).

35

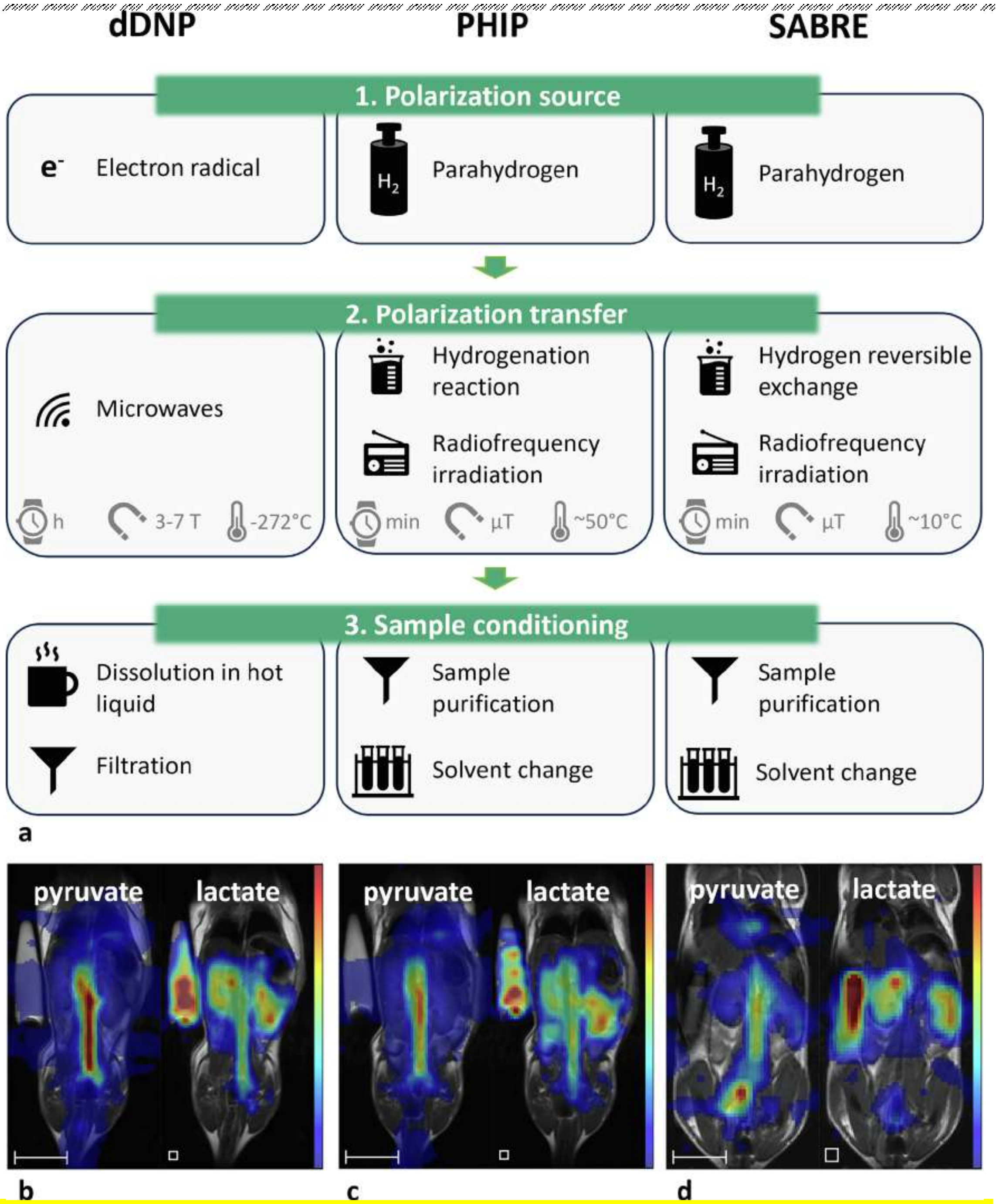
dDNP
PHIP
SABRE
1. Polarization source
e⁻ Electron radical
H2 Parahydrogen
H2 Parahydrogen
2. Polarization transfer
Microwaves
h
3-7 T
-272°C
Hydrogenation reaction
Radiofrequency irradiation
min
µT
~50°C
Hydrogen reversible exchange
Radiofrequency irradiation
min
µT
~10°C
3. Sample conditioning
Dissolution in hot liquid
Filtration
Sample purification
Solvent change
Sample purification
Solvent change
a
pyruvate
lactate
pyruvate
lactate
pyruvate
lactate
b
c
d

**13C Hyperpolarization techniques and examples of preclinical studies with hyperpolarized [1-13C] pyruvate in mice**

- ✓ (a ) Simplified schematic overview of dDNP, PHIP and SABRE hyperpolarization highlighting the most important steps in the polarization process. Parameter ranges for the polarization transfer do not indicate the full range of suitable conditions but rather predominantly applied regimes as well as the regimes corresponding to the images shown in b-d.
- ✓ (b )dDNP pyruvate and lactate projection from 3D bSSFP dataset (resolution 1.75 x 1.75 x 1.75 mm3, indicated in the image by a white voxel), 10 repetitions are averaged into the shown images, data reproduced from Nagel et al. [14].

- ✓ (c ) PHIP-SAH pyruvate and lactate projection from 3D bSSFP dataset (resolution 1.75 x 1.75 x 1.75 mm3, indicated in the image by a white voxel), 10 repetitions are averaged into the shown images, data adapted from [14].
- ✓ (d ) SABRE pyruvate and lactate projection from 3D bSSFP dataset (resolution 2.5 x 2.5 x 2.5 mm3, indicated in the image by a white voxel), 14repetitions are averaged into the shown images, data adapted from [15].
- ✓ Scale bars in (b,c,d) represent 10 mm.

# ***Biomarkers***

35

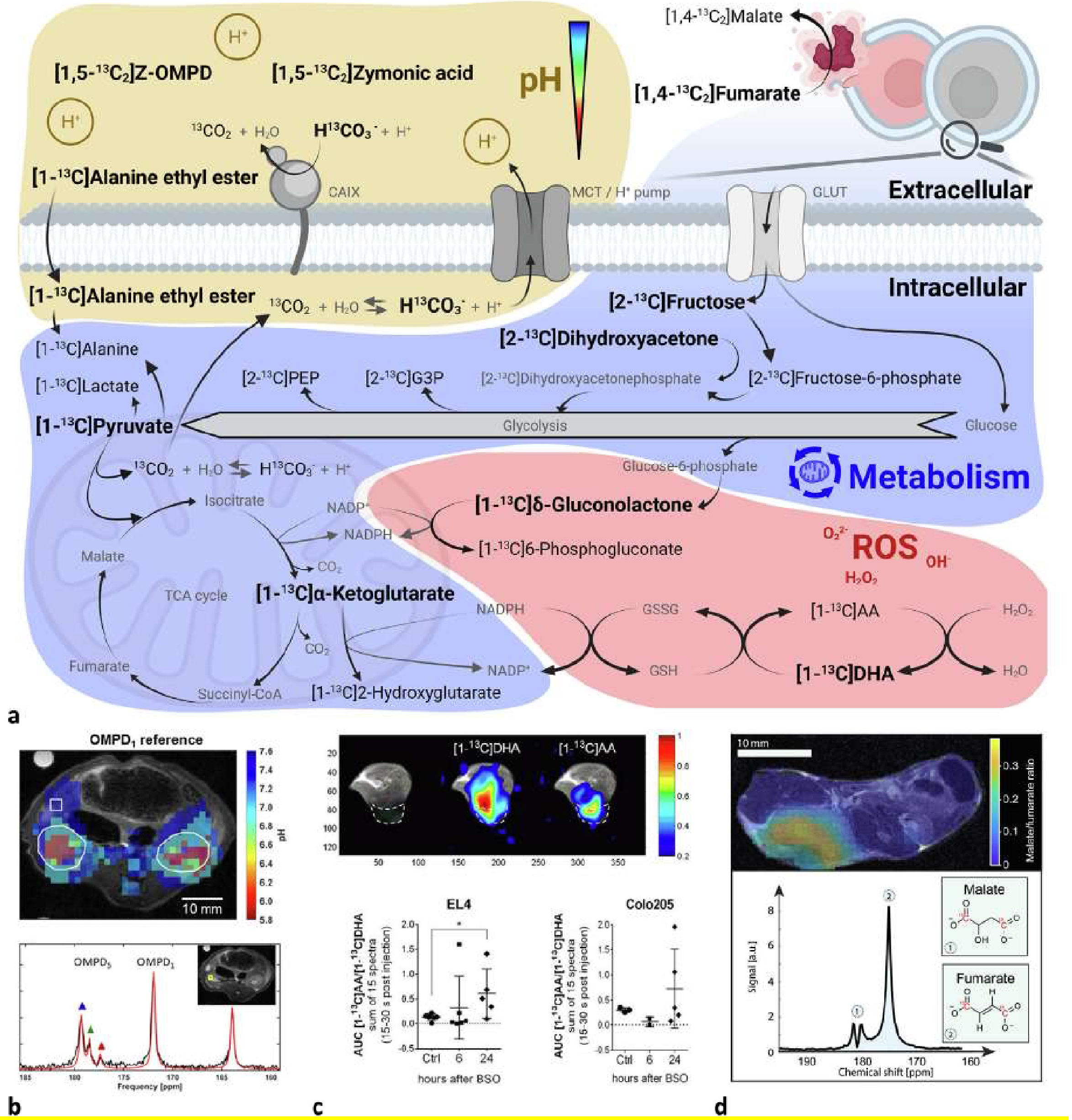
[1,5-13C2]Z-OMPD
[1,5-13C2]Zymonic acid
pH
[1,4-13C2]Malate
[1,4-13C2]Fumarate
13CO2 + H2O
H13CO3- + H+
H+
[1-13C]Alanine ethyl ester
CAIX
MCT / H+ pump
GLUT
Extracellular
Intracellular
[1-13C]Alanine ethyl ester
[2-13C]Fructose
[2-13C]Dihydroxyacetone
[1-13C]Alanine
[1-13C]Lactate
[2-13C]PEP
[2-13C]G3P
[2-13C]Dihydroxyacetonephosphate
[2-13C]Fructose-6-phosphate
[1-13C]Pyruvate
Glycolysis
Glucose
Glucose-6-phosphate
Metabolism
Isocitrate
NADP+
NADPH
[1-13C]δ-Gluconolactone
[1-13C]6-Phosphogluconate
ROS
Malate
CO2
TCA cycle
[1-13C]α-Ketoglutarate
NADPH
GSSG
[1-13C]AA
H2O2
Fumarate
Succinyl-CoA
[1-13C]2-Hydroxyglutarate
NADP+
GSH
[1-13C]DHA
H2O
a
OMPD1 reference
10 mm
OMPD5
OMPD1
Frequency [ppm]
[1-13C]DHA
[1-13C]AA
EL4
Colo205
AUC [1-13C]AA/[1-13C]DHA sum of 15 spectra (15-30 s post injection)
Ctrl
6
24
hours after BSO
10 mm
Malate/fumarate ratio
Signal [a.u.]
Malate
Fumarate
Chemical shift [ppm]
b
c
d

Metabolic biomarkers and enzymatic pathways accessible by hyperpolarized 13C-labeled probes

---

- ✓ (a ) Schematic overview of selected biomarkers in the extra- and intracellular space and related pathways that can be probed in vivo by imaging using hyperpolarized 13C-labeled probes. Substrates highlighted in this review are marked in black and bold and observable products are colored in black and are displayed with smaller font size. Unobservable products or contextual metabolites are colored in gray. 13C-bicarbonate as a substrate rather resides in the xtracellular and cytosolic compartment while 13C-bicarbonate produced from [1-13C]pyruvate originates from the intramitochondrial space.

- ✓ (b ) pH-sensitive probes such as [1,5-13C2]Z-OMPD enable detection of multiple pH compartments (bottom spectra) upon injection in healthy kidneys which correspond to the anatomical regions of cortex, medulla and pelvis (top image). Image adapted with permission from [59].

- ✓ (c ) [1-13C]DHA shows increased reduction to [1-13C]AA in tumors (top images) under oxidative stress, which can be monitored following treatment (bottom cluster plots). Color bar indicates voxel intensity relative to respective maxima. Image adapted with permission from [65].
- ✓ (d ) Conversion of [1,4-13C2]fumarate to [1,4-13C2]malate indicates cell death and related release of the intramitochondrial enzyme fumarase into the extracellular space in fast growing or treated tumors. Image adapted with permission from [75].

- ✓ The schematic graphic in (a) was created with BioRender.com.

  - CAIX: Carbonic anhydrase 9;
  - MCT: Monocarboxylate transporter;
  - GLUT: Glucose transporter;
  - PEP: Phosphoenolpyruvate;
  - G3P: Glyceraldehyde-3-phosphate;
  - TCA: tricaboxylic acid;
  - NADP+/NADPH: Nicotinamide adenine dinucleotide phosphate (oxidized and reduced form respectively);
  - GSSG: Glutathione disulfide;
  - GSH: Glutathione;
  - AA: Ascorbic Acid;
  - Succinyl-CoA: Succinyl-coenzyme A.

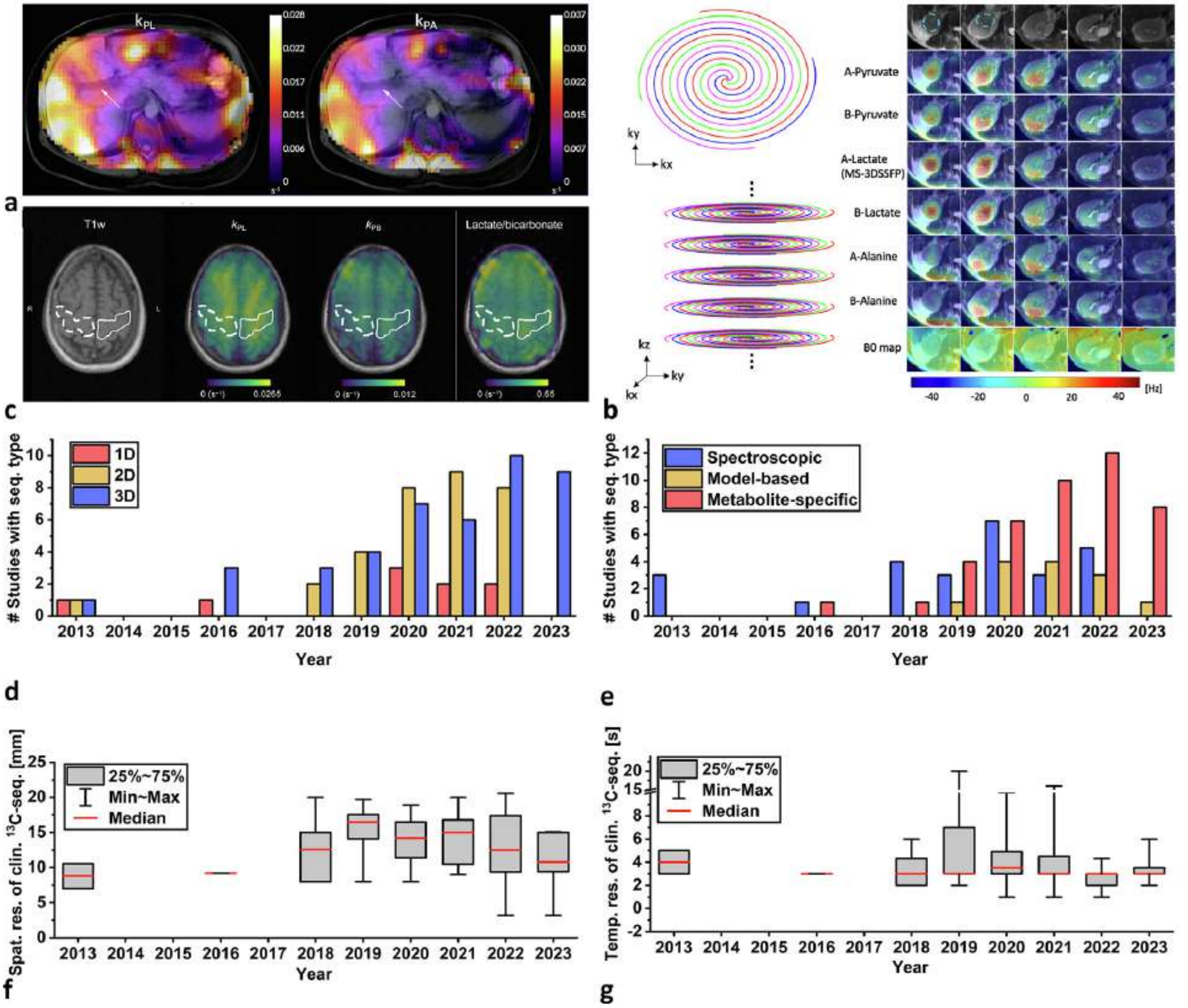

**Sequences, acquisition advances and performance trends in clinical hyperpolarized 13C MRI of [1-13C]pyruvate.**

- ✓ (a ) Three dimensional, whole-abdomen-covering conversion rate mapping in healthy volunteers. Image adapted with permission from [121].
- ✓ (b ) Fast stack of spirals readout trajectory and combination of sequences (gradient echo &bSSFP) that allows fine-tuning and optimization of magnetization usage and acquisition speed for hyperpolarized 13C MRI and e.g. enables sub-millimeter in-plane resolution, here
- ✓ demonstrated in ALS patients (c). Image in (b) and (c) adapted with permission from [128] and [47] respectively.
- ✓ Trend analysis for dimensionality reveals increased availability of 3D volume-covering scans (d) which rely more and more on metabolite-specific acquisition techniques (e).
- ✓ Improvements in more efficient signal usage and faster acquisition techniques are invested in favor of improving the spatial (f) and less so the temporal resolution (g).
- ✓ For trend analysis, hyperpolarized clinical research studies listed in the “Human HP C13
    - o publication list (v2, 15 September 2023) [12] were reviewed. Consecutive multi-slice sequences were classified as “3D” and spatial resolution represents the average spatial resolution in three dimensions. Sequences were considered spectroscopic when explicitly stated or spectra were displayed. Model-based sequences all rely on IDEAL reconstruction and were explicitly stated. Metabolite-specific sequences

encompass spectral-spatial, narrow bandwidth excitation approaches or other techniques explicitly stating this term. One publication could contain more than one acquisition strategy in terms of sequence type, and dimensionality and spatial and temporal resolution

35

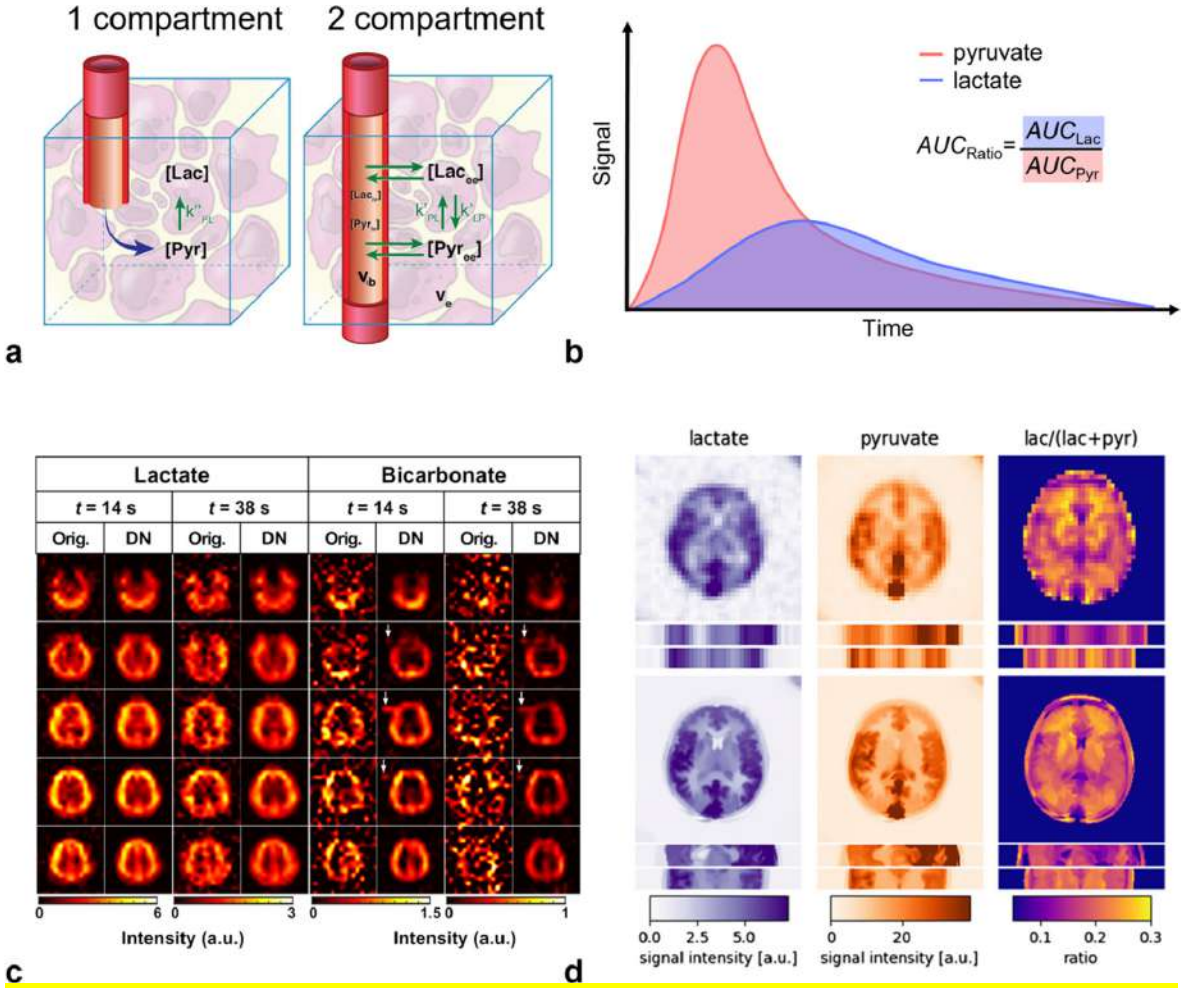
1 compartment
2 compartment
[Lac]
k''PL
[Pyr]
[Lacee]
[Lacb]
[Pyrb]
k'PL
k'LP
[Pyree]
vb
ve
a
Signal
pyruvate
lactate
AUCRatio = AUCLac / AUCPyr
Time
b
Lactate
Bicarbonate
t = 14 s
t = 38 s
t = 14 s
t = 38 s
Orig.
DN
Orig.
DN
Orig.
DN
Orig.
DN
0
6
0
3
0
1.5
0
1
Intensity (a.u.)
Intensity (a.u.)
c
lactate
pyruvate
lac/(lac+pyr)
0.0
2.5
5.0
signal intensity [a.u.]
0
20
signal intensity [a.u.]
0.1
0.2
0.3
ratio
d

**Kinetic models, biomarker and novel trends in analysis of hyperpolarized imaging data using [1-13C]pyruvate**

- ✓ (a ) One compartment model (left) and two compartment model (right), which includes the vascular blood volume fraction vb, the extracellular volume fraction ve, accounting for a vascular compartment and bidirectional conversion.
- ✓ (b ) Typical shape of fitted pyruvate (red) and lactate (purple) signal time curves obtained in a single-voxel. Figure inspired by [163].
- ✓ (c ) Patch-based HOSVD-denoising applied to human metabolic imaging brain data
- ✓ (d ) Human metabolic imaging brain data processed without (top row) and with applied (bottom row) structuralguidance super-resolution approach.

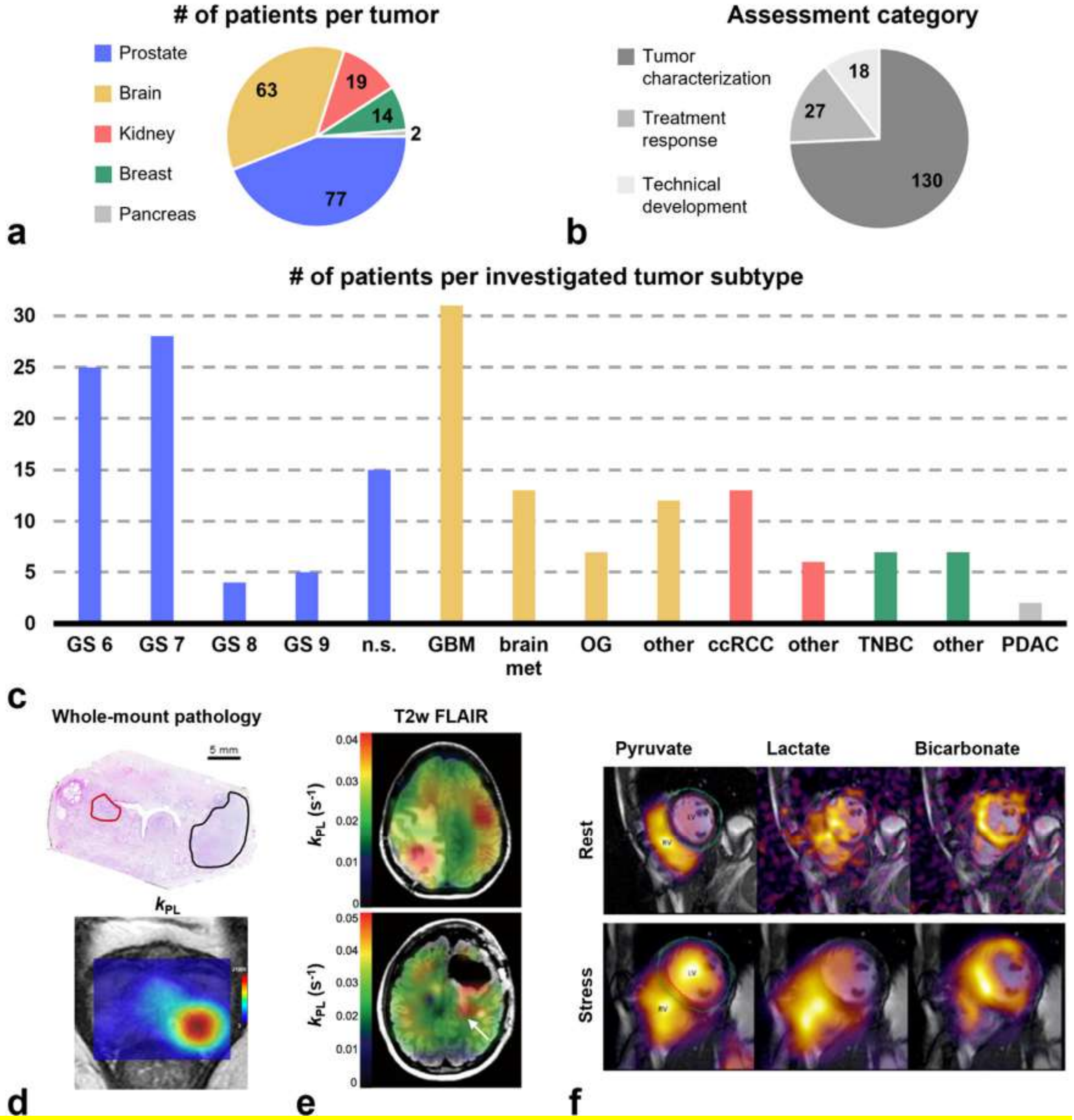

Statistics and exemplary data for clinical studies using hyperpolarized [1-13C]pyruvate MRI

- ✓ (a ) Division of patients into examined tumor organs.
- ✓ (b ) Classification of patient data into three different assessment categories.
- ✓ (c ). Subdivision of patients into examined tumor subtypes.
- ✓ (d )kPL in a prostate lesion is able to distinguish clinically relevant (black) from an indolent (red) lesion.
- ✓ (e )kPL increase (red) in T2w FLAIR enhancing lesions indicates radiological progression in brain
- ✓ tumor patients. Image adapted with permission from [192]. Analyzed data exclusively stems from published studies. The UCSF Department of Radiology & Biomedical Engineering published a summary of human scans worldwide, including non-published studies [227].
- ✓ (f ) Rest/stress test conducted in a healthy human heart.

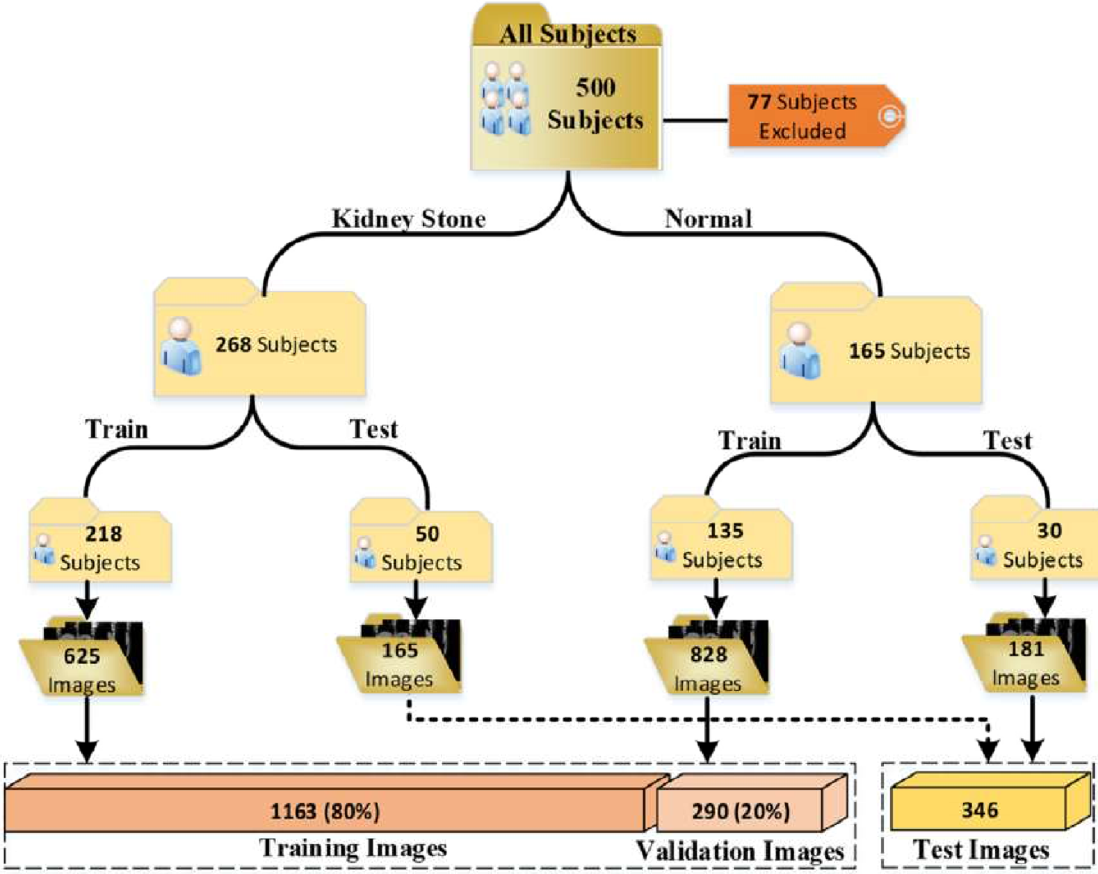
All Subjects
500 Subjects
77 Subjects Excluded
Kidney Stone
Normal
268 Subjects
165 Subjects
Train
Test
Train
Test
218 Subjects
50 Subjects
135 Subjects
30 Subjects
625 Images
165 Images
828 Images
181 Images
1163 (80%)
290 (20%)
346
Training Images
Validation Images
Test Images

Data distributions used for training and testing in this study

36

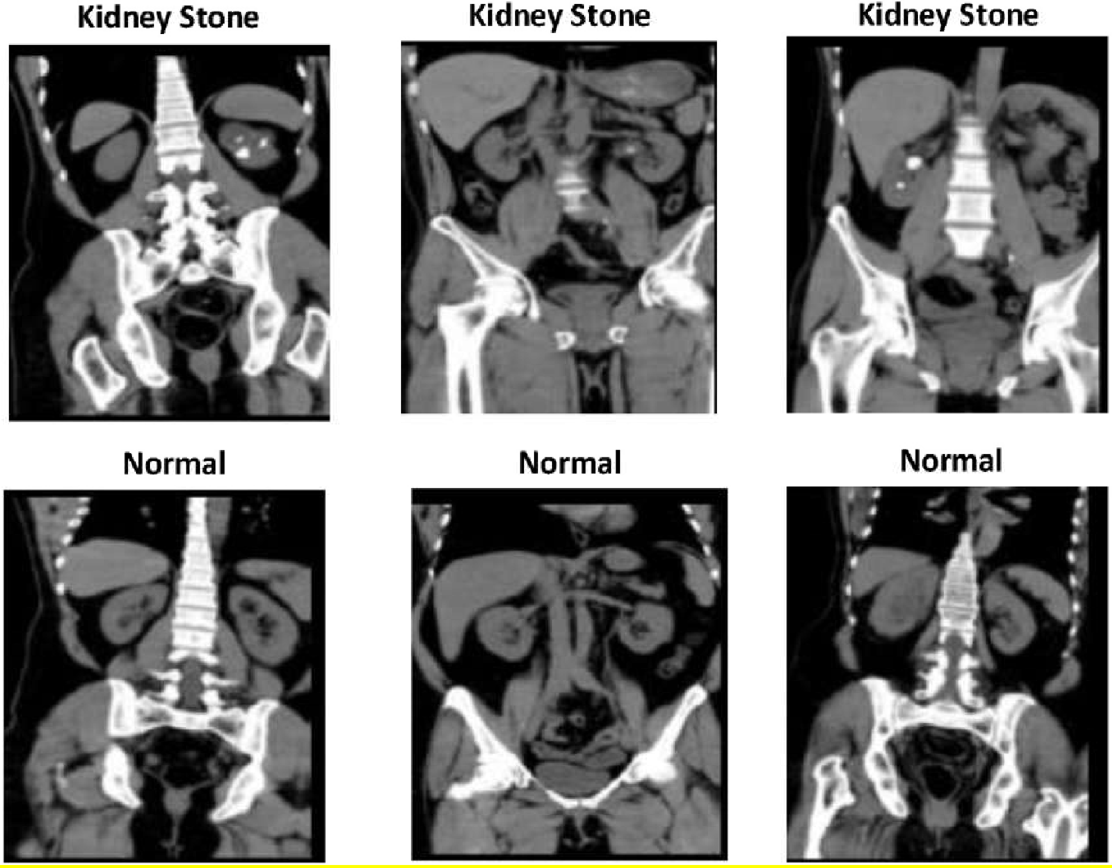
Kidney Stone
Kidney Stone
Kidney Stone
Normal
Normal
Normal

Typical examples of normal and kidney stone CT images obtained using various augmentation techniques

# XResNet-50
# CNN

36

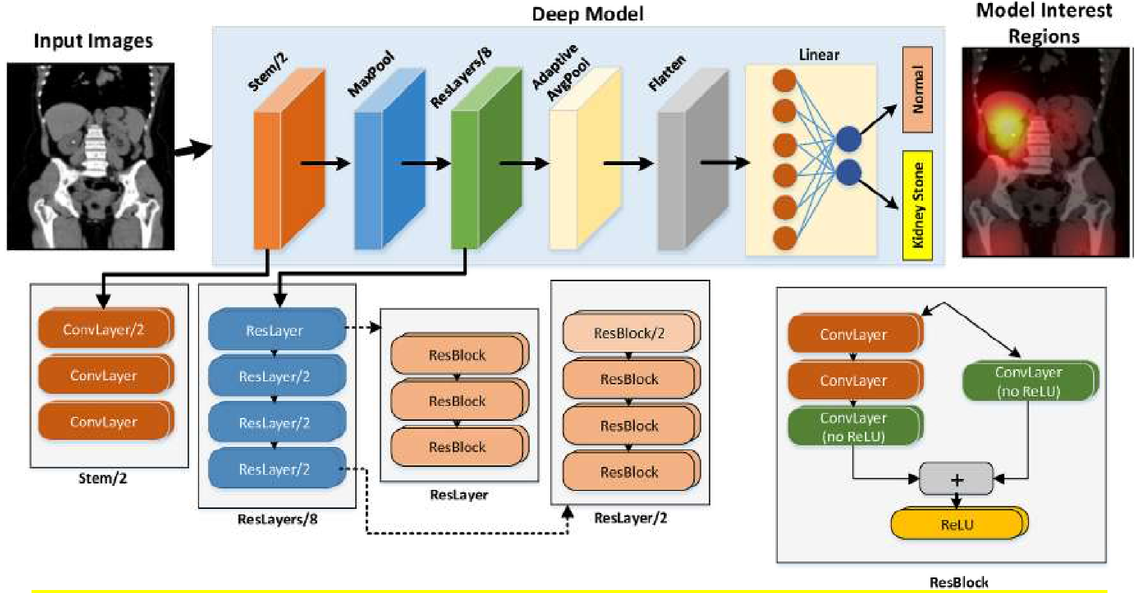
Input Images
Deep Model
Model Interest Regions
Stem/2
MaxPool
ResLayers/8
Adaptive AvgPool
Flatten
Linear
Normal
Kidney Stone
ConvLayer/2
ConvLayer
ConvLayer
Stem/2
ResLayer
ResLayer/2
ResLayer/2
ResLayer/2
ResLayers/8
ResBlock
ResBlock
ResBlock
ResLayer
ResBlock/2
ResBlock
ResBlock
ResBlock
ResLayer/2
ConvLayer
ConvLayer
ConvLayer (no ReLU)
ConvLayer (no ReLU)
+
ReLU
ResBlock

**Block representation showing the layer organization of XResNet-50 deep learning model employed for automated kidney stone detection**

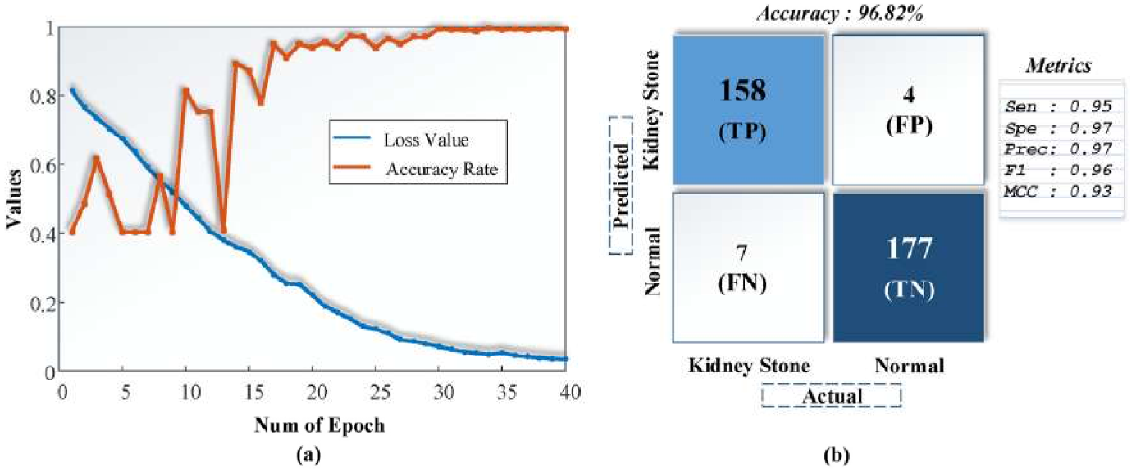

**(A) Graphs of loss values and accuracy rates obtained for various epochs during the training of model,**
**(b) confusion matrix obtained on the test data**

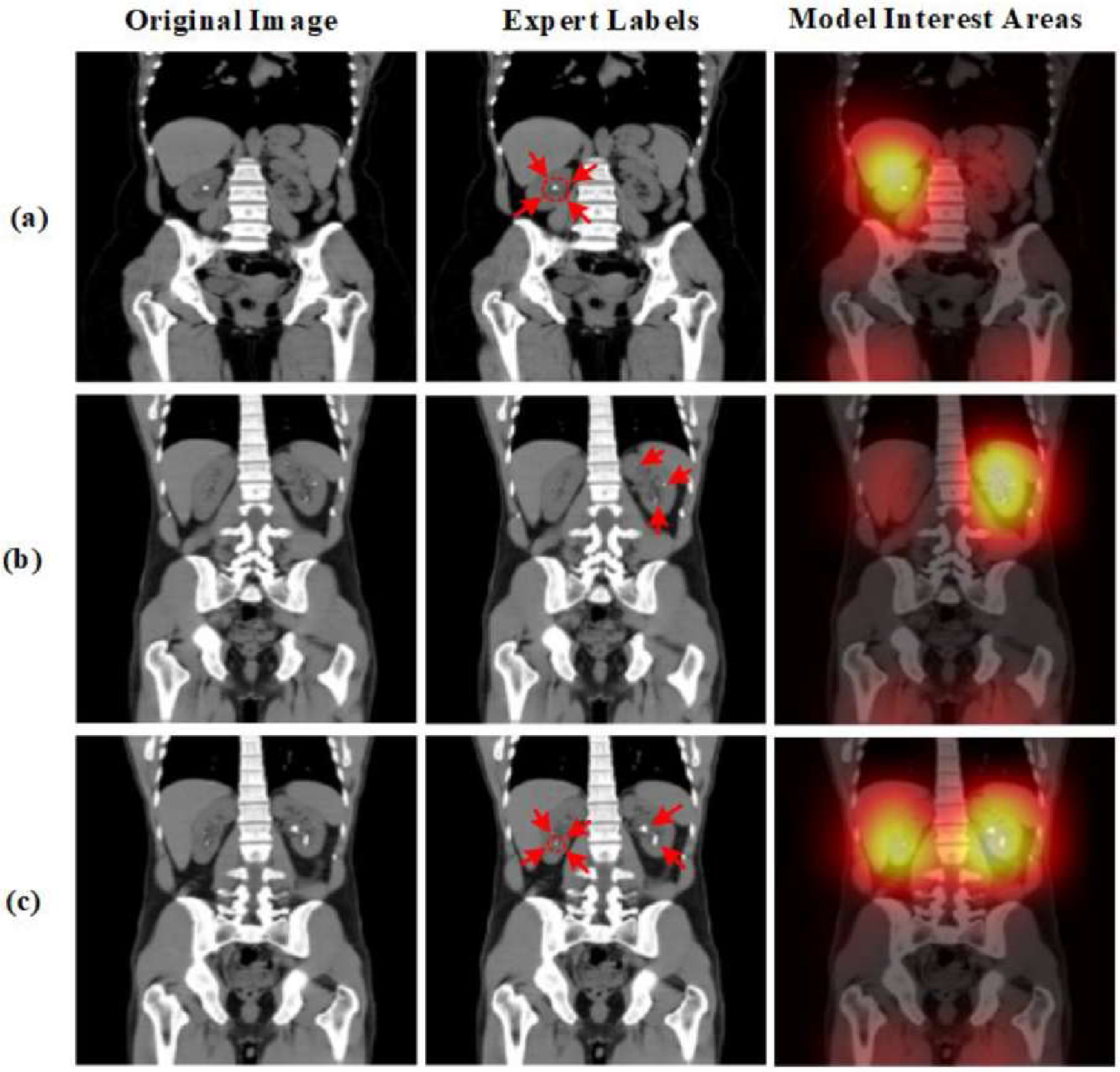
Original Image
Expert Labels
Model Interest Areas
(a)
(b)
(c)

Images misclassified by the model

- ✓ CT images fed as input to the model (left),
- ✓ Interested regions selected by the model for classification (right),
- ✓ Stones marked on the CT image by the experts (red arrows).

**Deep-Lrn-NN**
**CNN**

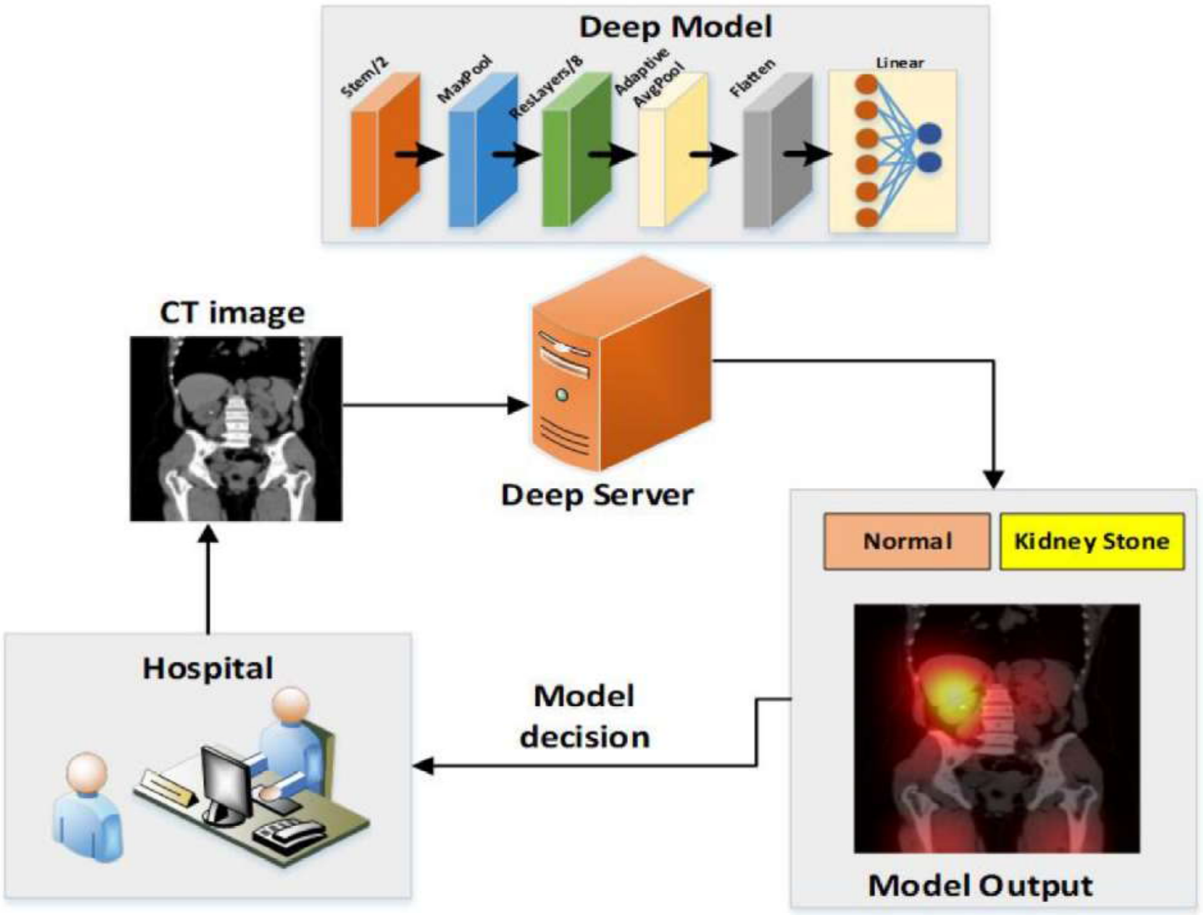
Deep Model
Stem/2
MaxPool
ResLayers/8
Adaptive AvgPool
Flatten
Linear
CT image
Deep Server
Normal
Kidney Stone
Hospital
Model decision
Model Output

Snapshot of the demonstration of deep learning model as an auxiliary tool in healthcare centers

**48**

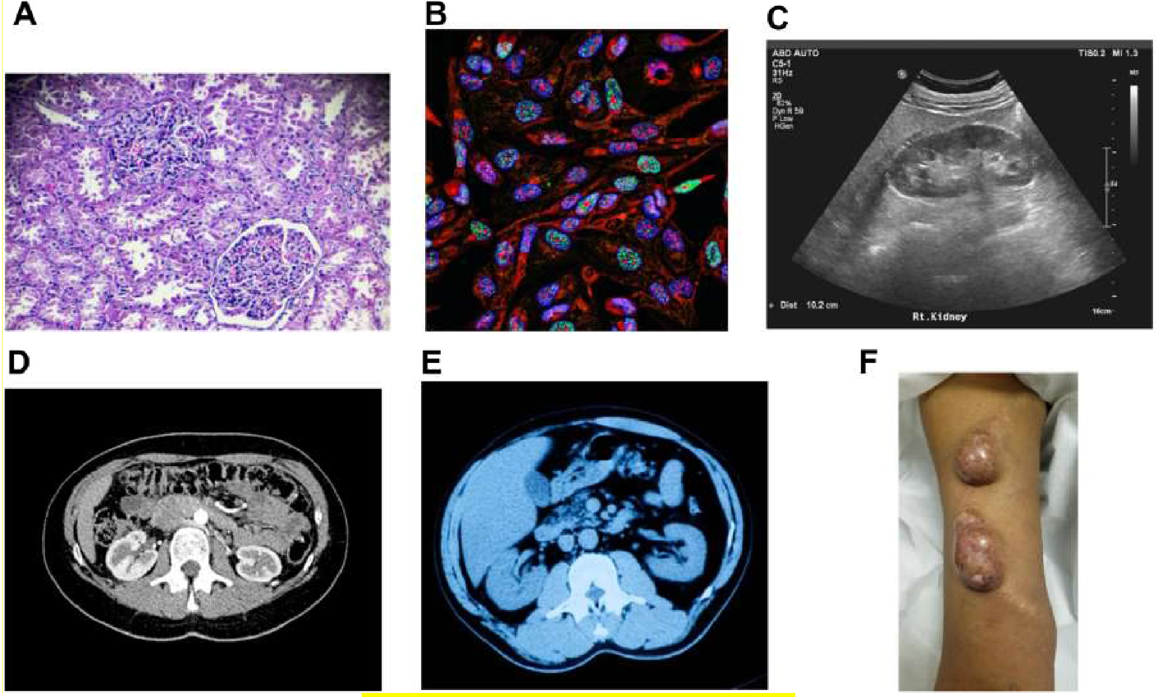
A
B
C
ABD AUTO
Rt.Kidney
Dist 10.2 cm
D
E
F

XDigital image types in kidney care

- ✓ (A ) Whole slide image;
- ✓ (B ) immunofluorescence image;
- ✓ (C ) ultrasound image;
- ✓ (D ) computed tomography scan;
- ✓ (E ) magnetic resonance image;
- ✓ (F ) arteriovenous access aneurysm (digital photographs).
  - A-E images downloaded from iStock.
  - Image "F" is from the first author's publication

59

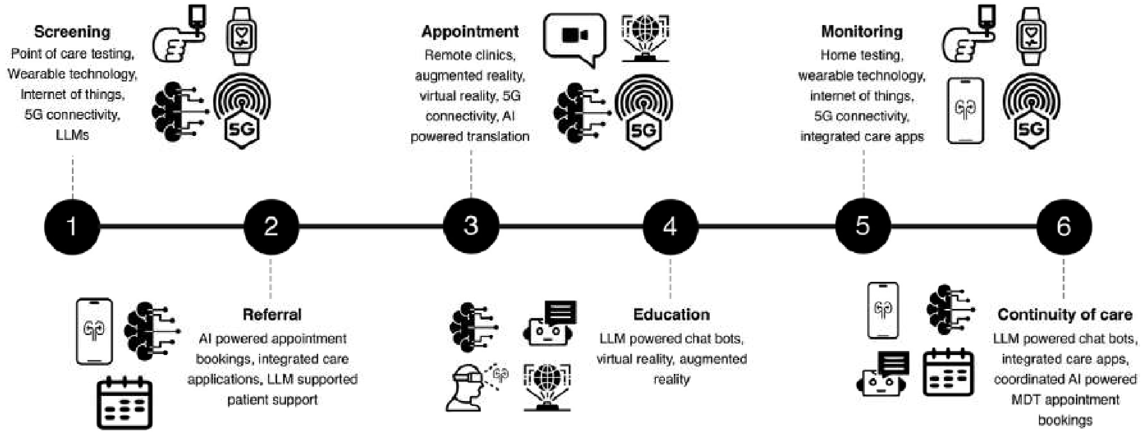
Screening
Point of care testing, Wearable technology, Internet of things, 5G connectivity, LLMs
5G
Appointment
Remote clinics, augmented reality, virtual reality, 5G connectivity, AI powered translation
5G
Monitoring
Home testing, wearable technology, internet of things, 5G connectivity, integrated care apps
5G
1
2
3
4
5
6
Referral
AI powered appointment bookings, integrated care applications, LLM supported patient support
Education
LLM powered chat bots, virtual reality, augmented reality
Continuity of care
LLM powered chat bots, integrated care apps, coordinated AI powered MDT appointment bookings

Technological innovations empowering a patient's health care journey

Technological innovations to support engagement.

- ✓ ) Home testing and wearable technology form an ‘internet of things’ network to continuously screen of risk factors
  - for progressive kidney disease, prompting a referral if anomalies (eg, proteinuria, hypertension) are detected.
  - The significant findings could be contextualized for patients through AI tools such as large language models (LLMs).

- ✓ ) Referrals can be facilitated by AI (recurrent neural network)-powered booking systems trained to pick appointments most suitable for patients to maximize engagement. Referrals could be made through integrated care applications that become the basis of patient communication and management, allowing complete transparency in management plans and decision-making.

- ✓ 3) Clinical appointments for those with scheduling challenges can be conducted remotely through tele or video conferencing powered by 5G connections, with augmented and virtual reality platforms facilitating counseling and education. For those with language barriers, AI tools may 1 day provide real-time translation.

- ✓ 4) Patient education in between clinic appointments can be facilitated by large language models as well as virtual and augmented reality platforms.

- ✓ 5) Health monitoring can be performed regularly through home testing and wearable technology, with results transferred to integrated care applications to allow patients and health care professionals to view trends in real time.

- ✓ 6) Integrated care applications can facilitate multidisciplinary team appointmentswith transparency for patients, with AI-powered tools adding context and answering questions in between appointments.  Icons with credit to thenounproject.com CC BY 3.0. AI, artificial intelligence

60

## Differential expression analysis of immune-related genes in ANCA-GN patients (GSE108113 and GSE104948 datasets, micro-dissected glomerular tissue)

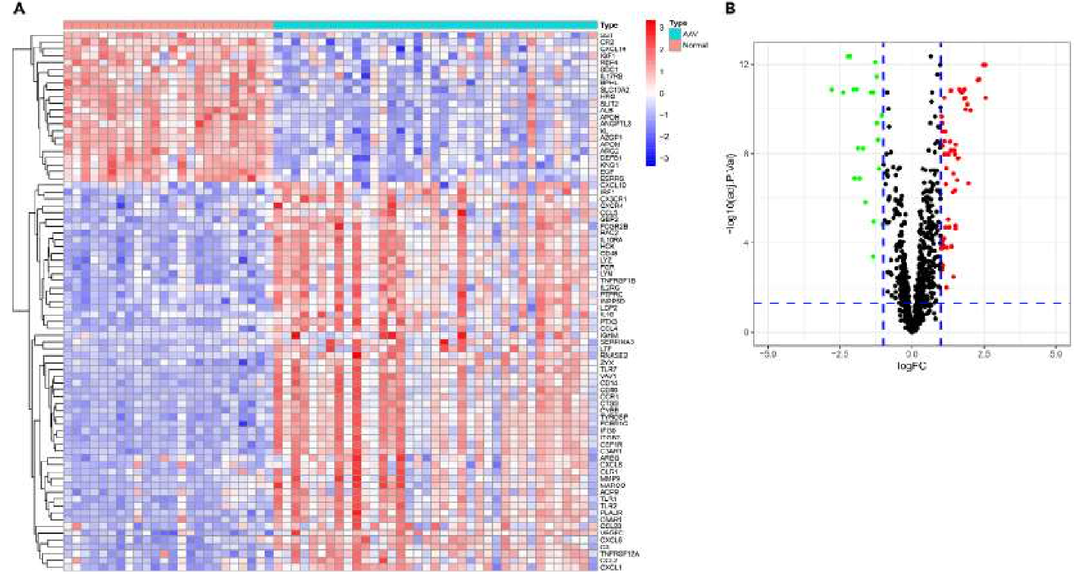

- ✓ (A ) Heatmap of immune-related genes. Legend on the top right indicates the log fold change of the genes. The vertical axis represents each differentially expressed gene. Blue and red colors represent low and high expression values, respectively.
- ✓ (B ) Volcano map of immune-related genes. Red dots indicate upregulated genes and green dots indicate downregulated genes. AAV, antineutrophil cytoplasmic antibody-associated vasculitis. ANCA-GN, antineutrophil cytoplasmic antibody-associated glomerulonephritis

# Protein-protein interaction network(PPIN)

**Construction of protein-protein interaction (PPI) network and expression levels of hub genes**

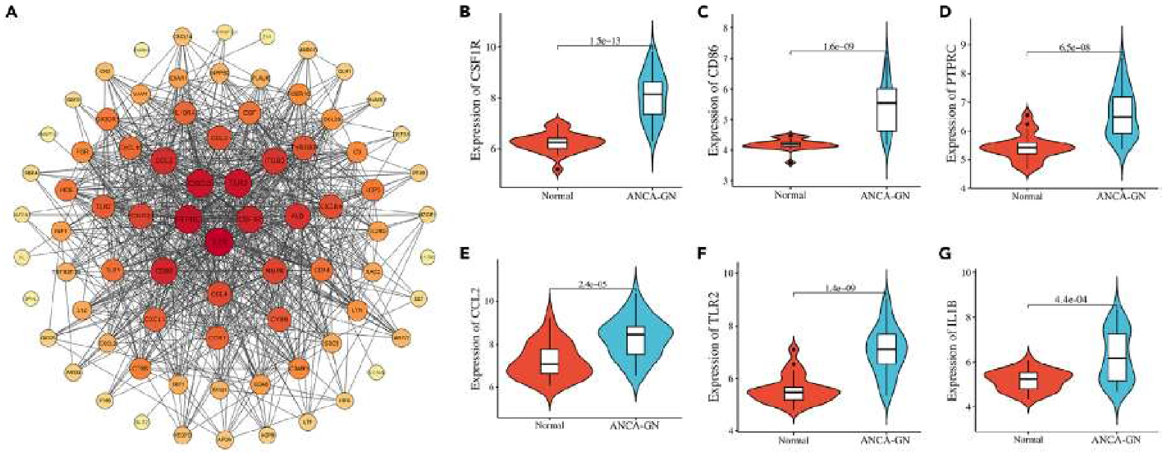

- ✓ (A ) PPI network for immune-related DEGs visualized by Cytoscape. Nodes represent target protein, edges represent interactions among genes. The darker the color and the larger the node are, the greater the degree is. Showing the comparison of six hub genes in ANCA-GN tissues and healthy control, CSF-1R

- ✓ (B ), CD86

- ✓ (C ), PTPRC (D), CCL2 (E), TLR2 (F), IL1B (G). DEGs, differentially expressed genes. ANCA-GN, antineutrophil cytoplasmic antibody-associatedglomerulonephritis.

## External dataset validation (E-MTAB-1944 dataset, micro-dissected kidney tissue) and correlation between the expression of hub genes in ANCA-GN glomeruli and GFR

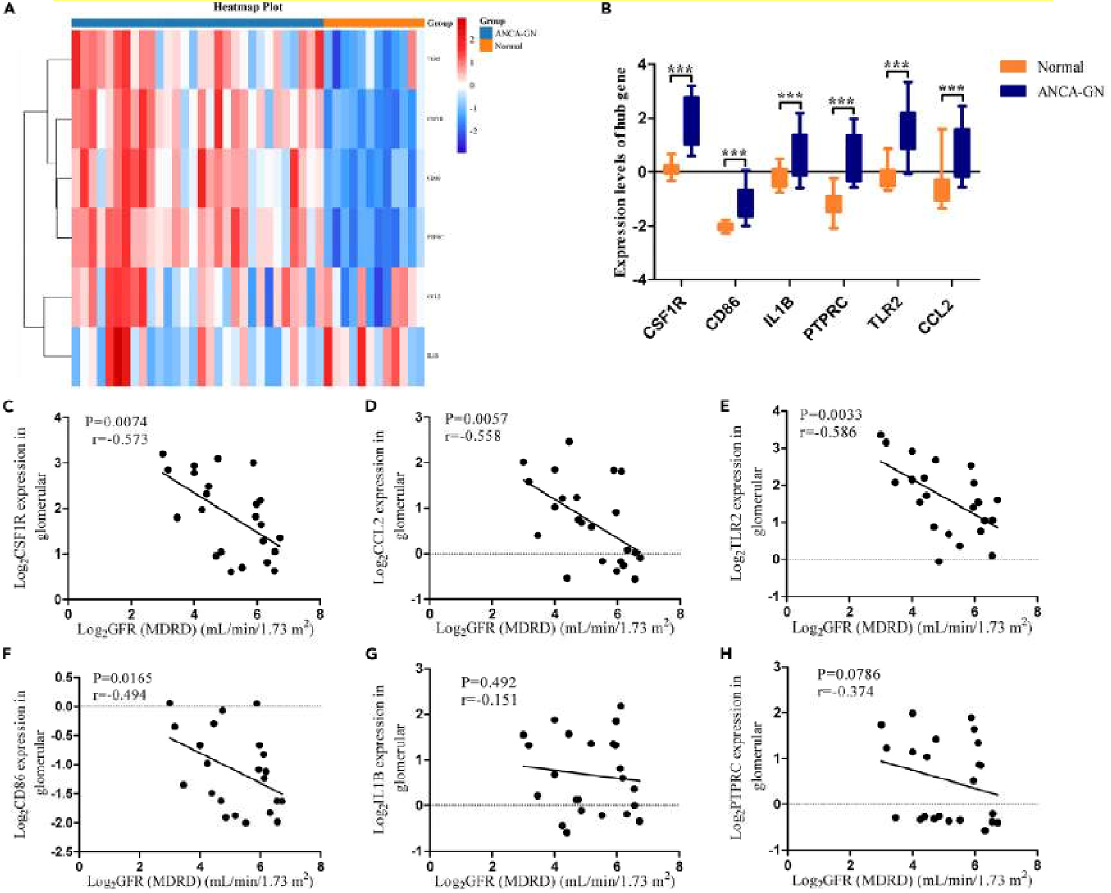

- ✓ (A ) The clustering of six hub genes in heatmap of dataset E-MTAB-1944.
- ✓ (B ) Expression levels of CSF-1R, CD86, IL1B, PTPRC, TLR2, and CCL2 were significantly upregulated in glomeruli of ANCA-GN patient in Nephroseq database (normal n = 21, ANCA-GN patients n = 23). Correlation analysis of GFR and the expression of CSF-1R
- ✓ (C ), CCL2 (D), TLR2 (E), CD86 (F), IL1B (G), and PTRPC (H) inANCA-GN glomeruli from Nephroseq database (n = 23). ANCA-GN, antineutrophil cytoplasmic antibody-associated glomerulonephritis. GFR, glomerularfiltration rate; MDRD, modification of diet in renal

disease. ***p<0.001

61

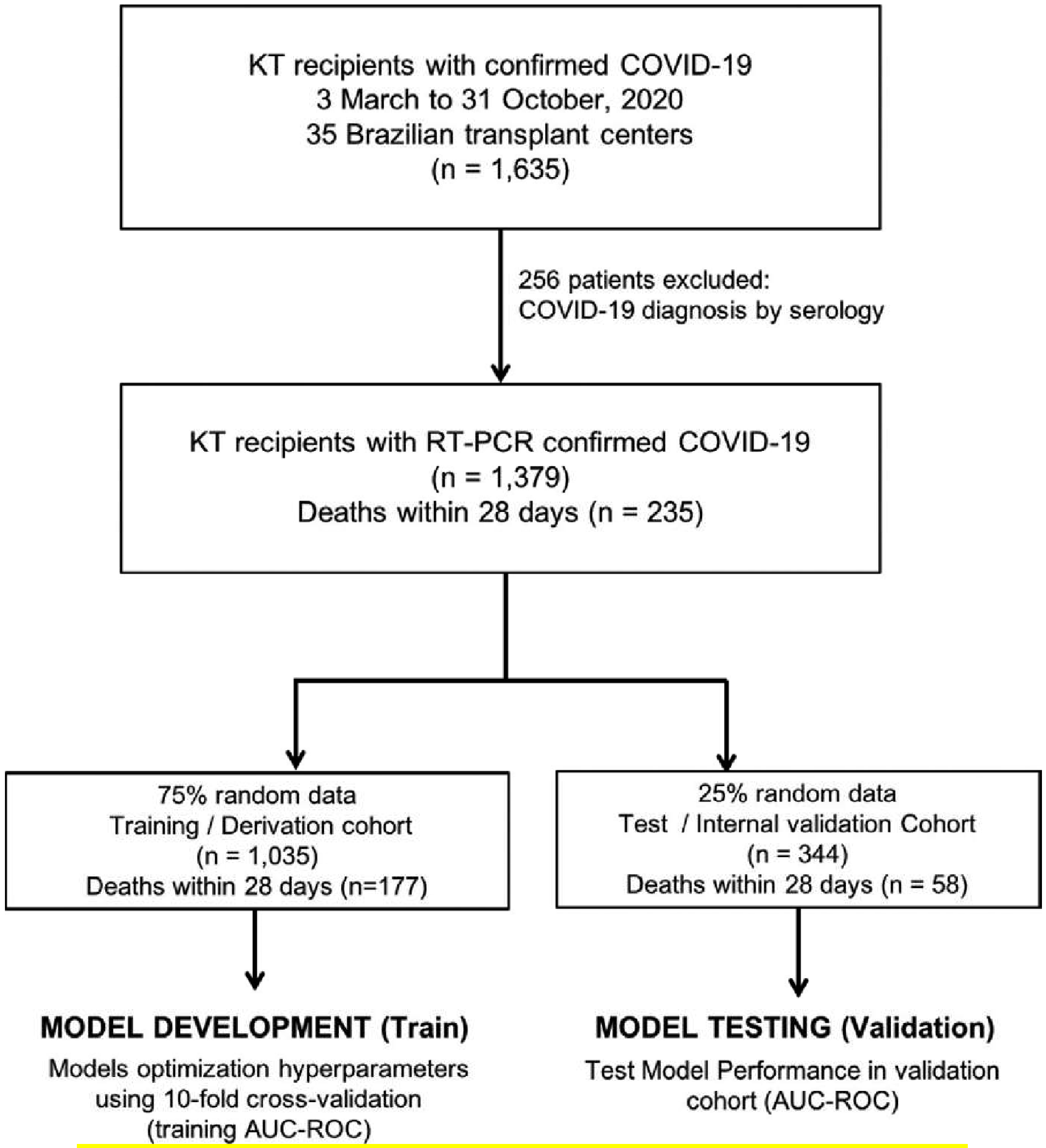
KT recipients with confirmed COVID-19
3 March to 31 October, 2020
35 Brazilian transplant centers
(n = 1,635)
256 patients excluded:
COVID-19 diagnosis by serology
KT recipients with RT-PCR confirmed COVID-19
(n = 1,379)
Deaths within 28 days (n = 235)
75% random data
Training / Derivation cohort
(n = 1,035)
Deaths within 28 days (n=177)
25% random data
Test / Internal validation Cohort
(n = 344)
Deaths within 28 days (n = 58)
MODEL DEVELOPMENT (Train)
Models optimization hyperparameters
using 10-fold cross-validation
(training AUC-ROC)
MODEL TESTING (Validation)
Test Model Performance in validation
cohort (AUC-ROC)

**Participant flow diagramand proportion of patients enrolled inthe derivation and validation cohorts**

61

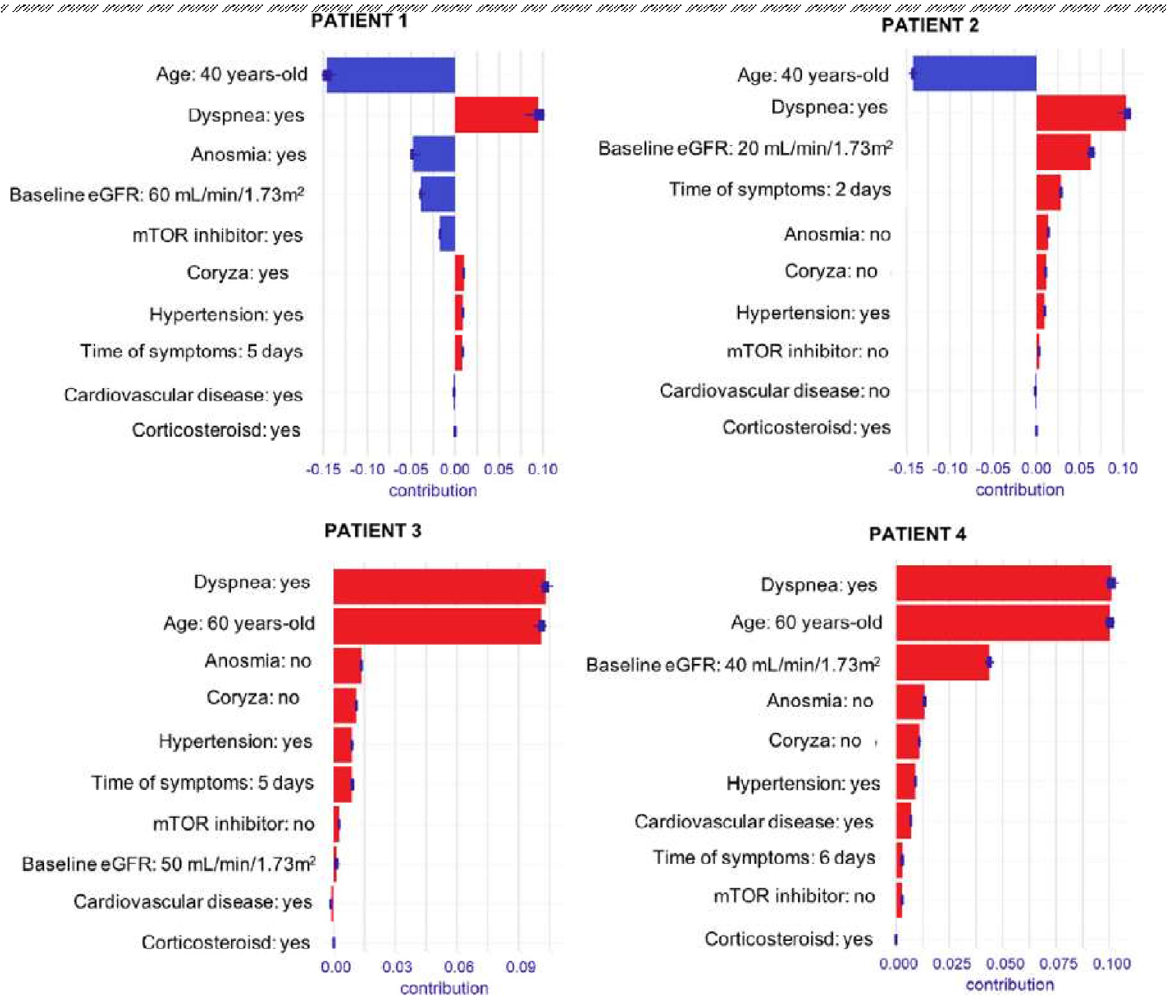

**Shapley Additive Explanations (SHAP plot)**

- ✓ Fig. shows contribution of each predictor in COVID-19-Associated death score in simulated transplant patients.
    - o The red bars represent variables with a positive coefficient that means a positive association between the predictor and the outcome, while the
    - o blue bars represent variables with a negative coefficient that means an inverse association between the predictor and the outcome.
- ✓ eGFR, estimated glomerular filtration rate;
- ✓ mTOR, mammalian target of rapamycin

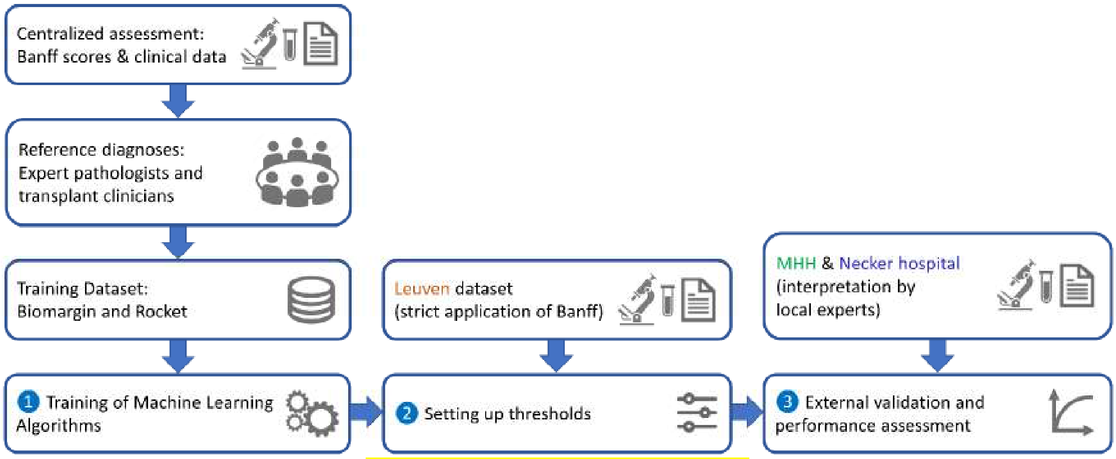
Centralized assessment:
Banff scores & clinical data
Reference diagnoses:
Expert pathologists and
transplant clinicians
Training Dataset:
Biomargin and Rocket
Leuven dataset
(strict application of Banff)
MHH & Necker hospital
(interpretation by
local experts)
1 Training of Machine Learning
Algorithms
2 Setting up thresholds
3 External validation and
performance assessment

Workflow diagram of the study

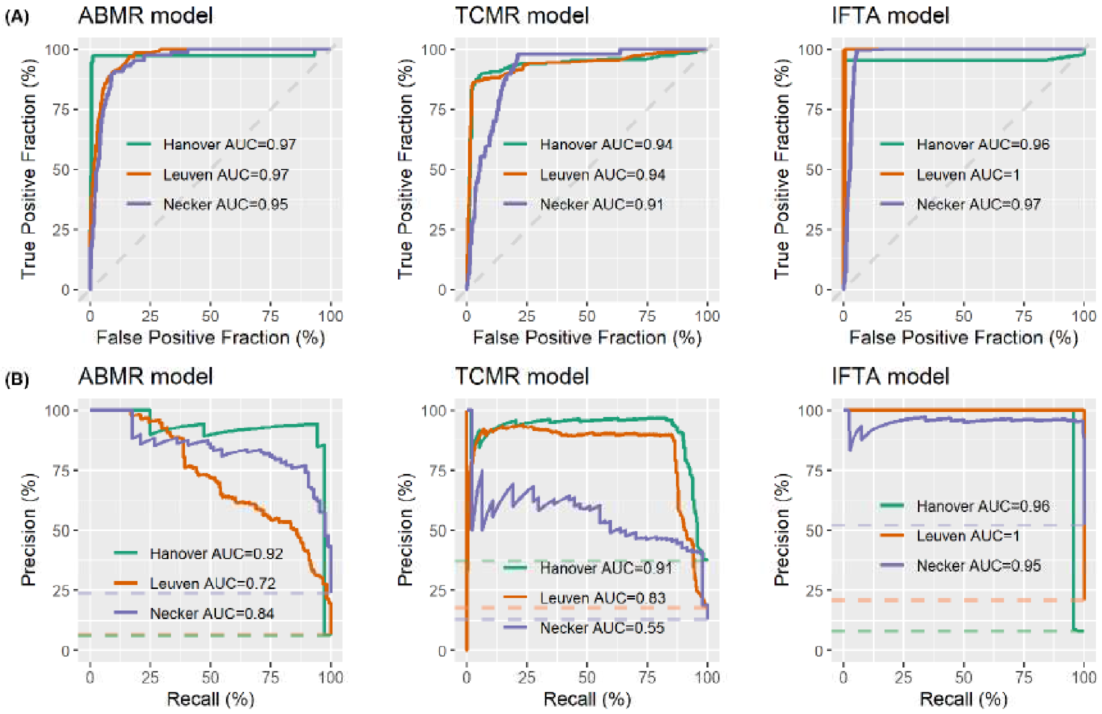

External validation of the machine learning estimators in three independent cohorts

- ✓ (A ) ROC curves of the ABMR model, TCMR model, IFTA model.
- ✓ (B ) PR curves of ABMR model, TCMR model, IFTA model.

- ✓ ABMR, active antibody-mediated rejection;
- ✓ IFTA, interstitial fibrosis/tubular atrophy grade II;
- ✓ Precision, positive predictive value; Recall, sensitivity; TCMR, T cell–mediatedrejection.

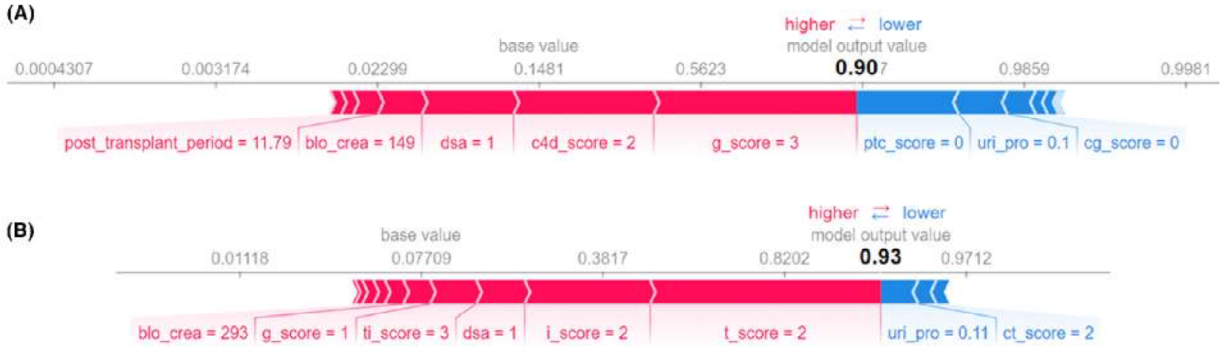

**SHAP explanation force plot for two exemplary cases**

- (A ) The first case has a high score for active ABMR (0.90, which qualifies for "positive"). High serum creatinine, positive DSA, and some specific elementary lesions (C4d = 2, g = 3) increase the score.
- Negative proteinuria (<0.3 g/L) and some negative criteria (ptc = 0, cg = 0) decrease the score.
- (B ) The second case has a high score for TCMR (0.93, which qualifies for "positive"). High serum creatinine, positive DSA, and some specific elementary lesions (i = 2, t = 2, ti = 3) increase the score. Negative proteinuria (<0.3 g/L) and nonspecific lesions (ct = 2) decrease the score.

- ABMR, active antibody-mediated rejection;
- C4d, linear C4d staining in ptc or medullary vasa recta; cg, chronic transplant glomerulopathy; ct, tubular atrophy in cortex;
- DSA, donor-specific antibodies;
- i, inflammation in non-scarred cortex;
- t, tubulitis in cortical tubules within non-scarred cortex;
- TCMR, T cell–mediated rejection;
- ti, total cortical inflammation

- SHAP, SHapley Additive exPlanations;

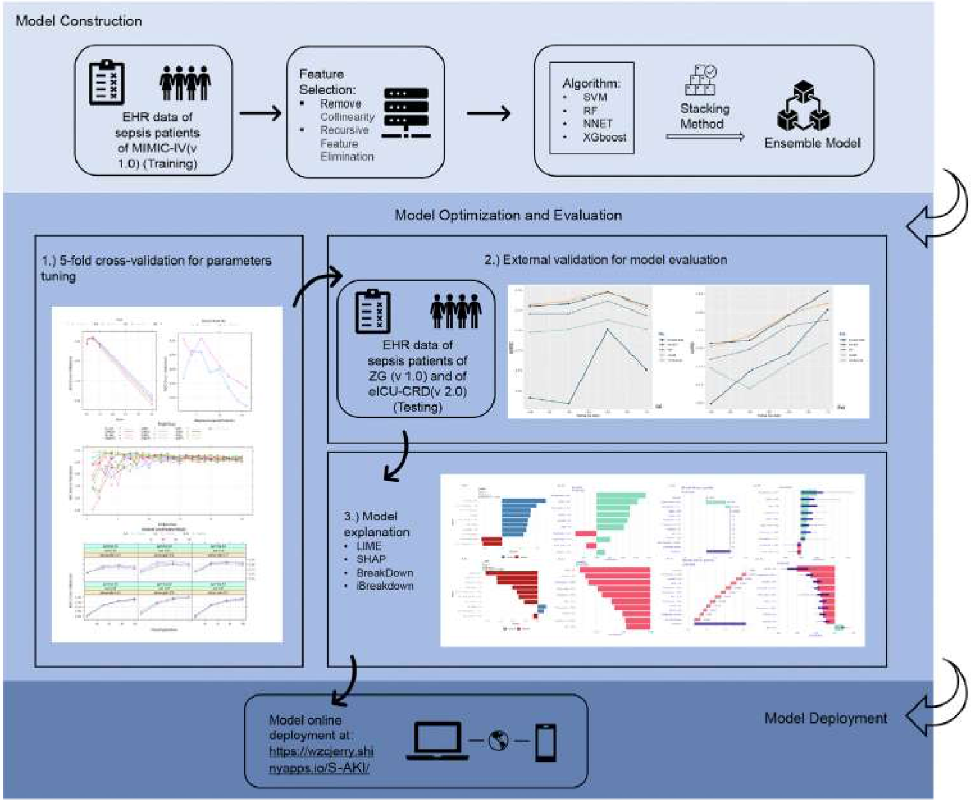
Model Construction
EHR data of sepsis patients of MIMIC-IV(v 1.0) (Training)
Feature Selection:
Remove Collinearity
Recursive Feature Elimination
Algorithm:
SVM
RF
NNET
XGboost
Stacking Method
Ensemble Model
Model Optimization and Evaluation
1.) 5-fold cross-validation for parameters tuning
2.) External validation for model evaluation
EHR data of sepsis patients of ZG (v 1.0) and of eICU-CRD(v 2.0) (Testing)
3.) Model explanation
LIME
SHAP
BreakDown
iBreakdown
Model Deployment
Model online deployment at: https://wzcjerry.shinyapps.io/S-AKI/

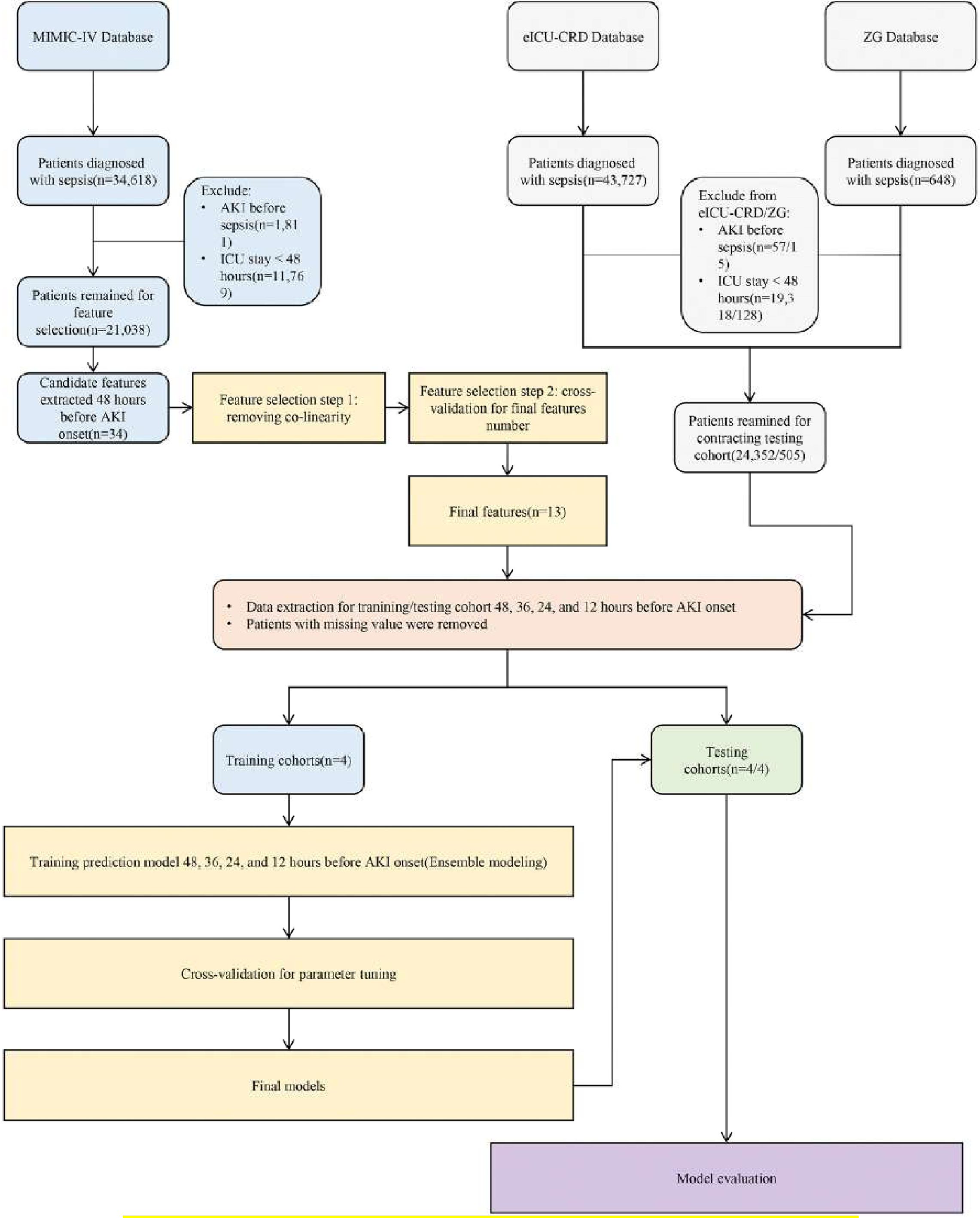
MIMIC-IV Database
eICU-CRD Database
ZG Database
Patients diagnosed with sepsis(n=34,618)
Exclude:
AKI before sepsis(n=1,811)
ICU stay < 48 hours(n=11,769)
Patients diagnosed with sepsis(n=43,727)
Patients diagnosed with sepsis(n=648)
Exclude from eICU-CRD/ZG:
AKI before sepsis(n=57/15)
ICU stay < 48 hours(n=19,318/128)
Patients remained for feature selection(n=21,038)
Candidate features extracted 48 hours before AKI onset(n=34)
Feature selection step 1: removing co-linearity
Feature selection step 2: cross-validation for final features number
Patients reamined for contracting testing cohort(24,352/505)
Final features(n=13)
Data extraction for traninin/testing cohort 48, 36, 24, and 12 hours before AKI onset
Patients with missing value were removed
Training cohorts(n=4)
Testing cohorts(n=4/4)
Training prediction model 48, 36, 24, and 12 hours before AKI onset(Ensemble modeling)
Cross-validation for parameter tuning
Final models
Model evaluation

**Flow chart for participant inclusion and model processing in the study**

93

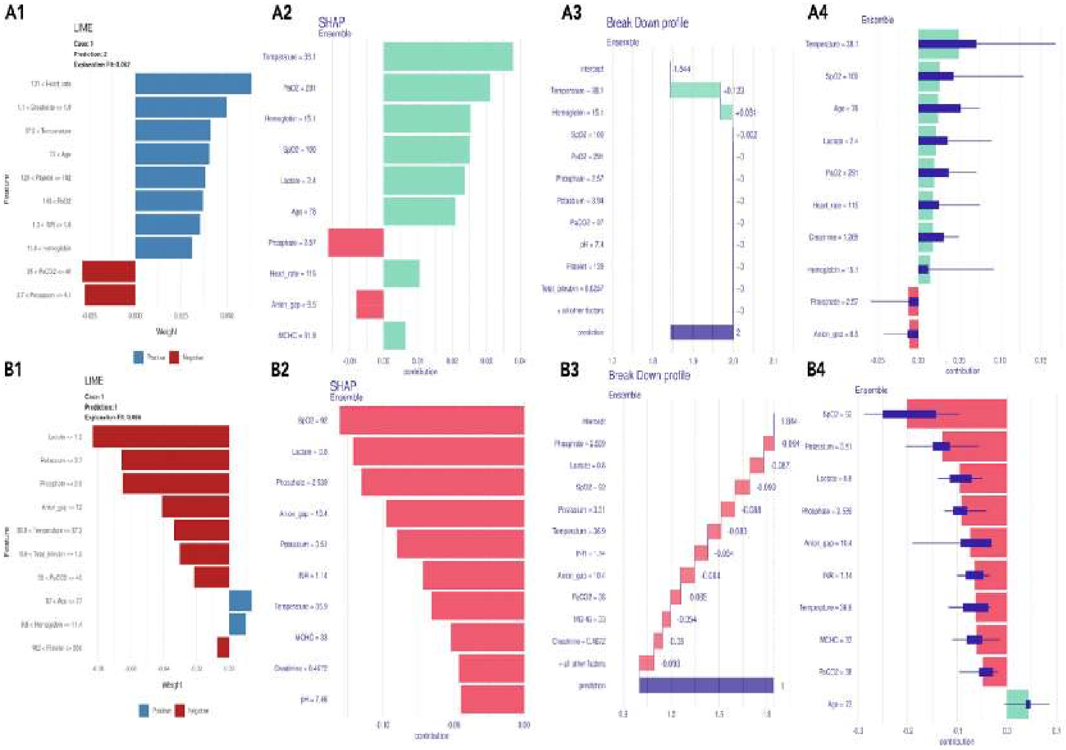

**Model explanations for the ensemble model**

- ✓ XAI methods for one S-AKI onset and one control patient are exhibited in (a) and (b);
- ✓ (a.1; b.1) represented LIME method;
- ✓ (a.2; b2) represented SHAP method,
- ✓ (a.3; b.3) represented Break Down method;
- ✓ (a.4; b.4) represented
  - iBreakDown method.
  - Bar plots to right direction represented positive predictionand bar plots to left direction represented negative prediction.
  - Boxplots for iBreakDown represented the uncertainty of features contributions

67

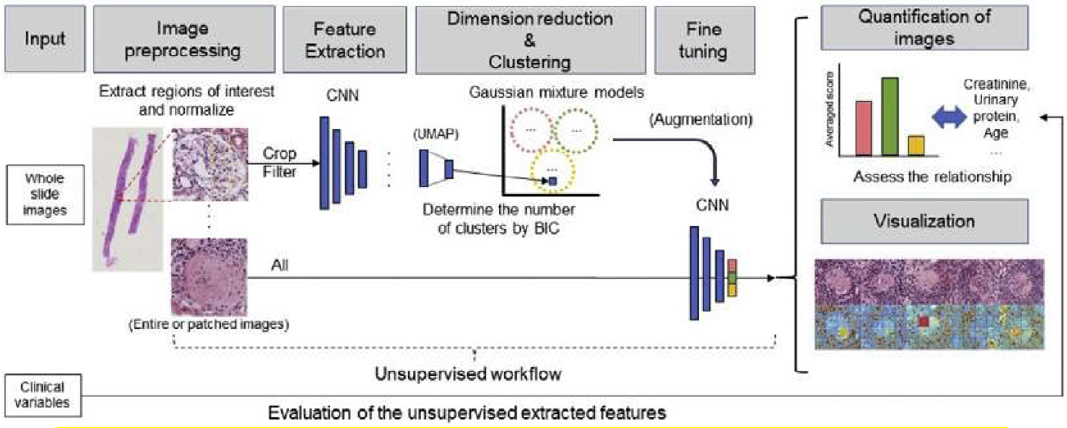
Input
Image preprocessing
Feature Extraction
Dimension reduction & Clustering
Fine tuning
Quantification of images
Extract regions of interest and normalize
CNN
Gaussian mixture models
(UMAP)
(Augmentation)
Crop Filter
Whole slide images
Determine the number of clusters by BIC
CNN
All
(Entire or patched images)
Averaged score
Creatinine, Urinary protein, Age
Assess the relationship
Visualization
Unsupervised workflow
Clinical variables
Evaluation of the unsupervised extracted features

**Overall workflow. The overall workflow of the proposed methods is visualized**

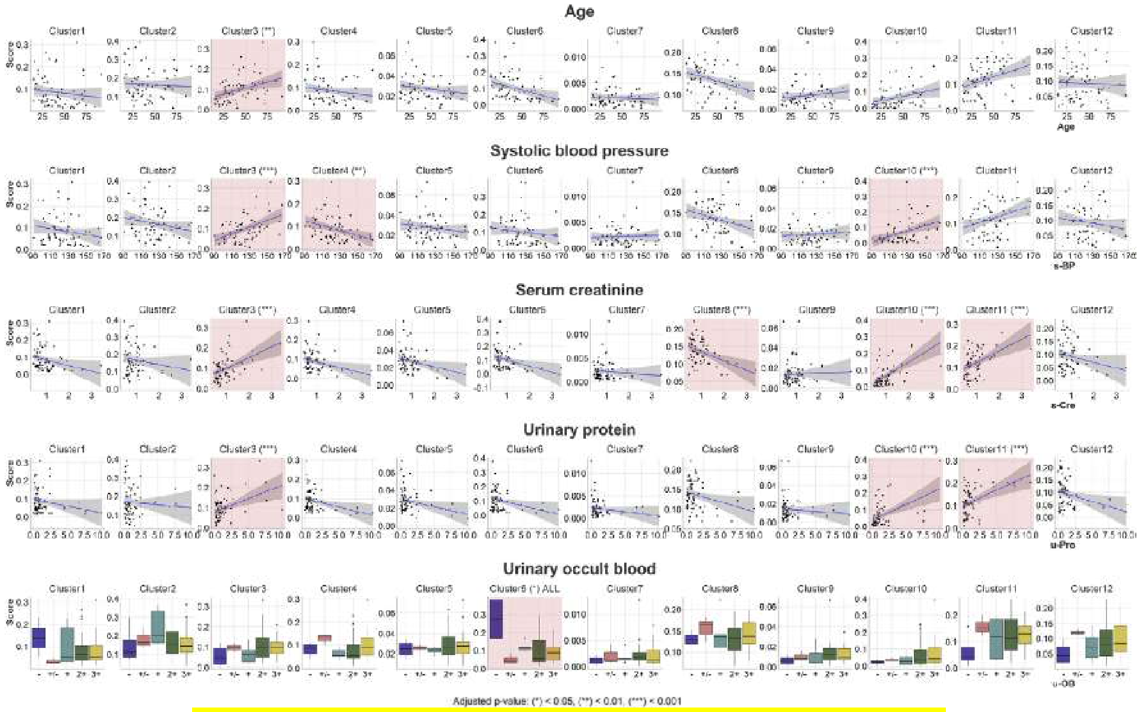

Relationship between histological scores and clinical variables

- The box plot (urinary occult blood)
- line plots (age, systolic blood pressure, serum creatinine, and urinary protein excretion)
- ✓ x axes represent clinical variables,
- ✓ y axes represent histological scores.
- Statistically significant clusters are presented with an asterisk and red background.

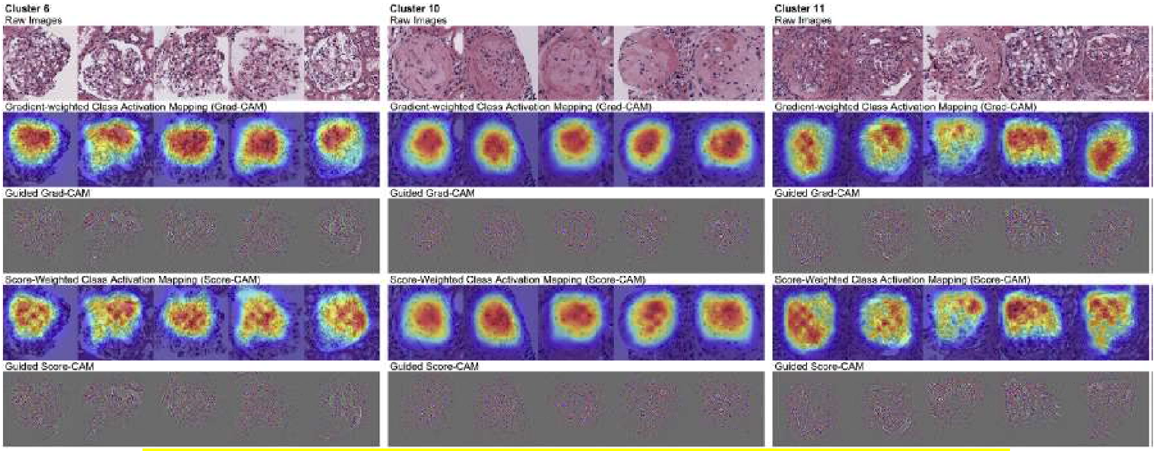
Cluster 6
Raw Images
Cluster 10
Raw Images
Cluster 11
Raw Images
Gradient-weighted Class Activation Mapping (Grad-CAM)
Guided Grad-CAM
Score-Weighted Class Activation Mapping (Score-CAM)
Guided Score-CAM

Visualization results of the rationale behind the prediction of each class

- The score-weighted class activation mapping, gradient weighted class activation mapping, and the results obtained by multiplication with guided backpropagation.

- Clusters 6 (left), 10 (middle), and 11 (right)

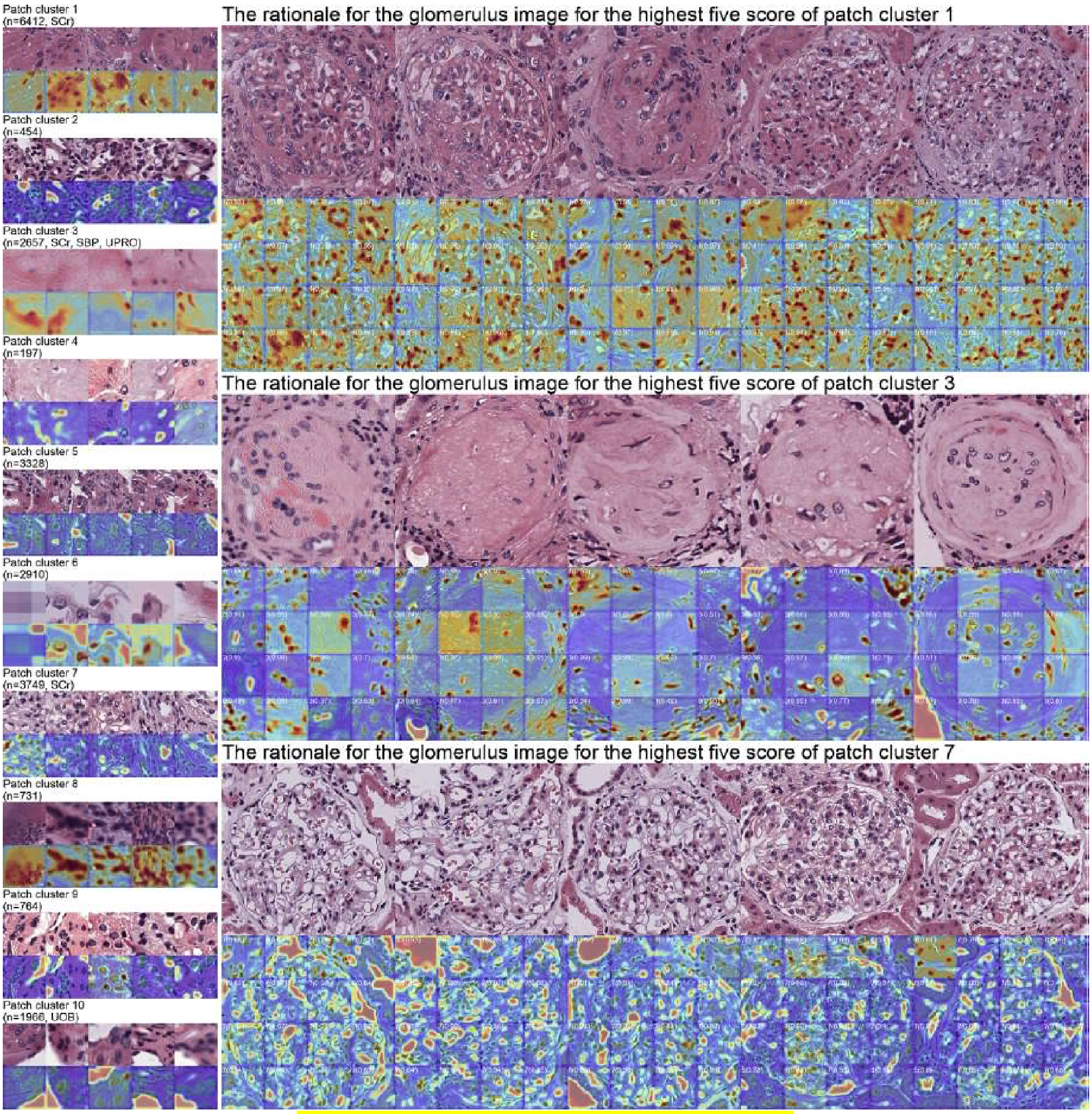
Patch cluster 1
(n=6412, SCr)
Patch cluster 2
(n=454)
Patch cluster 3
(n=2657, SCr, SBP, UPRO)
Patch cluster 4
(n=197)
Patch cluster 5
(n=3328)
Patch cluster 6
(n=2910)
Patch cluster 7
(n=3749, SCr)
Patch cluster 8
(n=731)
Patch cluster 9
(n=764)
Patch cluster 10
(n=1966, UOB)
The rationale for the glomerulus image for the highest five score of patch cluster 1
The rationale for the glomerulus image for the highest five score of patch cluster 3
The rationale for the glomerulus image for the highest five score of patch cluster 7

**Result summary of the patch-based analysis**

- **left panel** shows clustered patches and the rationale behind the clustering visualized by score-weighted class activation mapping.
  - The number of patches in the class,
  - clinical variables that had a significant relationship with the score of the patch class,

- **right panel** shows the rationale for the patches of the glomeruli with the highest scores of the respective cluster of patches.
  - The predicted cluster of each patch is shown in the upper left corner with the prediction probability

64

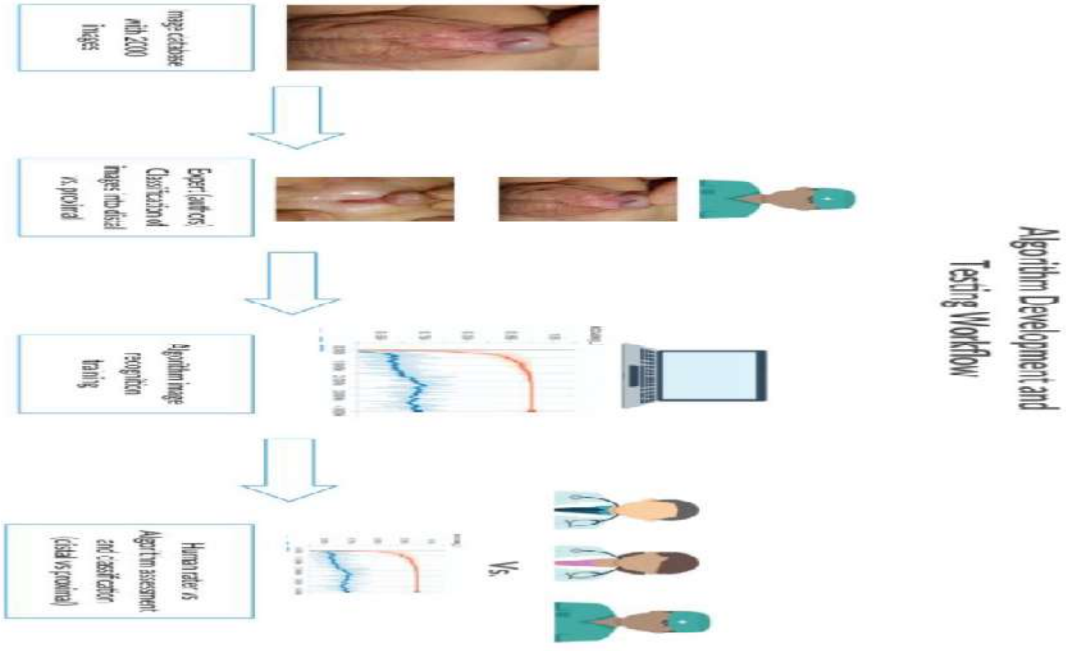
Algorithm Development and Testing Workflow
Image database with 2200 images
Expert (authors) Classification of images into distal vs. proximal
Algorithm image recognition training
Human rater vs Algorithm assessment and classification (distal vs proximal)
Vs.

**Algorithm creation and testing workflow**

64

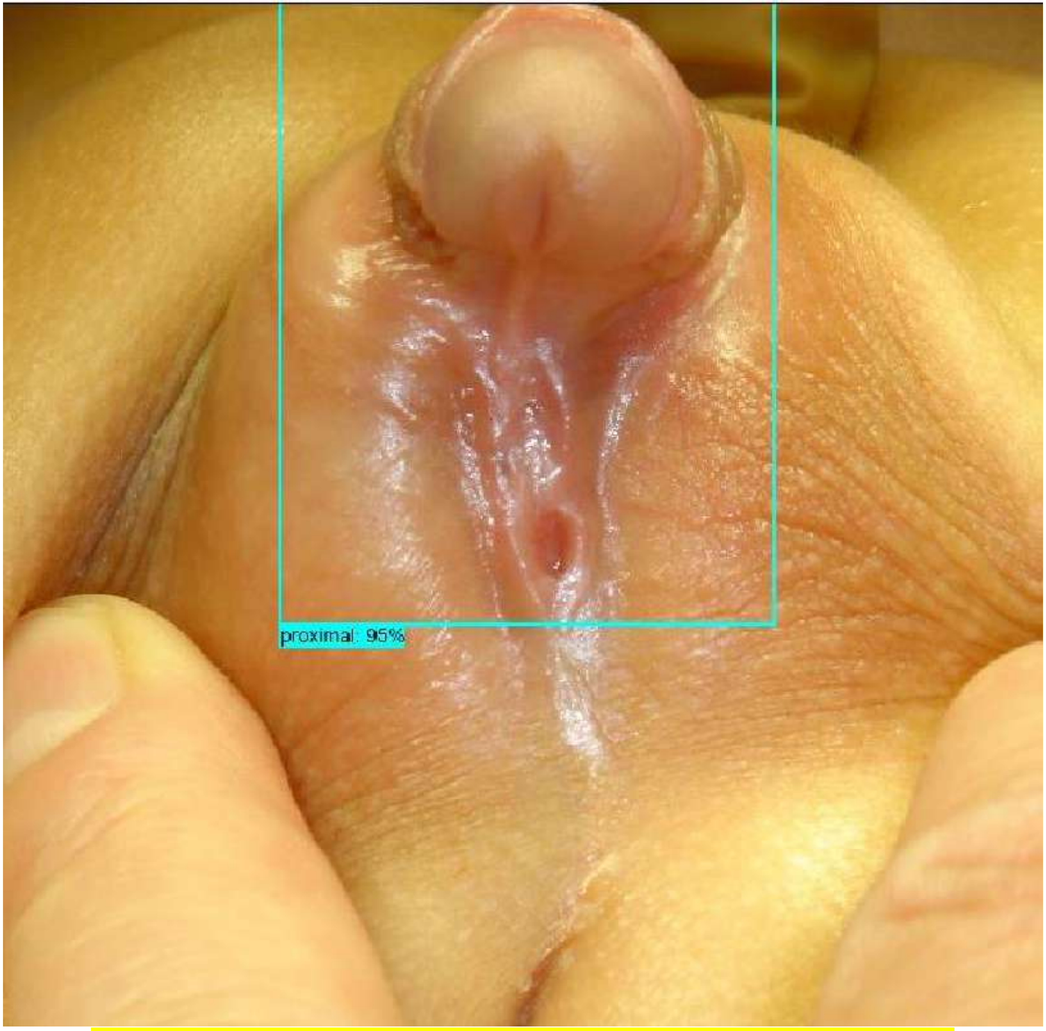

Output from the model showing a bounding box and confidence percentage

- Digital pattern recognition for the identification and classification of hypospadias using artificial intelligence vs. experienced pediatric urologist

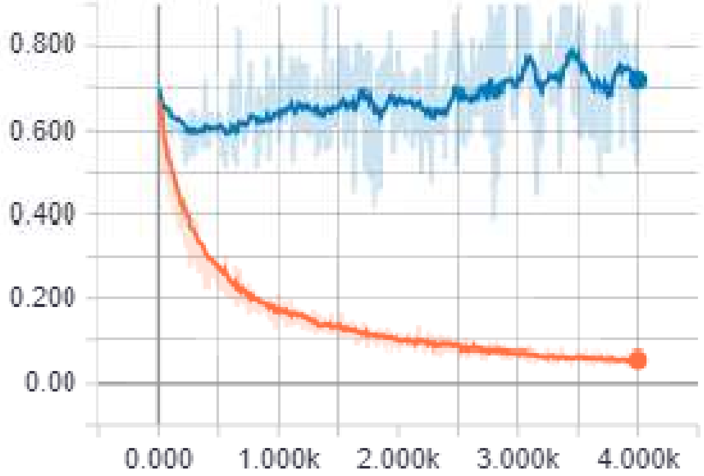

**Representation of values for each statistical measurement using first setof images (orange line) and validation process (blue line).**

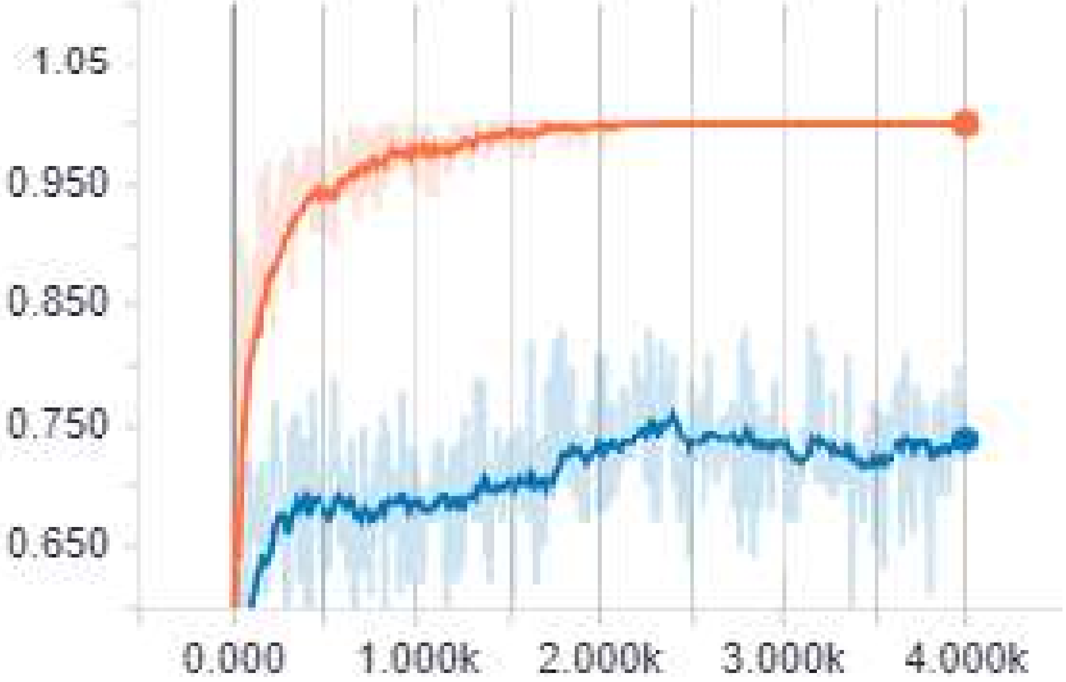

**Accuracy reached after algorithm training**

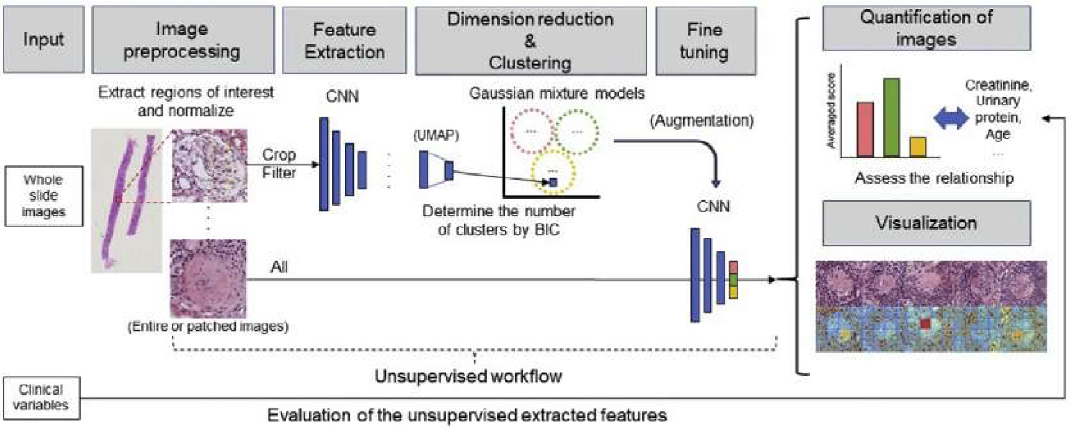
Input
Image preprocessing
Feature Extraction
Dimension reduction & Clustering
Fine tuning
Quantification of images
Extract regions of interest and normalize
CNN
Gaussian mixture models
(UMAP)
(Augmentation)
Whole slide images
Crop Filter
Determine the number of clusters by BIC
CNN
All
(Entire or patched images)
Averaged score
Creatinine, Urinary protein, Age
Assess the relationship
Visualization
Unsupervised workflow
Clinical variables
Evaluation of the unsupervised extracted features

Overall workflow. The overall workflow of the proposed methods is visualized

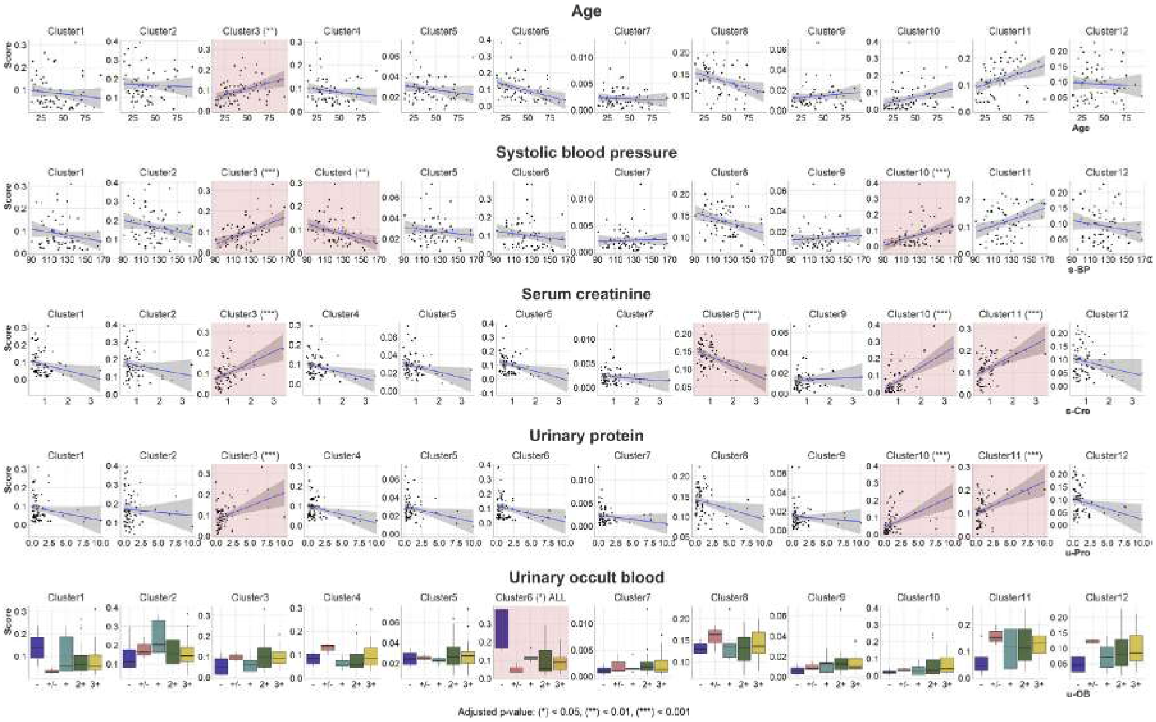

Relationship between histological scores and clinical variables

- ✓ The box plot (urinary occult blood) and line plots (age, systolic blood pressure, serum creatinine, and urinary protein excretion) show the relationship between histological scores and clinical variables.
    - o x axes represent clinical variables,
    - o y axes represent histological scores.
    - o Statistically significant clusters are presented with an asterisk and red background.

67

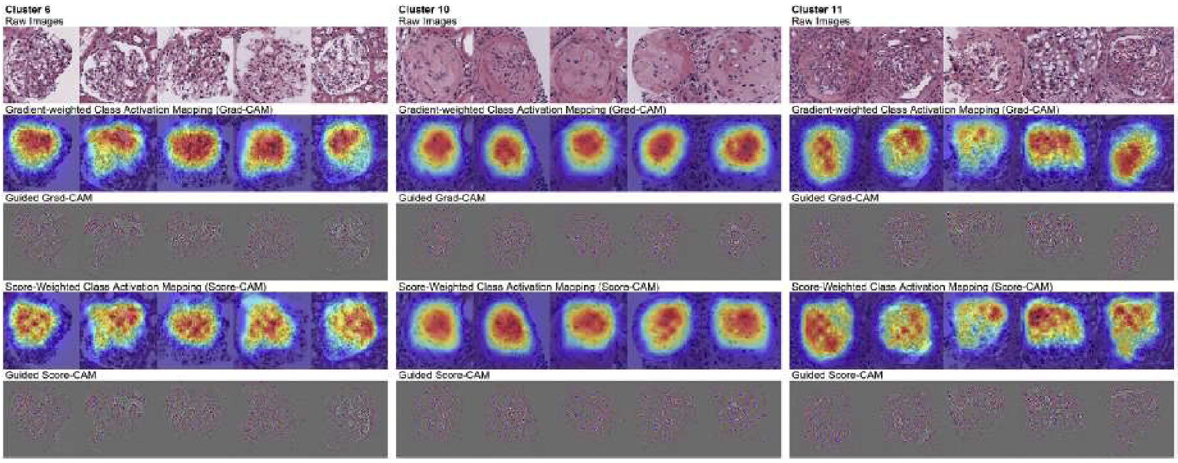
Cluster 6
Raw Images
Gradient-weighted Class Activation Mapping (Grad-CAM)
Guided Grad-CAM
Score-Weighted Class Activation Mapping (Score-CAM)
Guided Score-CAM
Cluster 10
Raw Images
Gradient-weighted Class Activation Mapping (Grad-CAM)
Guided Grad-CAM
Score-Weighted Class Activation Mapping (Score-CAM)
Guided Score-CAM
Cluster 11
Raw Images
Gradient-weighted Class Activation Mapping (Grad-CAM)
Guided Grad-CAM
Score-Weighted Class Activation Mapping (Score-CAM)
Guided Score-CAM

- ✓ Visualization results of the rationale behind the prediction of each class. The score-weighted class activation mapping, gradientweighted class activation mapping, and the results obtained by multiplication with guided backpropagation are shown. Clusters 6 (left), 10(middle), and 11 (right) are shown

67

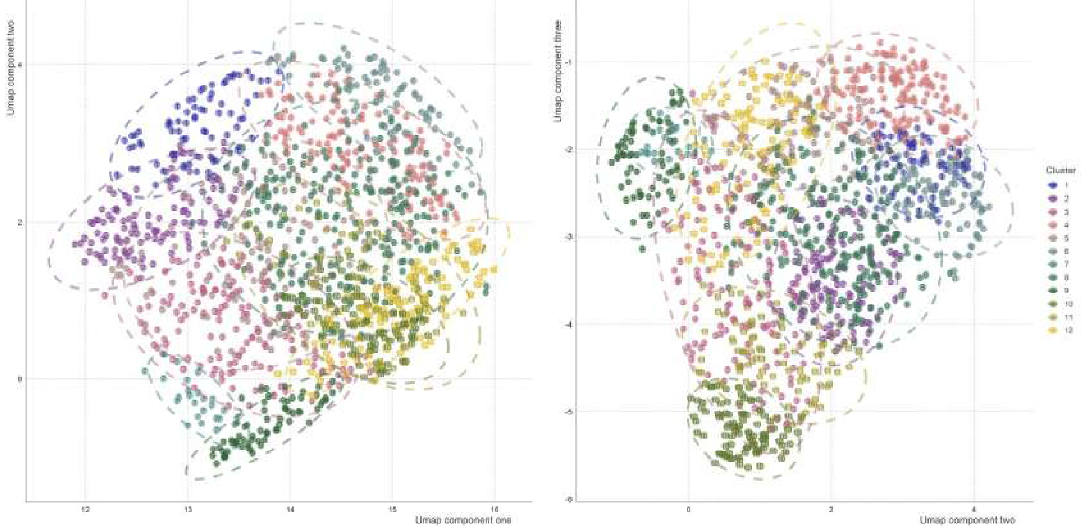

**Components one, two, and three of the UMAP results**

- ✓ Each point represents a glomerulus, with the color representing the class of the glomerulus. UMAP, Uniform Manifold Approximation and Projection

67

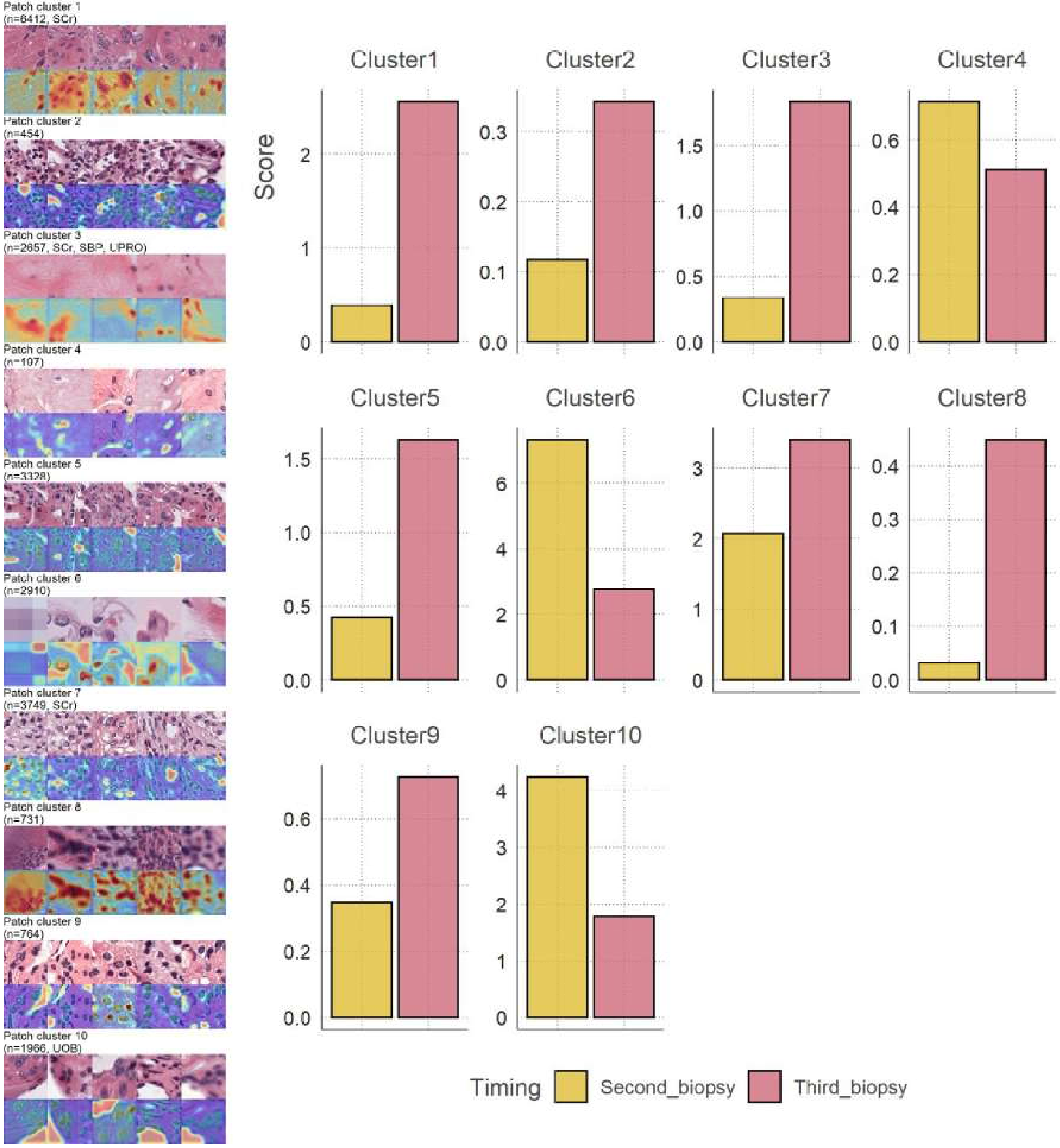

- ✓ **Left panel**shows the clustered patches and the rationale behind the clustering visualized by Score-weighted class activation mapping.
  - o The number of patches in the class, along with the clinical variables which had a significant relationship with the score of the patch class are shown.
- ✓ **Right panel**shows the bar plot depicting the score of the second and third biopsies.
    - ▪ UOB, urinary occult blood;
    - ▪ SBP, systolic blood pressure;
    - ▪ SCr, serum creatinine value;
    - ▪ UPro, urinary protein excretion

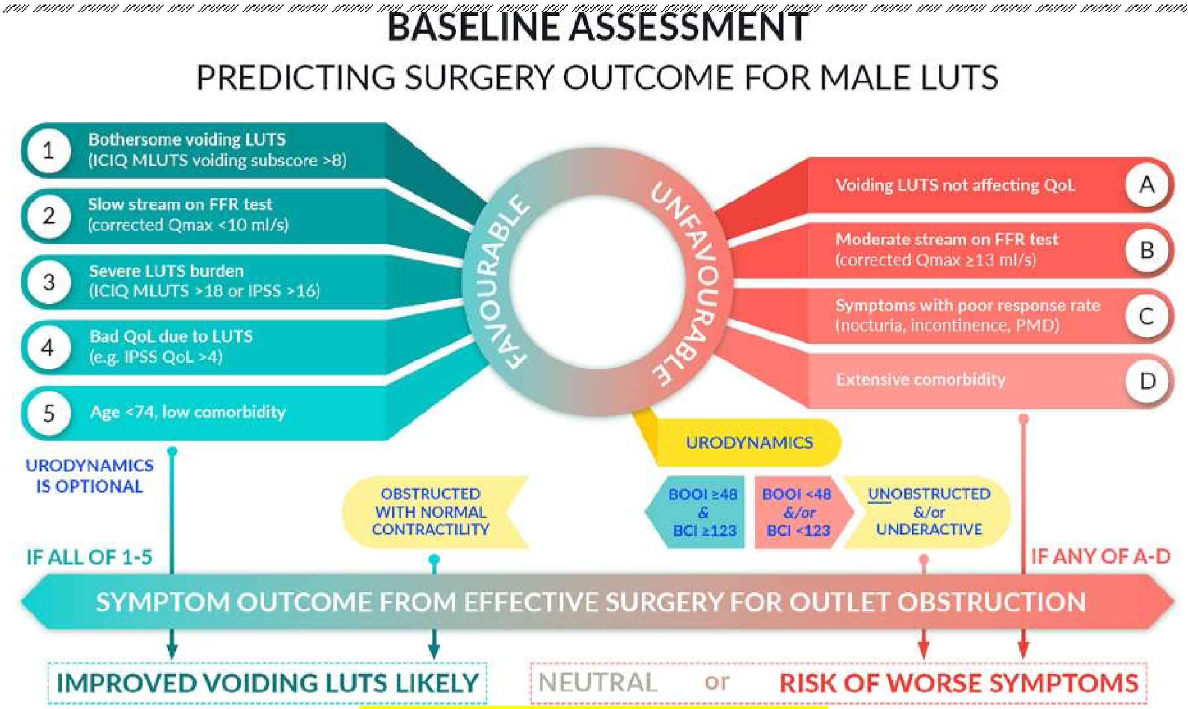
BASELINE ASSESSMENT
PREDICTING SURGERY OUTCOME FOR MALE LUTS
1 Bothersome voiding LUTS (ICIQ MLUTS voiding subscore >8)
2 Slow stream on FFR test (corrected Qmax <10 ml/s)
3 Severe LUTS burden (ICIQ MLUTS >18 or IPSS >16)
4 Bad QoL due to LUTS (e.g. IPSS QoL >4)
5 Age <74, low comorbidity
FAVOURABLE
UNFAVOURABLE
Voiding LUTS not affecting QoL A
Moderate stream on FFR test (corrected Qmax ≥13 ml/s) B
Symptoms with poor response rate (nocturia, incontinence, PMD) C
Extensive comorbidity D
URODYNAMICS IS OPTIONAL
IF ALL OF 1-5
URODYNAMICS
OBSTRUCTED WITH NORMAL CONTRACTILITY
BOOI ≥48 & BCI ≥123
BOOI <48 &/or BCI <123
UNOBSTRUCTED &/or UNDERACTIVE
IF ANY OF A-D
SYMPTOM OUTCOME FROM EFFECTIVE SURGERY FOR OUTLET OBSTRUCTION
IMPROVED VOIDING LUTS LIKELY
NEUTRAL or RISK OF WORSE SYMPTOMS

**Lower urinary tract symptoms (LUTS)**

- ✓ Key baseline clinical parameters for prediction of outcomes from surgery to treat BOO in male LUTS, incorporating overall findings from the UPSTREAM study.
- ✓ Two groups of men have a good chance of voiding symptom improvement from surgery, provided that BOO is properly relieved (‘‘effective surgery’’):

- ✓ ( 1 ) Those with all of the favourable predictive factors (shown in green on the left); and
- ✓ ( 2 ) Those for whom a urodynamics test finds BOOI ≥48 and BCI ≥123. Without these features, the outcome may be neutral (symptom score change below the minimally important difference) or even symptom deterioration, particularly in cases with any of the unfavourable factors shown in red.

  - o BCI = bladder contractility index;
  - o BOO = bladder outflow obstruction;
  - o BOOI = BOO Index;
  - o FFR = free flow rate;
  - o ICIQ MLUTS = International Consultation on Incontinence Questionnaire on male LUTS;
  - o IPSS = International Prostate Symptom Score;
  - o LUTS = lower urinary tract symptoms;
  - o PMD = postmicturition dribble;
  - o Qmax = maximum flow rate;
  - o QoL = quality of life

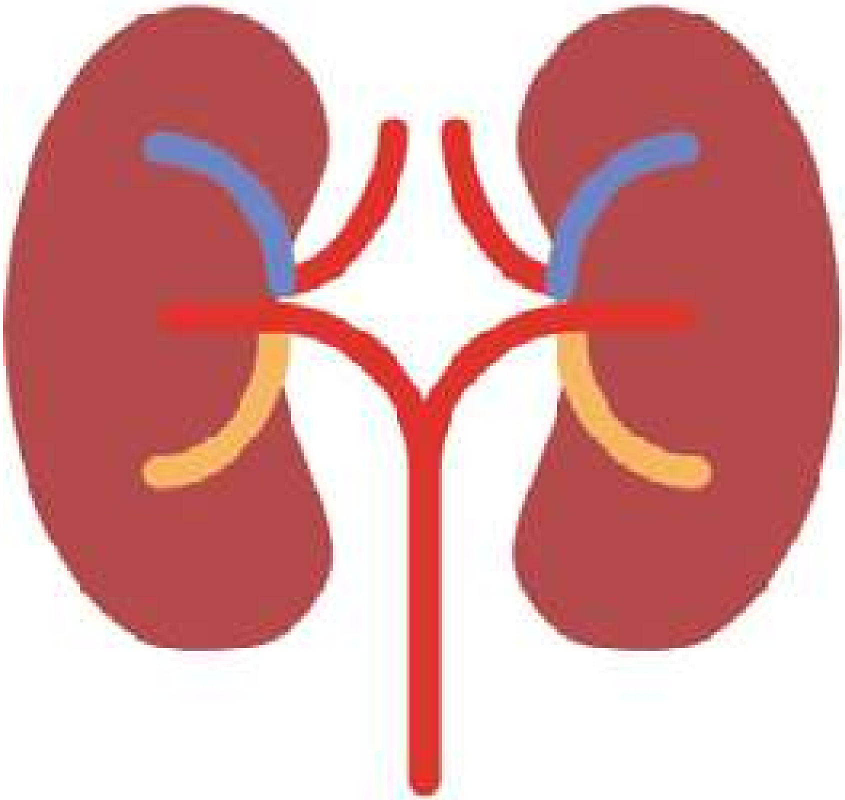

**Advances in targeted therapies**

**Overview of major contributors to clinical use of omics in nephrology**

76

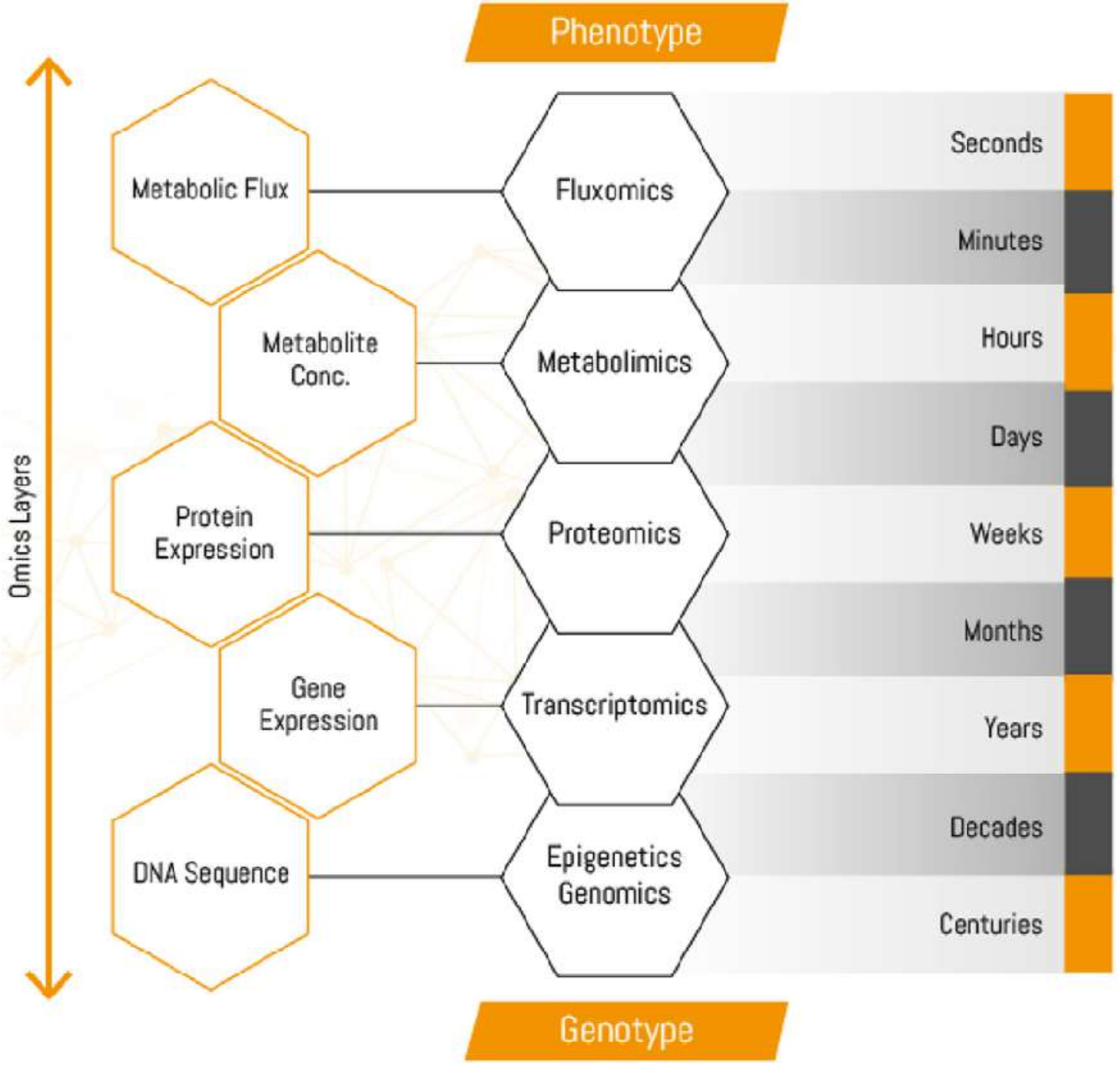
Phenotype
Omics Layers
Metabolic Flux
Metabolite Conc.
Protein Expression
Gene Expression
DNA Sequence
Fluxomics
Metabolimics
Proteomics
Transcriptomics
Epigenetics Genomics
Seconds
Minutes
Hours
Days
Weeks
Months
Years
Decades
Centuries
Genotype

**Various omics technologies characterize individual phenotypes and genotypes**

- Each omics layer represents a distinct set of interacting molecules with varying influence factors that are often changing at different chronological scales.

78

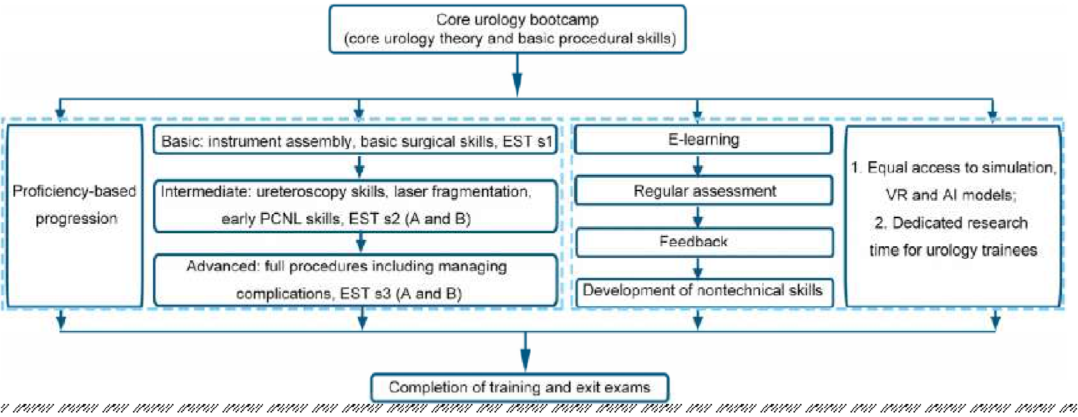
Core urology bootcamp
(core urology theory and basic procedural skills)
Proficiency-based progression
Basic: instrument assembly, basic surgical skills, EST s1
Intermediate: ureteroscopy skills, laser fragmentation, early PCNL skills, EST s2 (A and B)
Advanced: full procedures including managing complications, EST s3 (A and B)
E-learning
Regular assessment
Feedback
Development of nontechnical skills
1. Equal access to simulation, VR and AI models;
2. Dedicated research time for urology trainees
Completion of training and exit exams

A proposed pathway incorporating the EST curriculum

- EST, endoscopic stone treatment;
    - EST s1, EST step 1; EST s2, EST step 2;
- PCNL, percutaneous nephrolithotomy;
- VR, virtual reality;
- AI, artificial intelligence

79

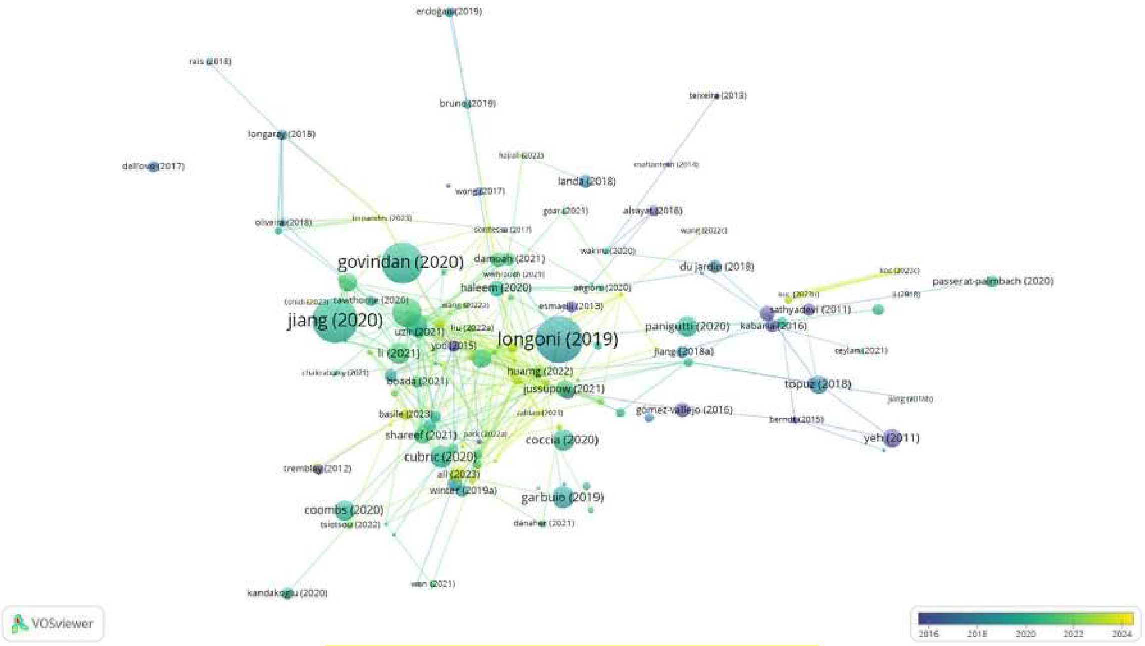
erdogan (2019)
rais (2018)
bruno (2019)
teixeira (2013)
longaray (2018)
dell'oglio (2017)
landa (2018)
wong (2017)
goar (2021)
alsayad (2016)
oliveira (2018)
govindan (2020)
damoah (2021)
du jardin (2018)
haleem (2020)
passerat-palmbach (2020)
jiang (2020)
sathyadevi (2011)
longoni (2019)
panigutti (2020)
kabaria (2016)
uzir (2021)
li (2021)
jiang (2018a)
huang (2022)
jussupow (2021)
topuz (2018)
boada (2021)
gómez-vallejo (2016)
basile (2023)
shareef (2021)
coccia (2020)
yeh (2011)
cubric (2020)
tremblay (2012)
ali (2023)
winter (2019a)
garbuio (2019)
coombs (2020)
tsiotsou (2022)
danaher (2021)
kandakoglu (2020)
wan (2021)
VOSviewer
2016
2018
2020
2022
2024

Bibliographic coupling of the documents

79

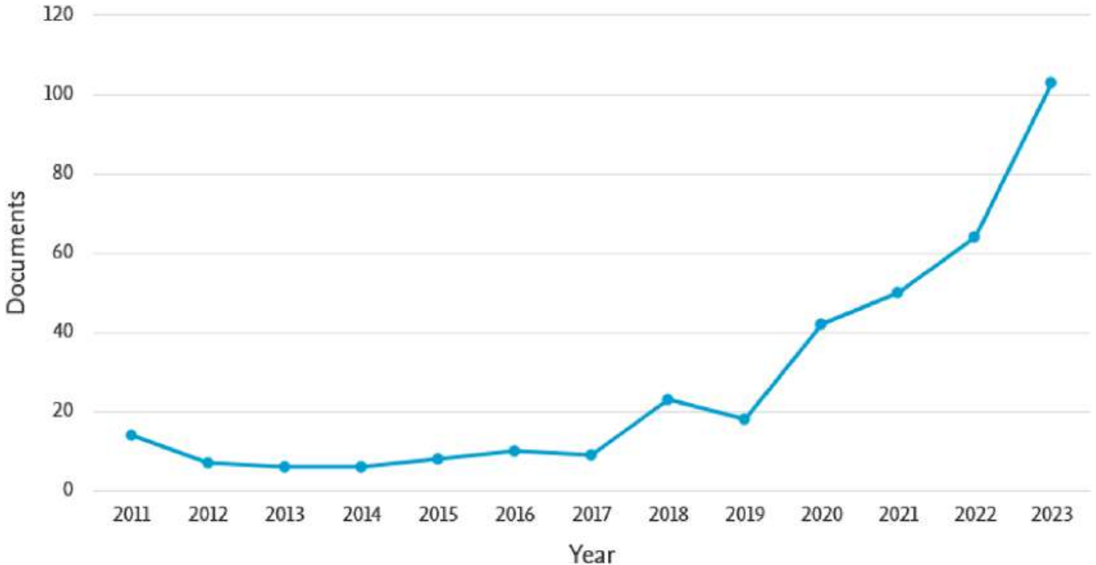

**Over time development of scholars' attention to the topic of AI and healthcare**

79

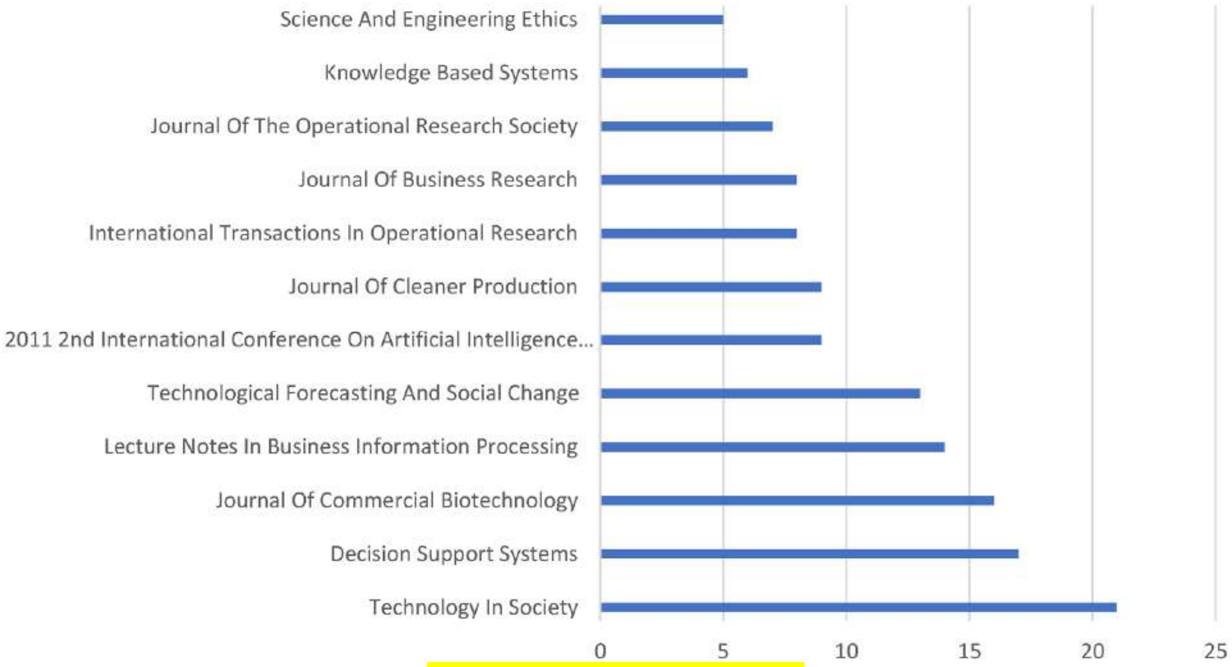

**Analyzed documents by source**

82

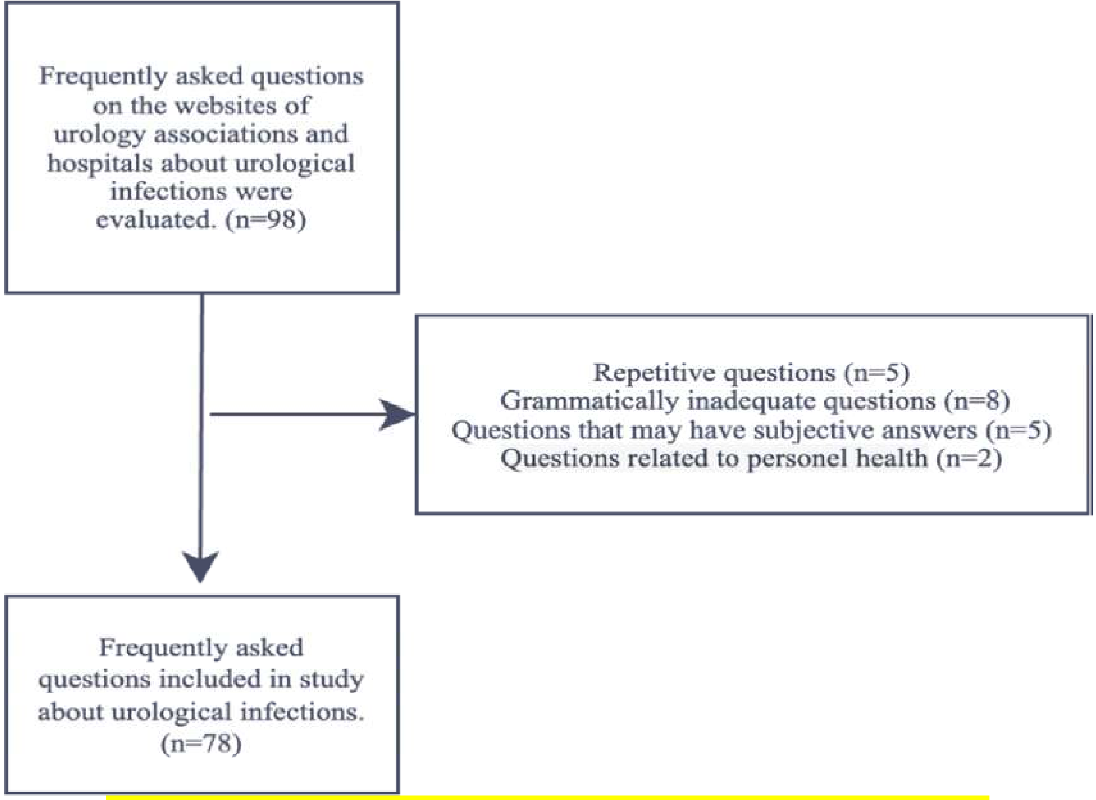
Frequently asked questions on the websites of urology associations and hospitals about urological infections were evaluated. (n=98)
Repetitive questions (n=5)
Grammatically inadequate questions (n=8)
Questions that may have subjective answers (n=5)
Questions related to personel health (n=2)
Frequently asked questions included in study about urological infections. (n=78)

**Flowchart of frequently asked questions included in the study Attention: Questions related to personal health**

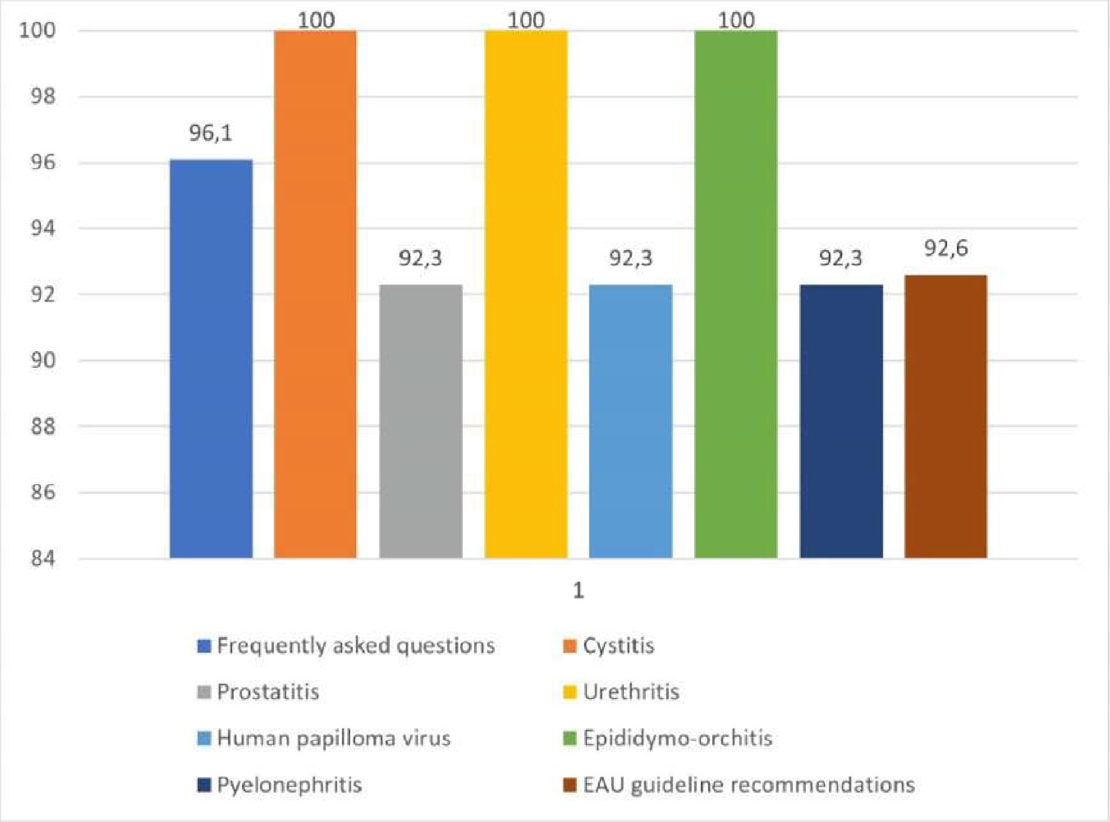

**Similarity rates of answers to questions**
**EAU: European Association of Urology**

84

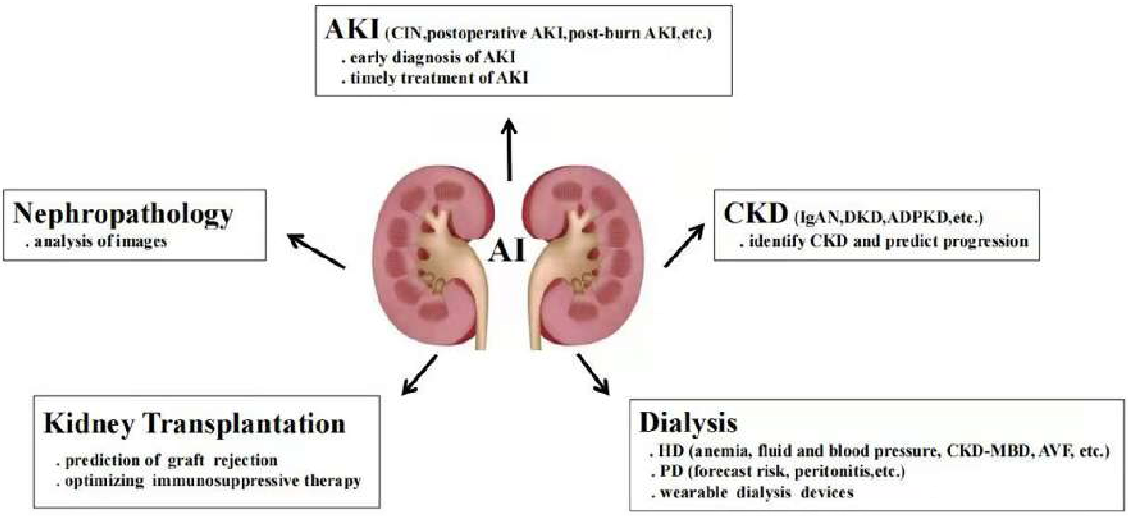
AKI (CIN,postoperative AKI,post-burn AKI,etc.)
. early diagnosis of AKI
. timely treatment of AKI
Nephropathology
. analysis of images
AI
CKD (IgAN,DKD,ADPKD,etc.)
. identify CKD and predict progression
Kidney Transplantation
. prediction of graft rejection
. optimizing immunosuppressive therapy
Dialysis
. HD (anemia, fluid and blood pressure, CKD-MBD, AVF, etc.)
. PD (forecast risk, peritonitis,etc.)
. wearable dialysis devices

Figure2. Clinical Applications of AI in Renal Disease

! Artificial intelligence (AI) is widely used in clinical diagnosis and treatment of renal diseases.

🔔 AI can assist in early diagnosis and timely treatment of

- acute kidney injury (AKI), including contrast-induced nephropathy (CIN), postoperative AKI and post-burn AKI

- AI helps to identify
    - CKD
    - Predict progression
    - Chronic kidney disease (CKD) patients such as
        - IgA nephropathy (IgAN),
    - diabetic kidney diseases (DKD),
    - autosomal dominant polycystic kidney disease (ADPKD),
- AI can
    - forecast risk and optimize
        - therapy For
            - hemodialysis (HD)
            - peritoneal dialysis(PD)
            - kidney transplant patients,
- AI can
    - analyze images of
        - renal biopsy in pathological diagnosis.

✓ CKD-MBD, Chronic kidney disease-mineral and bone disorder
✓ AVF, arteriovenous fistula

# CNN – 64b

## *Urologist/Nephrologist*

***is (Intelligentsystem)***

***m e(mental elevation/evolution)***

| | |
|---|---|
| International BusinessMachines | ***IBM*** |

| | |
|---|---|
| ***IBM Corporation*** | ***(1911)*** |

| | |
|---|---|
| **IBM** | **(1924)** |
| **IBM PC** | **(1981)** |

## Now (2020s)

**Information (Figure Image Table Script …)**

**Base (d) (Big Data)**

**Model ((Math/Stat/Fuzzy, ML, DeepArch, CNN,CapsN, Transformers, DeepLrn)**

**NI/AI/Si/Hi/Consc.)**

| | |
|---|---|
| **IBM** | **Is** |

- Nature’s/natural/Species/Human/Organ/Gene Intelligence
- Artificial/ General/Generative/Super/Hyper/Ultimate Evolving Intelligence
- Consciousness [Human, Universal, artificial]
- System [Animated species, Inanimate objects]
- Objects-of-study [System(s) Surrounding(s)
  Celestial, Macroscopic, microscopic, nano, molecular, atomic, electrons, nucleons, Boson etc.]

# MBI

# Medical/Mathematical method-Bots Based Information/Intelligence